DEVELOPMENT OF MOCK-UP RF MATCHING NETWORK FOR ICRH SYSTEM OF TOKAMAK AND ITS OPTIMIZATION WITH CONTINUOUSLY VARIABLE LOAD

A Thesis Submitted in fulfilment of the requirement for the award of the degree of

DOCTOR OF PHILOSOPHY

in

Electronics and Communication Engineering

Submitted by

ABHINAV JAIN

Reg. No. 901606002

Under the Supervision of

Dr. Rana Pratap Yadav
Associate Professor
TIET, Patiala (Punjab), India

Electronics and Communication Engineering Department

Thapar Institute of Engineering and Technology, Patiala-147004

March-2020

DECLARATION

I, **Abhinav Jain** hereby declare that the work contained in the thesis entitled **"Development of mock-up RF matching network for ICRH system of tokamak and its optimization with continuously variable load"** in fulfillment of the requirement for the award of degree **"Doctor of Philosophy"** submitted at **Department of Electronics and Communication Engineering, Thapar Institute of Engineering and Technology, Patiala** is an authentic record of research work carried out under the supervision of **Dr. Rana Pratap Yadav**, Associate Professor, Thapar Institute of Engineering and Technology (TIET). The matter presented in this thesis does not incorporate any material previously published or written by any other person except where due references are made in the text. The results obtained in this thesis have not been submitted in part or full to any other institute or university for the award of degree or diploma.

Abhinav Jain

Date: 24/07/21

Abhinav Jain

(Reg. No. 901606002)

CERTIFICATE

It is certified that the work contained in the thesis entitled "**Development of mock-up RF matching network for ICRH system of tokamak and its optimization with continuously variable load**" by Abhinav Jain (Reg. No. 901606002) has been carried out under my supervision and that this work has not been submitted elsewhere for any other degree.

Date: 02/08/2021

Dr. Rana Pratap Yadav
Associate Professor
Electronics and Communication Department
Thapar Institute of Engineering and Technology, Patiala

To my Family

ACKNOWLEDGEMENT

This thesis is the culmination of my journey of Ph.D., which was just like climbing a high peak step by step accompanied by encouragement, hardship, trust, and hard work. When I found myself at top experiencing the feeling of fulfillment, I realized though only my name appears on the cover of this dissertation, many people have contributed to accomplishing this huge task. First and foremost, I bow my head humbly before my greatest teacher, Almighty Mahavir Swami Ji and my Guru Jitendra Muni Ji for making me capable of completing my Ph.D. Thesis; only with their blessings, I have accomplished this huge task. I could have never done this without their blessings. I feel very fortunate to have their blessings during all these years of my life.

I owe a deep debt of gratitude to my institute 'Thapar Institute of Engineering and Technology, Patiala' for giving me an opportunity to complete this work.

I would like to express my sincere gratitude to my thesis supervisor Dr. Rana Pratap Yadav, for his excellent guidance, help and the time he spent throughout my period of association with him. He always encouraged me for everything. He has helped me at each and every point of my research work with patience and enthusiasm. The discussion at every step felt very energetic and full of energy. He ensures that the fire keeps burning, and being there at times when I required motivation and propelling me on the course of this thesis. The positive attitude I learned from him will remain with me forever. I thank him for everything he did for me to make my Ph.D. a success.

I am extremely thankful to my head of department Dr. Alpana Agarwal, for encouraging me throughout my research work. I also thank Dr. Amit Kumar Kohli, Dr. Amit Mishra, and Dr. D. P. Singh, being on my Ph.D. committee. Their suggestion and comments have helped me in bringing this thesis to the present shape. I would like to especially thank my lab colleagues and friends Ms. Gurkirandeep Kaur and Ms. Deepika Singh, for supporting me and helping me in different stages of work. I have learned a lot from them. Also, I would like to thank Ms. Amandeep Kaur, Ms. Aditi Bajaj, and Ms. Anmol Gupta for being friendly and helpful towards me on various occasions.

My acknowledgement would be incomplete without thanking the biggest source of my strength, my family. I would like to thank my family for standing by me through all the joys and sorrows that life had to offer. My heartfelt thanks and life-long gratitude go to my parents, who have raised me and wanted me to study more and more and do best in life. They made things seem a lot easier than they were, with their tireless support. A very special thanks to my

sister Mrs. Saloni Jain, Mr. Rajan Jain (brother-in-law), and both nieces Ms. Samridhi Jain and Ms. Swasti Jain, for their continuous love, support, and encouragement throughout.

No research is possible without the Library, I take this time to express my gratitude to all the library staff for their services and special thanks to Dr. Shri Ram, who has helped me in solving different issues regarding the Ph.D. thesis work. I would also like to thank Thapar Administration, non-teaching staff of the ECED department, for their kind help.

I am grateful to the different authors of the Literature I have gone through, without which it would have been impossible for me to carry out this exciting research. I have tried to express my gratitude to every person who contributed to this work directly or indirectly, there may still be someone hiding behind the veils of my forgetful part of memory. Last but not the least; I would like to thank all such great souls.

Abhinav Jain

TIET, Patiala (Punjab), India

ABSTRACT

In Tokamaks, RF power of few MW is feed to the ICRH antenna for heating the plasma for the fusion reaction. The plasma offers continuously variable load impedance, which changes dynamically with time. These variations are mainly due to the collective effect of the spatial change of plasma density and Edge Localized Modes (ELMs) inside the tokamak. These variations might be in the order of few milliseconds. Such fast variations are very difficult to match, and to a certain extent, developed matching networks fail to cope-up with the faster variation of the plasma load impedance. Therefore, the development of a matching network is inevitable to match the fast variation of plasma.

The real ICRH systems of the tokamaks are spatially distributed in very long distances and unreliable for implementation of the research problem. Therefore, the idea is to develop a mock-up of the ICRH system on the test bench. To reduce the size of the mock-up, and make it accommodate at the test bench, the mock-up is designed for lower power handling capability and scaled at five times the ICRH frequency. Now, the mock-up can be a useful set-up on a single test bench where research problems related to the ICRH system of Tokamak can be tested before final implementation.

The proposed work has been completed in several stages which are briefed as follow:

- The components of the mock-up ICRH system, such as 3dB hybrid coupler, directional couplers, rigid coaxial tapped transmission line, coaxial stub tuners, line stretcher, RF antenna, variable water load has been developed. Since these component designs are novel in many respects, it is a part of our research objective.
- The developed components of the mock-up have been integrated as in the similar layout of the ICRH system and tested using VNA for the desired performance.
- A computational program has been developed with a defined control sequence to control the detectors and matching components. The developed system has been optimized for the best possible speed using the developed program.
- The developed system is capable of automatically match any arbitrary load and tested for load resilient behavior as per our thesis objective.

LIST OF PUBLICATIONS

P1. A. Jain, R. P. Yadav and S. V. Kulkarni, “Design and development of 2kW, 3 dB hybrid coupler for the prototype Ion Cyclotron Resonance Frequency (ICRF) system,” *International Journal of Microwave and Wireless Technologies*, vol. 11, no. 1, pp. 1-6, 2019.
DOI: 10.1017/s175907871800137x

P2. A. Jain, R. P. Yadav and S. Kumar, “Design and development of resonant loop antenna for mock-up ion cyclotron resonance frequency system of tokamak,” *in IET Microwaves, Antennas & Propagation*, vol. 13, no. 7, pp. 976-981, 12 6 2019.
DOI: 10.1049/iet-map.2018.5797

P3. A. Jain, R. P. Yadav and S. Kumar, “Design and development of high power variable dual-directional radio frequency coupler,” in *IET Microwaves, Antennas & Propagation*, vol. 13, no. 14, pp. 2544-2550, 2019.
DOI: 10.1049/iet-map.2018.5855

P4. A. Jain, Anurag and R. P. Yadav, "Design and Development of Coaxial Line Based 2kW, 10-30dB Variable Dual Directional Coupler," *2017 IEEE MTT-S International Microwave and RF Conference (IMaRC)*, Ahmedabad, 2017, pp. 1-5.
DOI: 10.1109/IMaRC.2017.8449709

P5. A. Jain, R. P. Yadav and S. Kumar, "Design and Development of high power matching network for variable load," *2018 IEEE MTT-S International Microwave and RF Conference (IMaRC)*, Kolkata, India, 2018, pp. 1-4.
DOI: 10.1109/IMaRC.2018.8877143

P6. A. Jain and R. P. Yadav. "Design and development of rigid coaxial line based variable stub tuner" Frequenz, vol. 75, no. 5-6, 2021, pp. 153-158.
DOI: 10.1515/freq-2020-0085

COMMUNICATED

P1. A. Jain, R. P. Yadav, “Design and Development of 20 dB directional coupler for radio frequency applications,” International Journal of Electronics letters

P2. A. Jain, R. P. Yadav, “Development of mock-up ICRF system with a new algorithmic approach for automatic impedance matching for Ion cyclotron resonance frequency (ICRF) system of Tokamak,” in Fusion Engineering Design.

LIST OF ABBREVIATIONS

DT	Deuterium Tritium
SST-1	Steady State Superconducting Tokamak -1
JET	Joint European Torus
WEST	Tungsten Environment in Steady-state Tokamak
ITER	International Thermonuclear Experimental Reactor
ICRH	Ion Cyclotron Resonance Heating
ECRH	Electron Cyclotron Resonance Heating
ICRF	Ion Cyclotron Resonance Frequency
MW	Megawatt
ELMs	Edge Localised Modes
RF	Radio Frequency
HF	High Frequency
VHF	Very High Frequency
UHF	Ultra-High Frequency
dB	Decibel
HMI	Human Machine Interface
AC	Alternating Current
eV	Electron Volt
PPPL	Princeton Plasma Physics Lab
PLT	Princeton Large Torus
TFTR	Tokamak Fusion Test Reactor
ATC	Adiabatic Toroidal Compressor
NBI	Neutral Beam Injection
GHz	Gigahertz
MHz	Megahertz
EM	Electromagnetic
ASDEX	Axially Symmetric Divertor Experiment
TEXTOR	Tokamak Experiment for Technology Oriented Research
VME	Versa-Module Euro Card
ms	Millisecond
kW	Kilowatt
VSWR	Voltage Standing Wave Ratio

PLC	Programmable Logic Controller
SCADA	Supervisory control and data acquisition
μs	Microsecond
NSTX	National Spherical Torus Experiment
TOPICA	TOrino Polytechnic Ion Cyclotron Antenna)
3D	Three Dimensional
CST	Computer Simulation Technology
CNC	Computer Numerical Control
VNA	Vector Network Analyzer
CW	Continuous Wave
BNC	Bayonet Neill-Concelman
ORNL	Oak Ridge National laboratory
RDLs	Resonant Double Loops
CRLH-TL	Composite Right/Left Handed-Transmission Line
LH	Left Handed
RH	Right Handed
LPA	Low Power Amplifier
MEMS	Micro-Electromechanical System
DC	Direct Current
IC	Integrated Circuit
RADAR	Radio Detection and Ranging

GLOSSARY OF SYMBOLS

P_P	Maximum peak power
Z_O	Characteristic impedance
V_O	Maximum voltage
P_{av}	average power handling capability
T_{amb}	Ambient temperature
T_{max}	Maximum temperature
ΔT	Rise in temperature
b	Gap between conductor
k	Thermal conductivity
L	Length of coupled line
W	Width
t	thickness
ε_r	dielectric constant of air
W_e	Effective width
α_c, α_d	Loss coefficient of conductor and dielectric
$\Delta P_c, \Delta P_d$	Power dissipation due to losses in inner conductor and dielectric
R_s	Sheet resistivity
$tan\delta$	loss tangent of air dielectric
σ	conductivity of copper
f	frequency
D	gap between inner and outer conductor
$C_{11,}\ C_{22}$	Self-capacitance between coupled loop element and inner coaxial conductor in ground reference,
$C_{12,}\ C_{21}$	Mutual capacitance between the loop element and the inner conductor of a coaxial line
Z_{oe}	Even mode impedance
Z_{oo}	Odd mode impedance
v_P	phase velocity of wave
$C_{e,}\ C_o$	even and odd mode capacitance
$S_{Z_{oe}}^{C}, S_{Z_{oo}}^{C}$	sensitivity as a function of even and odd mode impedances
$\Delta C_{max}/C$	fractional change of coupling coefficient

K	complete elliptic integrals of the first kind
w_{se}	Series resonance
w_{sh}	Shunt resonance
L_S	Series Inductance
C_{se}	series capacitance
Z_{11}	input impedance
e	antenna radiation efficiency
e_r	reflection efficiency
e_c	conduction efficiency
e_d	dielectric efficiency
Z_{sA}	impedance of short circuited stub tuners
β	phase constant
λ	Wavelength
y_{ant}	Antenna admittance
g_{ant}	Antenna conductance
b_{ant}	Antenna susceptance
y_s	Normalized admittance
b_{sA}, b_{sB}	Susceptance of Stub A and B
l_{sA}, l_{sB}	Length of stub 1 and stub 2
P_d	Detector output power
P_{df}, P_{dr}	Forward and reflected output power
V_{df}, V_{dr}	Forward and reflected output voltage
Γ	Reflection coefficient

LIST OF FIGURES

LIST OF TABLES

TABLE OF CONTENTS

Page No.

CHAPTER 1

INTRODUCTION AND LITERATURE REVIEW

1.1. Overview

The consumption of energy has drastically increased over the decades, as the population increased. Therefore, the focus on alternative sources of energy is inevitable. The energy consumption in India is the third biggest after China and the USA. In India, about 92% of the total energy consumption is fulfilled through crude oil (29.55%), coal (55.88%), and gas (6.17%) and around 8% contributed through nuclear energy, hydroelectricity, and renewable power as per data available of 2018 [1]. About 75% of India's electricity generation is from fossil fuels. The total energy consumption is expecting to exceed 53% by 2030, so it will largely depend upon the export of fossil fuel to meet its energy demands. Also, fossil fuel poses a serious threat to the environment as it liberates around 10.65 billion atmospheric carbon dioxide (CO_2) per year, which contributes to global warming. There is a need to explore environmentally sustainable energy options to meet the current requirement. We have to consider various options to fulfill the demand. Fusion energy seems to have the potential to offer a secure and sustainable energy option because of numerous advantages [2]. Fusion energy is liberated from the fusion reaction, where two hydrogen isotopes that fuse to form the heavier helium element, a neutron, and also releases a large amount of energy [3]. The same mechanism is considered to be responsible at the core of our sun. Every second, the sun turns 600 million tons of hydrogen into helium, releasing an enormous amount of energy. The reaction between two hydrogen (H) isotopes, deuterium (D) and tritium (T) are identified as the most efficient reaction in fusion science. The DT fusion reaction produces the highest energy gain at the "lowest" temperatures. Scientists from various organizations around the world join hands to develop a powerful reactor known as the International Thermonuclear Experimental Reactor (ITER) in Cadarache, south of France, to demonstrate the feasibility of fusion energy [3-4]. In 2005, India became the solemn member of the ITER project and is responsible for delivering the Ion Cyclotron Resonance Heating (ICRH) system along with other systems.

This chapter explores the comprehensive literature review, starting with the concept of fusion energy, generation in the laboratory along with the practical problems involved. Further, the literature survey is focused on the latest research carried out in this direction of the development

for an efficient ICRH system. Several types of research studies have been carried out in respect to ICRH heating system, but still there exist many gaps which have been identified during the literature survey which has been presented in next chapter. The literature survey includes the previous study involved in the design and development of the ICRH system with a detailed study on matching techniques for matching the load impedance with source impedance.

1.2. Fusion Energy

Fusion energy is liberated from the fusion reaction, where two hydrogen isotopes that fuse together to form the heavier helium element, a neutron, and also releases a large amount of energy [1-2]. This same mechanism is considered to be responsible for energy sources like sun, stars and other illuminating celestial objects. The core of the sun composed of a tremendous amount of heat and gravity, which is responsible for fusion. In the laboratory, fusion has been achieved in Tokamak devices that used magnetic fields to contain and control the plasma for the production of energy. The plasma is produced with deuterium gas, and tritium is added in the form of pellets in the plasma to have fusion reaction. For a fusion reaction to occur in sun or stars, about 10 million degrees temperature is adequate due to high gravitational forces whereas, on earth, it requires above 100 million degrees Celsius temperature, i.e. about 10eV in a fusion reactor. This is one of the requirements to achieve fusion. Second is the requirement of sufficient plasma particle density such that most of the collisions between the nuclei do occur. Third is the requirement of sufficient plasma confinement time which is a sort of practical problem. Plasma confinement is needed to kept plasma at a safe distance from the reactor in order to prevent melting [3].

1.3. Plasma Confinement

Plasma as like gas, will occupy the whole volume when it's not confined. The inertial confinement uses the high energy focused laser beams to confine the dense plasma for a short period of time. The magnetic confinement device uses magnetic fields to confine the plasma. The first device used for magnetic confinement is a linear device which uses open field lines [4]. The losses in the linear device led to the formation of a torus structure that uses toroidal as well as poloidal fields called as Tokamak [3-5]. The Tokamak concept is given by the soviet physicist, and till now, it is the most successful configuration in terms of output fusion power.

1.4. Tokamak

1.4.1. History

Tokamak is an experimental reactor or machine in the shape of torus designed to harness the energy of fusion [2]. Tokamak is a magnetic confinement device, which is used to control and confine the high-temperature plasma to have a controlled fusion reaction for future energy generation [4]. The fusion reaction between the atoms releases enormous amount of energy which is absorbed as heat by the sidewalls of the device. This heat will generate the steam in the fusion power plant, and then by the use of turbines or generators, this will be converted to electricity.

A brief of the world-known experimental reactors [5-49] are given in Table 1.

Table 1.1: Various Tokamak and its description:

Tokamak	Power	Frequency Range
Aditya [5]	200kW	(22-47) MHz
SST-1 [6-14]	1.5MW	(22-91.2) MHz
Alcator C-Mod [15-22]	4MW	(40-80)MHz
ASDEX upgrade [23-27]	6MW	30-120MHz
JET [28-34]	36MW	(25-55) MHz
WEST (formerly Tore Supra) [35-37]	17MW	(40-80) MHz
ITER [38-49]	20MW/Antenna	(40-55) MHz

Tokamak is till now the foremost leading candidate for the practical fusion reactor. But the history of nuclear fusion on earth started around 1934, when a scientist like Mark Oliphant, Paul Hartack and Ernest Rutherford [4] tried to fuse deuterium nuclei with metal foil using a particle accelerator. But the experiment results in the scattering of particles due to the low cross-sectional area of reaction.

The scattering will create a loss in energy and do not undergo fusion. In 1944, to maintain the fusion, Enrico Fermi calculated the temperature around 50,000,000 K; that will self-sustain the reaction. In 1945, UK scientist George Paget gave various unsuccessful attempts to build a practical fusion machine using a pinch effect, which is a promising technique but gave up due to the funding problems. The Russian physicist Sakharov and Tamm initially suggested not to use external magnets as the current in the plasma is strong enough to confine [4]. Golovin and Natan Yavlinsky were the only scientists that favor the static toroidal arrangement. The linear pinch concept found many instabilities. One is the sausage, and the other one is kink. [4] One additional

concept of ‘stabilized pinch’ is introduced in which extra magnets outside the chamber are used, which created a field before the plasma discharge. Sakharov again gave a new idea to stabilize the plasma by reducing the current and use of strong external magnets to confine the plasma. To suppress the instabilities, the safety factor (q) concept is developed, which state that q must always be greater than 1. In 1958, the first Tokamak T-1 began operational. In T-1 demonstrated high energy losses due to the impurities in plasma. To find the solution, a small device T-2 was constructed. The results make way for the Tokamak construction around the world like TM-2 in 1965, T-3, T-4 in 1968, “The Culham Five” late in 1968. During the mid-1970s, many countries started working on Tokamak, and in the late 1970s many results suggest the practical conditions to achieve the fusion but not in a single reactor. Princeton Plasma Physics Laboratory (PPPL) proposed the magnetic compression, whereas neutral beam injection is proposed by Oak ridge laboratory. The results on beamforming heating shown by Princeton Large Torus (PLT) form the basis of a future fusion reactor. The T-7 Tokamak in 1979 successfully used superconducting magnets. After that, various Tokamaks like T-15, Alcator C-mod [15-22], JT-60 [25], JET [28-34], TFTR [35],TEXTOR [37] etc. started to work on the instabilities, and these were run on the fuel of deuterium and tritium. These machines also demonstrated new problems that limit their performances and to mitigate the challenges, a more expensive and bigger unit is required which is beyond the ability of a single country. So, an agreement is signed between European Union, USA, Japan, and Soviet Union in1986 to build a larger and more powerful machine with a q factor of nearly 10, and the organization is known as International Thermonuclear Experimental Reactor (ITER) organization [4]. In 2005, India became the solemn member of the ITER project. Till now, only JET has the highest fusion output of 16MW from the 24MW input power.

1.4.2. Plasma Heating

As the fusion is directly related to the temperature of plasma inside the vessel. In the mid-1970s, when the stellarator results were not encouraging, the PPPL and Oak Ridge laboratory [80] started working on heating the plasma by external sources, and the initial results confirmed success in heating the plasma. For a fusion reaction to take place inside the Tokamak, plasma temperature should be maintained to about 100 million degrees Celsius [2-3]. To achieve such a high temperature is the main key challenge for scientists. Plasma, as an ionized gas makes it electrically conductive and strongly responsive to electromagnetic fields. So, the plasma is initially heated by inducing a current obtained using a transformer coil around the perimeter of the vessel. It is also

called ohmic or resistive heating, as the same occurs in electric heater or electric bulb. The heat generated within the Tokamak depends upon the amount of electric current running and resistance of plasma. The ohmic heating becomes ineffective with the increase in plasma temperature, and thus, the resistance decreases. There are many limitations, as discussed by R. Koch and D. Van Eester [4]. This type of heating can attain about 20-30 million degrees Celsius. To obtain the optimum temperature where fusion can occur, various methods have been developed for heating the plasma-like ICRH (Ion cyclotron resonance heating), ECRH (Electron cyclotron resonance heating), Neutral beam injection, Magnetic compression, etc. [5-30].

1.4.2.1. Magnetic Compression

Magnetic compression is a technique in which the plasma is compressed by increasing the confinement of the magnetic field. This compression brings the ions closer together and makes the required plasma density for the fusion reaction. This type of heating was used in the early research of fusion and was used in ATC. Since then the magnetic compression is not used but the concept is a part of general fusion design.

1.4.2.2. Neutral Beam Injection (NBI)

NBI is the technique in which a beam of high energy neutral particles is injected into the plasma. The particles transfer the energy to plasma via Coulomb collisions. Oak Ridge Laboratory first proposed the NBI in mid-1970s [4, 15]. The neutral beam injection facility of ITER in Padova is the first to start operation. This technique is basically used to heat the plasma but also used as a diagnostic tool and in feedback control by making a pulsed beam.

1.4.2.3. Electron Cyclotron Resonance Heating (ECRH)

In ECRH, the microwave energy is absorbed at electron resonance frequency to heat the plasma to fusion temperature. It happens when the frequency of incident waves collides with the frequency of electrons in the magnetic field [15, 27]. The ECRH system frequency may vary from 28 to 170GHz depending on the magnetic field inside Tokamak, and these frequencies are produced by special free-electron lasers and gyrotron tubes.

1.4.2.4. Ion Cyclotron Resonance Heating (ICRH)

During the last few decades, continuous study on the interaction of electromagnetic waves with the plasma has been studied. Various fusion devices such as stellarator [15], mirror machines [4], and Tokamak [4-50] uses plasma heating by EM waves. Radio Frequency (RF) heating is the technique in which energy of high-frequency electromagnetic waves is transferred to the plasma.

The waves are generated using RF oscillators/generators outside the vessel. The resonant interaction of EM waves with plasma increases the kinetic energy of ions, this energy is transferred to other plasma particles by collisions, and hence the heating takes place.

1.5. Detailed description on ICRH system

India is a part of the ITER Tokamak project and is responsible for the delivery of ECRH, ICRH heating systems, power supplies, etc. Inside Tokamak, plasma is heated up to several tens of million degrees centigrade to achieve the required rate of the fusion reaction. The heating of Tokamak plasma using the ICRH system is one of the promising methods due to effective heating in low densities, low magnetic field. Also, the technology involved in high power RF generation and transmission is relatively cheaper. The ICRH system consists of RF generator, transmission lines, a detection unit, matching network, and RF antennae [6].

RF power of few MW is feed to ICRH antenna to transfer power from source to antenna, and then these RF antennae radiate the RF waves inside Tokamak at ICRF frequency of plasma for heating the plasma for the fusion reaction. Plasma condition varies dynamically in front of RF antennae, which results in variation of antenna impedance [6-14], [38-41]. The antenna impedance not only depends on antenna structure; it also depends on the boundary condition of plasma such as plasma density, density gradient in front of the antenna. The variations in impedances have a time scale of few milliseconds, which are very difficult to control and match. These impedance variations can limit the power delivered to the plasma in a Tokamak to achieve the fusion temperature. It can also damage the generator with the reflected power. Various studies have been presented in detail with respect to the ICRH system. The detailed description of various studies carried out on the ICRH system of Tokamak around the world, its structure, working frequency range, various matching networks, detection units, and then problem identification related to the ICRH system has been explained below in detail.

1.5.1. Structure of ICRH system

The ICRH system used in each Tokamak [5-53] basically consists of high power RF generators, long transmission lines, a detection unit, a matching unit, a feedback unit, and an RF antenna. The high power generators used in some of the Tokamaks such as ASDEX upgrade [23-27] use four generators, each with power capability of 2 MW, C-mod Tokamak [15-22], D-III-D [25], NSTX [25], Tore Supra [35-36], TEXTOR [37] consist of 2MW power with multiple generators whereas

JET [28-34] uses 16 generators for its ICRH system each having power capability of 2 MW, in similar way JT-60U [25] consists of 8 generators with 1.5 MW power generation from each unit. The ICRH system on Aditya [5] uses a 200 kW generator, whereas SST-1 [6] uses a 1.5MW generator for the operation. ITER [47] proposed 20MW of power coupled to ICRH antenna. The RF power of a few MW is transferred to the RF antenna through high power transmission lines. In Aditya Tokamak [5], 9" coaxial transmission line (TL) is used, which is about 53m long whereas in SST-1 [6, 9] it is100m long. The TL carries the high power to the RF antennae which radiates the RF waves inside the Tokamak at ICRF frequency of plasma for heating the plasma. The operating frequency of the various system of Tokamaks are described as below,

1.5.2. Operating Frequency

Many experiments on different Tokamaks like JET, Tore Supra, ASDEX Upgrade, KSTAR, TEXTOR, SST-1, Aditya, ITER, etc. around the world have been carried out to enhance/explore the capability of the tokamak. ICRH system used in some of the well-known Tokamaks such as ASDEX Upgrade worked in the frequency range of 30-120 MHz, D-III-D from 60-120 MHz, Aditya [5] from 22-47 MHz, SST-1[9] Tokamak at 22-91.2 MHz, C-mod Tokamak [16] in the range of 40-80 MHz, TEXTOR [36] from 25-38 MHz, JET [26-28] at 25-55 MHz, Tore Supra [35] from 35-80MHz whereas ITER [47] plan to operate at 40-55 MHz range of frequency.

1.5.3. Detection, matching and feedback system with its components

Plasma property varies dynamically in front of RF antennae, which results in variation of antenna impedance. The antenna impedance variations have a time scale of few milliseconds, which are very difficult to control and match. Also, it can damage the generator with the reflected power. So, to protect the system and to deliver full input power to the plasma, a matching system along with a detection unit, which is used to calculate the amount of reflection on the generator is integrated into each ICRH system of the Tokamak. Here detailed analysis about the detection, matching and feedback system used in various system of Tokamak has been discussed,

Bora et al., [6] reported the commissioning and testing of the SST-1 ICRF system, which is one of the major heating schemes used in SST-1 where the system consists of two branches, and 3dB hybrid coupler is used to split the power to drive both the antenna. The study and installation of 3dB coupler in different Tokamaks proved to be very successful as it diverts the reflected power to the isolated port terminated by dummy load and protects the RF generator from backscattered waves. An ultra-wideband two-section 3dB coupler study was reported by H. J. Kim et al., [51]

which is developed for high power handling capability in fusion Tokamak. Yadav et al., [54-56] has also successfully designed the 3dB coupler using strip-line technology in the frequency range of 38 to 112MHz. He also explains about the junction discontinuity effect in high power scenario and explains the bandwidth enhancement by using multi-section coupled lines. Noterdaeme et al., [25] reported the use of 3dB coupler and conjugate-T provides a better handling capability to suppress the reflections. Messiaen et al., [38, 40, 42, 46] and Grine et al., [47] successfully tested four hybrid couplers for mock-up of the ITER Tokamak system and found response very similar as expected.

The detection unit consists of directional coupler, tapped transmission line, i.e. RF probes section. The directional couplers are used to detect the forward and reflected power to calculate the mismatching in the system. Different Tokamaks such as in Aditya [5], SST-1 [6-14] Parihar et al., [8] uses 24 probe signals in the transmission line to calculate the VSWR, which is processed using a controller to control the matching system to achieve the desired output. The directional couplers [59-70] are also placed in the transmission line to calculate forward and reflected power, which is used in error signal calculation. Grine et al., [47] also calculated the voltage for forward and reflected signals to find the error signal for matching of variable load.

The matching networks are used to transform the load impedance with that of source impedance, to transfer the total input power to the plasma for the ignition of fusion reaction. The matching units that are used on different Tokamaks consist of a combination of fixed and variable stub tuners, phase shifters/line stretchers, de-couplers, and service stubs. Tokamaks around the world have been operated on different combination of matching systems. Some of the well-known Tokamaks such as ASDEX upgrade [25] uses a combination of double stub and hybrid coupler, C-mod uses combination of Trombone (basically a phase shifter/line stretcher) and stub, D-III-D uses only hybrid couplers whereas JET, JT-60U and NSTX [25] uses Trombone and stubs, TEXTOR utilizes Stubs, trombones and capacitors whereas tore supra uses resonant double loop (capacitors) for the matching unit. Aditya Tokamak [5] uses an offline matching system that consists of directional coupler, probe section, fixed and variable phase shifter, variable stubs for matching purposes. As the matching system operates in offline mode, so the response time of the matching system is very slow. Bora et al., [6] reported the use of two matching systems in SST-1, one is slow matching system that consists of stub and phase shifter whereas the other is the fast matching system which is an online system that uses variable capacitor and stubs. Presented work

reported to match the system within few seconds as the movement of stub is very slow. SST-1 system uses the VERSA-Module Euro card (VME) based data acquisition system for real-time control. SST-1 system reported around 30-40% reflections during the operations, which is very high, and plasma impedances changes within a few milliseconds (ms). Joshi et al., [9] reported to match the load impedance with source impedance within 120 ms, where poloidal antennae are used. The offline system uses stub and phase shifter, while the online system uses a capacitor and two stubs. The offline matching is achieved within a few seconds whereas online matching achieved in ~120ms. Parihar et al., [8] tested the system at 45.6MHz for variable conditions made using variable capacitor and resistor as same as the condition of plasma inside the Tokamak. Joshi et al., [9] integrated and tested the PLC-based control and acquisition system in SST-1, where SCADA based interface is used for matching. The offline system has been tested and integrated, which consists of static stubs, two variable stubs with two voltage variable capacitor and one variable shifter have been employed for the offline system. Noterdaeme et al., [25] reported that the reflections might be as fast as 50μs. The variation of impedance values in JET and ASDEX are ranging from 1 to 10 ohm in the real part. Noterdaeme suggested matching methods to control the impedance variations such as, to make the antenna variations small by reconfiguring boundary conditions or use of traveling wave antenna, use of capacitors, inductors to transform the impedance, use of hybrid coupler and T-conjugate by suppressing the reflected power. In JET [25] the matching component such as stub moves at a speed of 5cm/sec, trombone at 16.5cm/sec, which matches the variations of impedance in few seconds whereas in JT-60 U trombone at 0.5 cm/sec and stub at 2cm/sec.

Various experiments have been performed to test the condition for the proposed ITER Tokamak. Messiaen et al., [42] reported a mock-up for ITER Tokamak to test the load resilience behavior based on antenna array with varying water load conditions as same as plasma variations. Here, Messiaen developed an array of 24 radiating straps [40, 42] where the mutual coupling effects have been analyzed, and the effects of the variation of mutual coupling between the straps have been controlled by anti-node voltage distribution and use of the de-coupler circuit. The system uses four hybrid couplers, CT junctions and de-coupler, and the feedback-controlled stub. The load resilience performance and the antenna spectrum obtained by modeling is very similar to TOPICA simulation and is true for the ITER system. The Prototype has been scaled to five times the ITER ICRH which means, the system has increased the frequency and decreases the size to five times

than the real system, to test and control the effects of mutual coupling, loading variations. Messiaen utilize the saltwater load for similar variation like plasma. Grine et al., [47] stated the results obtained on the prototype developed for the ITER ICRH system. They have utilized different matching techniques for the impedance matching in real-time. The system is scaled to low power, and 3dB matching technique is used with 24 strap antenna forming the eight four-port junctions. The matching components like de-coupler, stub tuners, phase shifters are used to provide the necessary reactance or phase for matching. The system operated on 210 MHz, and the response is very similar as expected in the real system. Grine reported a real/Img algorithm based on error function that can match the impedance variations in real-time. Messiaen [38] reported the testing of simulated salt water load in front of the developed array of antenna straps. The saltwater can act like the plasma load conditions due to the high dielectric constant of water, which is similar in variations, and the impedance matrix also remain the same when the proposed system is scaled in terms of frequency and power. The analysis reported by Messiaen shows that loading variation in front of the antenna can be changed by varying the distance between the antenna straps and the water tank. Salt is added to decrease the effect of reflection from the walls of the tank. Messiaen [40] utilized the electrostatic screen in front of the antenna that has been realized to decrease the effect of plasma loading. Kumazawa et al., [73] uses liquid stub tuner for Alcator C-Mod Tokamak but the response time of the stubs remain in seconds which is quite slow whereas, Lin et al., [19] implemented fast ferrite tuner using triple tuner scheme for matching the variations in real-time but the RF losses due to biasing is the major issue with the ferrite tuner. This technique has been previously deployed in several Tokamaks such as D-III-D [25], ASDEX-upgrade [23-25], etc. Durmortier [43] shows the optimization of the ICRF antenna in terms of current distribution, RF losses, etc. using CST microwave studio. The optimization is performed using a single triplet strap and is designed on scaled frequency. The service stub is also attached with the antenna which increases the coupled power and provides the broadband frequency response. Vervier [37] reported about the de-coupler circuit that is used to modulate the power transfer as well as to reduce the mutual coupling between different straps of the antenna. Durmortier [45] described the ITER ICRH antenna design and matching circuit, which consists of straps, pre matching elements, pressurized transmission lines, faraday screen, and also the use of single stub, double stub, de-coupler, ELM resilient schemes such as Conjugate-T and hybrid coupler has been explained briefly. The topic is still under research where scientists, researchers from various organizations

are working on it to mitigate the effect of impedance variations for maximum transfer of input RF power to the plasma. The literature review presents the study related to the design and development of the ICRH system in different Tokamaks for matching of variable load using various matching techniques.

In general, ICRH systems are RF network which has been rated for MW power handing capability in HF and VHF range. The real ICRH systems of the Tokamaks are spatially distributed in very long distances and very inflexible to changes due to its rigid configuration. Thus, any change in the system consumes much time and requires large number of manpower and planning. It is very difficult to utilize such a diversified system to study the research problems, where changes inside the system are required in a very frequent manner.

Therefore, the idea is to develop a low power prototype of the ICRH system at five times scaled frequency on test bench where new concept or technique can be easily implemented, studied, and tested for the ICRH system of Tokamak. This can be very useful to solve the research problems related to the ICRH system without facing the practical complexity of the high power ICRH system of Tokamak. So, the author is motivated to intensify his research on the development of a fast ICRH network and optimize it using simple and efficient algorithms, to enhance the capability of the ICRH system to deliver the maximum power to the load at any mismatch conditions. The general description of the proposed mock-up is discussed as follows:

1.6. Proposed mock-up ICRH system

The mock-up ICRH system consists of important RF components such as 3dB hybrid coupler, directional couplers, power detectors, coaxial stub tuners, line stretchers, service stubs, RF antennae, variable water load, and feedback-controlled drives, which are designed for low power and scaled at five times of ICRH frequency to reduce the size. Without introducing any significant effect on the system performance size of mock-up can be reduced by scaling the design at a higher frequency so that it can be implemented at a single test bench. The layout of the proposed mock-up ICRH system is shown in Fig.1. Each component shown in the layout has been discussed herewith in detail.

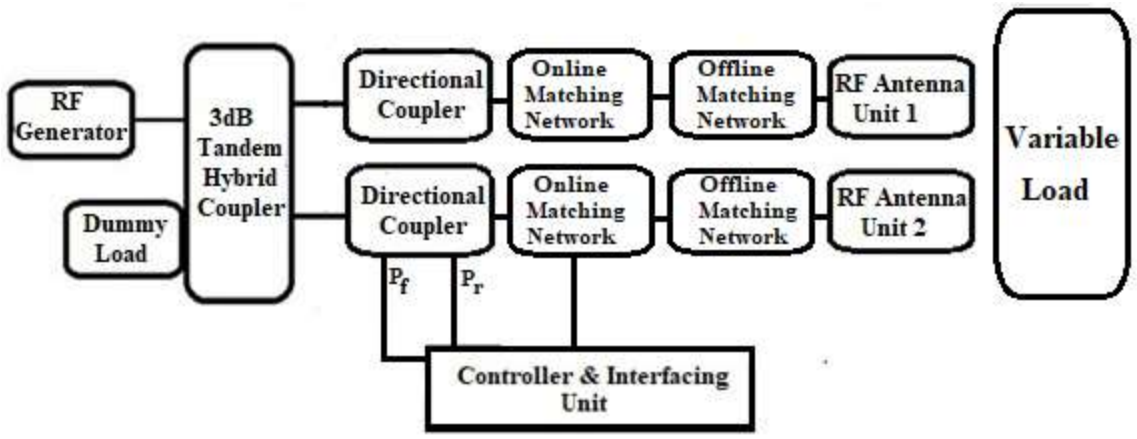

Figure 1.1: Layout of the proposed experimental set-up.

1.6.1. RF source

The RF source provides input to the mock-up system for active test and measurement. An RF signal generator is used for the waveform generation, which is being amplified with Low power amplifier (LPA). The combination of a signal generator and LPA offers an output of 100 watt RF power in the frequency range, 50 to 500MHz. The RF power is supposed to be sufficient for the operation of the mock-up.

1.6.2. The 3dB Hybrid Coupler [50]

A 3 dB hybrid coupler is used to divide the RF power between two antennae of the prototype and also provide the essential protection to the RF generator by coupling the reflected power at matched terminated isolated port [51-56]. The hybrid coupler provides the load-resilience to fast load excursions. Indeed, the use of hybrid splitters ensures that no reflections occur at the generator when the reflections on the output are equal both in magnitude and in phase, in which case the reflected power is diverted to the dummy load.

1.6.3. Tunable and Fixed Type Directional Coupler [57-58]

These are used to detect the forward and reflected power taken out for error signal calculations of the Matching network [59-70].

1.6.4. Components of Matching Network

***Stub Tuners*:** These are the motor-driven variable-length shorted stubs, which provides the online matching to the variable load and minimize the reflected power [71-78].

***Line Stretchers*:** The motor-driven line stretchers with shorted terminations on one of the two ports. This provides the required phase matching to the variable load [79-82].

***Service Stubs*:** This is utilized for broad banding and optimization of the frequency response of antenna [61-78].

De-coupler: This is utilized to reduce the mutual coupling between the RF antennae.

1.6.5. RF Antenna [83]

RF power is fed through the antenna to the variable load. These are designed to deliver the maximum power to the load in a perfectly matched condition [84-93].

1.6.6. Variable Load

To emulate the plasma load variation, a moveable water tank based variable load can be utilized [38, 40-41].

1.6.7. Controller and Interfacing Unit

The real-time matching shows the auxiliary hardware systems, including (i) the controller unit, motor drivers, analog to digital converter (ii) Human Interface Unit (HMI) (iii) the AC servo motors and power supplies (iv) A desktop computer/laptop used to run the acquisition and control part as well as Human Machine Interface (HMI) software, respectively [6-13].

The layout of the mock-up ICRH system is arranged in a similar way to that of SST-1 Tokamak [6]. The mock-up consists of two branches where each branch comprises of the directional coupler, power detectors, double stub arrangement, line stretcher, service stub, antenna, and variable water load. The stub tuners, line stretchers, service stubs are attached with electrically controlled fast drives that provide needful mechanical movement for required matching. The controller automatically senses the forward and reflected voltages through a power detector connected to the directional coupler and responds as per developed algorithms. The matching algorithm incorporates various matching steps which have been interpreted for the controller program to control devices used in the matching network. The speed of the matching network depends on the response of the inbuilt diagnostic and applied matching algorithms. Various matching techniques have been developed and applied for the fast load resilient matching of ICRF heating of the Tokamak.

1.7. Summary

This chapter provides introduction and a background review of different ICRH system of Tokamak, study of various detection and matching components involved, and its development. Different matching techniques have been studied to deliver optimum power to plasma for the unknown load. This topic still requires a continuous effort to make the system more reliable, accurate, and fast. Therefore, based on the literature survey, the research gaps have been identified and are presented in the next section.

1.8. Organization of the Thesis

The thesis deals with the design and development of a mock-up ICRH matching network where each component of the system is indigenously designed for lower power and scaled at five times of ICRH frequency to reduce the size. Then the fabrication and testing of every component have been completed. After that, the integration of the developed components into a matching system using coaxial transmission lines has been done. At last, the optimization with a continuous variable load has been carried out using simple and efficient algorithms.

Chapter 1 deals with the introduction and literature survey of fusion Tokamak, various heating phenomena, and brief about the ICRH heating, its limitations, challenges, and the structure of the thesis is also discussed in this chapter.

Chapter 2 deals with Research gaps and motivation of doing present research work, objectives, methodology to achieve the goals are elaborated in this chapter.

Chapter 3 deals with the design and development of various components of mock-up ICRH system which are developed for low power and scaled at five times of ICRH frequency to reduce the size. Simulation, fabrication, and test results have been presented in this chapter.

Chapter 4 presents the development of a high power double stub automated matching network along with a computational program based on a double stub RF matching hypothesis to achieve the optimum matching speed.

Chapter 5 deals with the integration of the whole mock-up ICRH system of Tokamak using developed components and implementation of different matching techniques on a developed system to provide the optimum power to the load in mismatch condition has been presented in this chapter.

Chapter 6 provides the conclusion of the thesis and also discusses the future work that could be taken up to extend the results of this effort.

CHAPTER 2

RESEARCH GAPS, OBJECTIVES AND METHODOLOGY

2.1. Research Gaps and Objectives

2.1.1. Research Gaps

The ICRH is used in Tokamak to heat the plasma at the required temperature for the fusion reaction. In Tokamak, plasma offers continuously variable load impedance, which changes dynamically with time. These variations are collective results of the variable spatial plasma density, Edge Localize Modes (ELMs), etc. inside the Tokamak. The plasma load varies in order of few milliseconds, and it is very difficult to match. Therefore, researchers are working on the development of a fast RF high power matching network to cope-up the plasma load variation inside Tokamak. The topic is still under research, where significant research contribution is expected [4-8, 18-20]. In general, ICRH systems are RF network which has been rated for Megawatt (MW) power handing capability in HF and VHF range. The real high ICRH systems of Tokamaks are spatially distributed fixed structures that are very unreliable for frequent changes required in research. Therefore, the idea is to develop a low power prototype of the ICRH system at five times scaled frequency on test bench where new concept or technique can be easily implemented, studied, and tested for the ICRH system of Tokamak. The thesis is mainly based on the design and development of load resilient mock-up ICRH system of the Tokamak. The work has been planned in various steps that decides the thesis objectives. The main objectives of the thesis are given as follows,

2.1.2. Objectives

1. Design and simulation of components of the mock-up ICRH system.
2. Optimization of each component in operating frequency range, 170-190MHz for the optimum performance.
3. Fabrication and testing of components and its integration for the development of proposed mock-up ICRH system used for matching of continuously variable load.
4. Optimization of mock-up ICRH system to deliver the optimum power to the load in mismatch condition.

2.2. Methodology to achieve the Objectives:

The work presented in the thesis is mainly based on the development of mock-up ICRH system of Tokamak. In order to get the fast matching speed, various matching concept has been developed. The work has been completed in many steps which have been explicitly discussed as follow,

The proposed system comprises of various RF components such as directional coupler, power detectors, coaxial stub tuners, phase shifters, RF antenna, variable water load, and feedback-controlled drives. The development of each component of the mock-up is a part of the thesis objective. Therefore, a detailed investigation has been carried out in a very early stage.

These components have been mainly developed using air-cored RF transmission line by taking into consideration of high power application. Initially, each component of the mock-up is theoretically designed, and the performance of these are verified using 3D Electromagnetic simulation software, CST. The simulation results in terms of S-parameters, VSWR, radiation characteristics, etc. have been analyzed for the desired results. The complete study on simulation of each component has been presented in Chapter 3, and the task has also been mentioned as the ***first objective*** of the thesis.

The next objective of the work is to design the RF components which can be upgradable up to MW power handling capability and optimize these for desirable parameters. These designs should also be compatible with the high-speed matching system. Therefore, air-cored coaxial transmission lines used in the fabrication of the matching components like variable stub tuner and phase shifter, directional coupler, etc. The variable stub tuner and phase shifters designs are based on belt pulley linear arrangement instead of a lead screw as found in conventional systems. Pulley arrangement is much faster than the lead screw, and it will move with the precision of 3.9mm/msec. These component designs incorporate the peripheral arrangement for mechanical movement for the tuning of components, which leads to transmission line discontinuity. The effect of this discontinuity significantly deteriorates the performance of the components from the desired response. Therefore, each of the components needs to be optimized by compensation of the induced discontinuity effect. So, the ***second objective*** of the thesis is based on the optimization of the designed components for the desired performance in the prescribed frequency range 170-190MHz. The complete study has been presented in Chapter 3.

The detailed engineering drawings of components have been prepared by taking into account of fabrication feasibility. The development of each component involves discussion on the

material used and mechanical fabrication processes such as CNC, milling, wire cutting, die casting, etc. that are the part of the analysis. The fabrication details have been discussed in chapter 3. After fabrication, each component has been tested and characterized using Vector Network Analyzer (VNA). The output performance of these components has been discussed in Chapter 3.

These components have been integrated as per the proposed layout of the mock-up as shown in Fig.1. The variable matching components such as stub tuners and phase shifters are integrated with AC servo motors, which are controlled and drive using feedback controller in the real-time domain. The fabrication, testing, and integration of the components are proposed as the **third objective** of the thesis.

The speed of the matching network depends on the response of the inbuilt diagnostic and applied matching algorithms. Therefore the next objective of the thesis is mainly based on the development of matching concepts and efficient algorithms for the operation of mock-up ICRH system. A high power double stub automated matching network along with a computational program based on a double stub RF matching hypothesis has been developed a stage before the development of a full mock-up ICRH system, which has been discussed in Chapter 4. The layout of the mock-up ICRH system is arranged in a similar way to that of SST-1 Tokamak. The mock-up has been designed to control the matching components and consists of two branches, where each branch consists of the directional coupler, power detectors, double stub arrangement, line stretcher, service stub, antenna, and variable water load. The stub tuners, line stretchers, service stubs are attached with electrically controlled fast drives that provide needful mechanical movement for required matching. The controller automatically senses the forward and reflected voltages through a power detector connected to the directional coupler and responds as per developed algorithms. The matching algorithm incorporates the various matching steps which have been interpreted for the controller program to control devices used in the matching network. Various matching techniques have been developed and applied for the load resilient matching of ICRF heating of Tokamak as detailed description presented in Chapter 4 and Chapter 5. The work has been mentioned as the f**ourth objective** of the thesis.

Chapter 6 provides a summary of the thesis and discusses the future work that could be taken up to extend the results of this effort.

CHAPTER 3

DESIGN AND DEVELOPMENT OF RF MATCHING COMPONENTS OF MOCK-UP ICRH SYSTEM

3.1. Overview

This chapter briefly explains the design and fabrication of components used in the development of the proposed mock-up ICRH system. The real ICRH system of Tokamak spreads over long area and not suitable for changes required for research and development. The main objective of the thesis is to develop a prototype called mock-up of ICRH system on the test bench. The proposed mock-up is designed for low power handling capability and scaled at five times of ICRH frequency, i.e. 182.5MHz. So that it can be implemented at a single test bench. The layout of the proposed mock-up of ICRH system is shown in Figure 3.1. It comprises of various RF components such as RF source, 3dB hybrid coupler, directional couplers, power detectors, coaxial stub tuners, line stretcher, RF antenna, variable water load, and feedback-controlled system. The RF power coming from the RF source is divided equally between the two RF antennae using a 3dB hybrid coupler. Antennae are out faced with a variable water load which emulates the mismatch condition like plasma inside the Tokamak. The components like directional coupler, power detectors, and RF probe array are used to detect the magnitude and phase of forward and reflected power for the analysis of the mismatched condition. Similarly, the other components like motorized stub tuners, line stretcher, service stub are utilized to provide necessary reactance for matching the load impedance to source impedance. A feedback control system has been designed to control the matching component on the basis of feedback received from the detectors.

The components of the mock-up are theoretically designed and modelled for the 3D Electromagnetic simulation. The design components has been simulated and optimized for the desired performance in the prescribed frequency range 170-190 MHz with the help of 3D Electromagnetic simulation software, CST. The dielectric loss is one of the major concerns in high power RF devices. Therefore, the components of the proposed mock-up have been designed using air-cored RF transmission lines. The detailed engineering drawings of components have been prepared and used for the fabrication of the respective component of the proposed system. A detailed study about each component is discussed in this chapter.

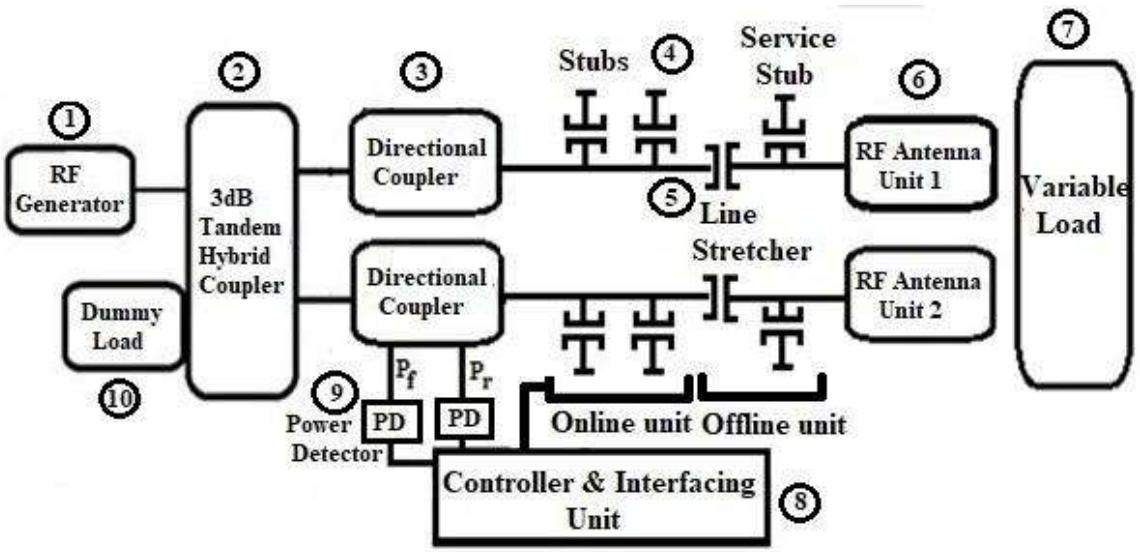

Figure 3.1: Layout of Proposed mock-up ICRH system.

3.2. Estimation of Power Handling capability

The peak power handling capability of the strip-line is limited by dielectric breakdown, whereas an increase in conductor temperature and dielectric losses limit the average power rating.
The peak power handling of strip-line depends on the maximum voltage that can be applied without causing dielectric breakdown. The maximum peak power P_P is given by [14, 55, 94]:

$$P_P = \frac{V_O^2}{2Z_O}. \tag{3.1}$$

where, Z_O is the characteristic impedance of strip-line and V_O is the maximum voltage that can withstand. The separation between inner to ground conductor can support higher voltage. At atmospheric temperature and pressure, the breakdown strength of air is approximately 3×10^6 V$/m$ or 1.47×10^6 $V_{rf(peak)}/m$ [94]. Thus, the maximum electric field on the surface of the strip conductor should be less than this value.

The average power handling capability (P_{av}) of the strip-line components depend upon the conductivity of the material, transmission losses, and ambient temperature, which is responsible for the rise of temperature in the conductor from T_{amb} to T_{max} and is given by [14, 95, 96]

$$P_{av} = \frac{T_{max} - T_{amb}}{\Delta T} \tag{3.2}$$

T_{max}= Maximum allowable operating temp, T_{amb}= Ambient temperature of medium surrounding the strip-line, ΔT = Rise in temperature of strip line and is given as

$$\Delta T = \frac{b}{k}\left(\frac{\Delta P_c}{W_e} + \frac{\Delta P_d}{2\times W_{eff(f)}}\right)\frac{C}{W} \tag{3.3}$$

where, b is gap between conductor, k is thermal conductivity of air = 0.0286 wm/K, W is the width, t is thickness, ΔP_c and ΔP_d are the dissipation per unit length of the line due to losses in inner conductor and dielectric respectively, Z_o(Impedance of line) = 50 Ω, ε_r (dielectric constant of air) = 1.

$$W_e = \frac{120 \times \pi \times b}{Z_o}, \quad \Delta P_c = 1 - exp(-0.2303 \times \alpha_c)$$

$$\Delta P_d = 1 - exp(-0.2303 \times \alpha_d)$$

where, α_c and α_d are the loss coefficient of conductor and dielectric respectively and are given as,

$$\alpha_c = \frac{0.0231 R_s \varepsilon_r Z_o}{30\pi(b-t)}\left[1 + \frac{2W}{b-t} + \frac{(b+t)Z_o\sqrt{\varepsilon_r}}{(b-t)\pi} ln\left(\frac{2b-t}{t}\right)\right]$$

$$\alpha_d = 27.3\sqrt{\varepsilon_r}\, tan\delta/\lambda_o$$

As, $tan\delta$ (loss tangent of air dielectric) = 0. So, α_d becomes 0. Also, R_s is the sheet resistivity of the conductor and is given as $R_s = \sqrt{\pi f \mu_o/\sigma}$ Ω/m, σ (conductivity of copper) = $1/(1.68 \times 10^{-8})$. By substituting above values, we can get a rise in temperature ΔT. The maximum allowable operating temperature of a strip-line circuit to be the one in which its electrical and physical characteristics within the acceptable limits.

3.3. High Power RF Components

3.3.1. TANDEM HYBRID COUPLER

The 3dB hybrid coupler [50] is an important component of the ICRH system. It divides the RF power coming from the RF source to feed the two RF antennae inside the Tokamak [51-56]. It also provides the essential protection to the RF generator by coupling the reflected power at the matched terminating isolated port. In case both the antennae interface pass through a similar mismatch condition, the total reflected power is being coupled to isolated port. A 3dB tandem

hybrid coupler has been developed by considering the high-power application. The place of the hybrid coupler is mentioned in Figure 3.1 as 2.

3.3.1.1. Concept, design and simulation

A single 3dB coupled line section provides narrow coupling gap which limits the power handling capability of the coupler. To achieve the higher power handling capability, two 8.34dB TEM broadside coupled strip-line sections in tandem are chosen to get the overall 3dB coupling. Schematic of the 3dB tandem hybrid coupler is shown in Figure 3.2. In case, RF input is given at port-1 that is to be equally divided between port-2 and port-3 with 90^0 phase difference, whereas port-4 is isolated. It is a symmetrical device in which any one of the ports can be taken as an input port.

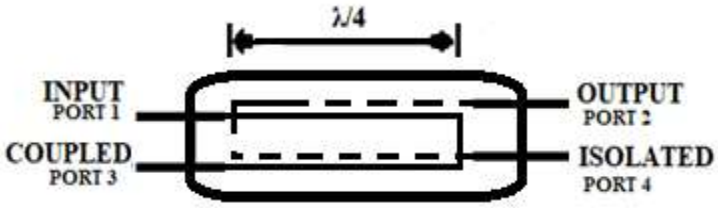

Figure 3.2: Schematic of the 3 dB tandem hybrid coupler.

The detailed drawing of the designed hybrid coupler is shown in Figure 3.3. The two identical U-shaped copper strip-lines with opposite faces are hanged to overlap and separated by a calculated coupling gap to form the assembly of tandem coupler. The hanging of U-strip is supported by Teflon studs with outer metallic enclosure. The assembly of 3dB hybrid coupler consists of two 8.34dB coupled line sections and a non-coupled connecting patch. The length of coupled line section is taken as λ/4 whereas non-coupled section is optimized with short length i.e. λ/40 at the operating frequency, 182.5 MHz. A coupling gap of 8.34dB coupled line section is selected in such a way that it can provide essential breakdown strength at 2kW RF input. Air is used as a dielectric that provides space for heat dissipation and gives better average power handling in continuous wave (CW) application.

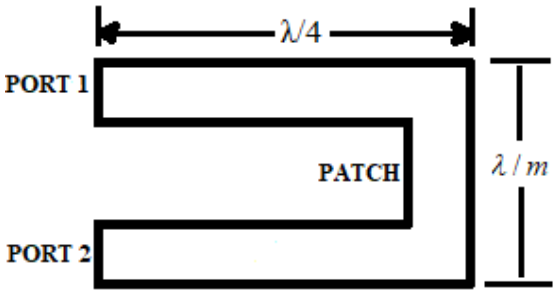

(a) U-shaped Coupled Strip-line

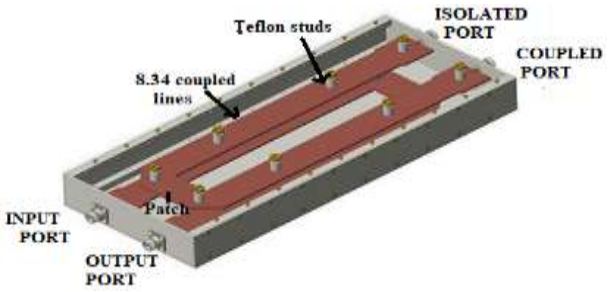

(b) Layout design of the prototype 3dB coupler

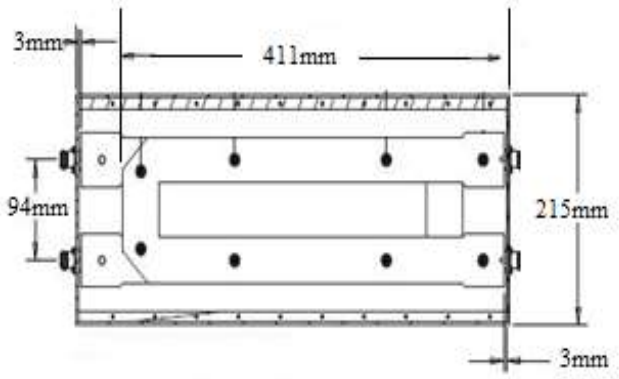

(c) Top view with detailed dimensions

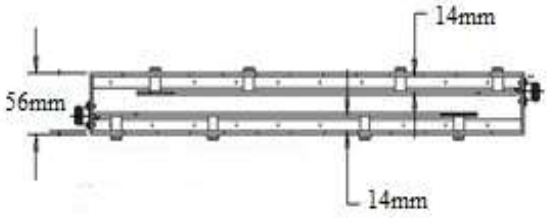

(d) Side view of Assembly drawing

Figure 3: Detailed Assembly drawing of the prototype tandem hybrid coupler ((a) U-shaped Strip-line (b) Layout design (c) Top view (d) Side view of prototype coupler).

The dimensions of strip-line sections are calculated using standard equations [97, 98].

The characteristic impedance (Z_o) of coupled strip-line depends on the amplitudes of even and odd mode impedances $(Z_{oe}\ and\ Z_{oo})$ and given by [99],

$$Z_{oe} = \frac{59.952\pi}{\sqrt{\varepsilon_r}} \frac{K(k')}{K(k)}, \quad Z_{oe} = \frac{94.172\pi\, {}^{d}/_{b}}{\sqrt{\varepsilon_r tanh^{-1}(k)}} \tag{3.4}$$

Where $k' = \sqrt{1-k^2}$, $K(k')and\ K(k)$are the complete elliptic integrals of first kind which are mentioned as [100],

$$k = \left[1 - \left[\frac{0.5\exp^{\pi\frac{K(k)}{K(k')}} - 1}{0.5\exp^{\pi\frac{K(k)}{K(k')}} + 1}\right]^4\right]^{1/2} \qquad and$$

$$\frac{w}{b} = \frac{2}{\pi}\left[tanh^{-1}\sqrt{\frac{k-\frac{d}{b}}{1-k-\frac{d}{b}}} - \left(\frac{d}{b}\right)tan^{-1}\sqrt{\frac{k-\frac{d}{b}}{k\left(1-k-\frac{d}{b}\right)}}\right] \quad (3.5)$$

Here w, b, d, t and ε_r represents strip width, total height of the conductor box, coupling gap, inner strip thickness and relative permittivity of medium respectively.

For finite value of coupling coefficient c, $Z_{oe} \neq Z_{oo}$ are limited by the overall characteristic impedance(Z_o), where

$$Z_o = \sqrt{(Z_{oe} \times Z_{oo})} \quad (3.6)$$

The coupling coefficient (c) is defined as,

$$c = \frac{Z_{oe} - Z_{oo}}{Z_{oe} + Z_{oo}}. \quad (3.7)$$

The coupling coefficient, c for 8.34dB coupled lines corresponds to 0.3828 in linear scale. $Z_{oe} = 78.84\Omega$ and $Z_{oo} = 22.23\Omega$ has been calculated for coupling coefficient c = 0.3828 using equation (3.6 and 3.7). The dimensions of strip line for given impedances are shown in Figure 3.4 (a) with its perspective annotations. The non-coupled 50Ω patch section has been optimized and the resulting dimensions of the patch are given in Figure 3.4 (b)

(a) Dimensions of 8.34dB coupled line **(b) Dimensions of Patch section**

Figure 3.4: Dimensions of (a) Coupled line and (b) Patch section.

The designed model of hybrid coupler has been simulated and optimized in 3D Electromagnetic simulation software, CST. The simulation outcomes are shown in Figure 3.5. The Figure 3.5 (a), (b), (c) and (d) present the coupling S_{31}, output S_{21}, return loss S_{11} and isolation S_{41} parameters of the hybrid coupler respectively. The coupling and output parameters are found as, -3.001dB and -3.031dB at the center frequency, 182.5 MHz and these are found under -3 ± 0.3 dB in an entire

frequency band of 155-225MHz. The return loss and isolation are found as -39 dB and -37 dB respectively, at center frequency and found better than -30dB in an overall band.

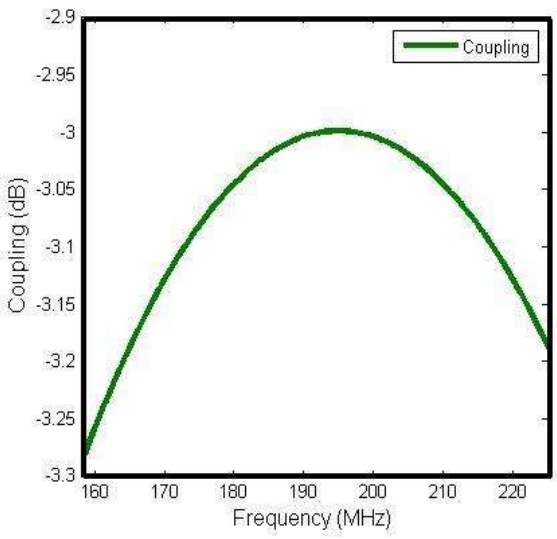

(a) Simulated Coupling in dB

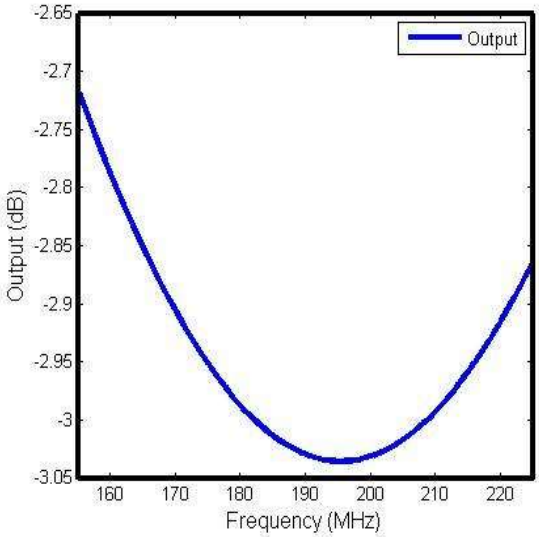

(b) Simulated Output in dB

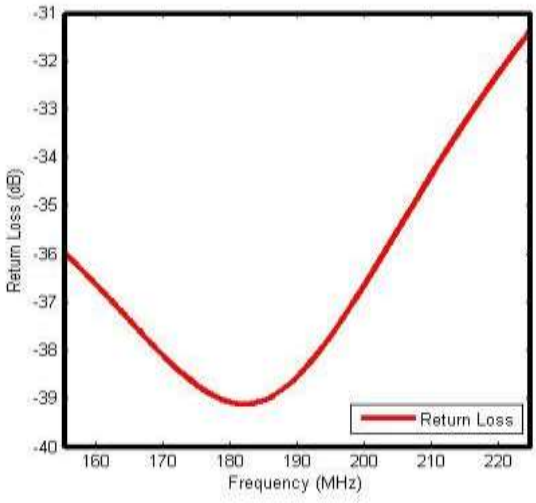

(c) Simulated Return Loss in dB.

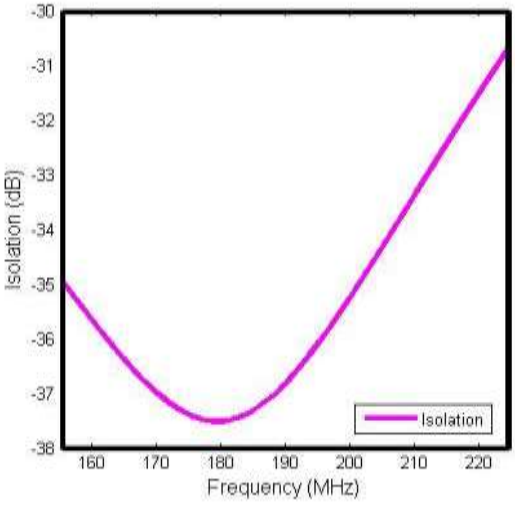

(d) Simulated Isolation in dB.

Figure 3.5: Simulated S-parameters using CST software ((a) Coupling, (b) Output, (C) Return Loss and (d) Isolation) in dB.

The electric field distribution inside the designed hybrid coupler is analyzed at 2kW RF input using CST simulation. Simulation outcome is shown in Figure 3.6. Here, the maximum electric field is found to be $6.6 \times 10^4\ V/m$ below the breakdown strength. The peak power handling capability depends on various losses and the maximum value of an applied electric field. To prevent the

electric breakdown, maximum applied electric field should be under the limit of $1.47 \times 10^6\ V/m$ [94, 98]. In simulation result, the maximum electric field is found significantly less than the breakdown limit which verifies the power handling capability of the coupler i.e. 2kW.

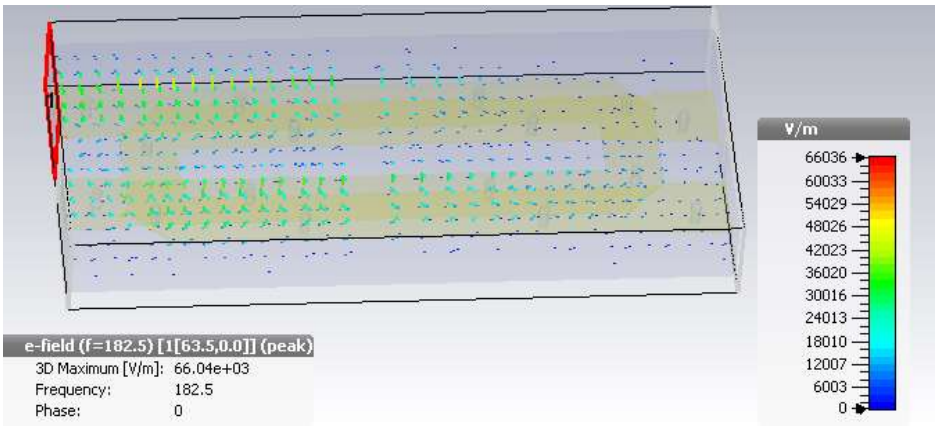

Figure 3.6: Electric field plot of tandem hybrid coupler.

3.3.1.2. Fabrication and Test results

A photograph of the fabricated hybrid coupler is shown in Figure 3.7. The fabricated hybrid coupler is having two U-shaped copper strip each of 3mm thickness. The outer rectangular box with dimensions $51.7 \times 21.5 \times 5\ cm^3$ is designed with 3mm thick aluminum sheet where air is used as a dielectric. Teflon studs are used for the insulation of U-shaped copper strips and also to provide support for the strip-line in a metallic enclosure. Coaxial N-type connectors are applied for input/output terminals which can withstand high voltage.

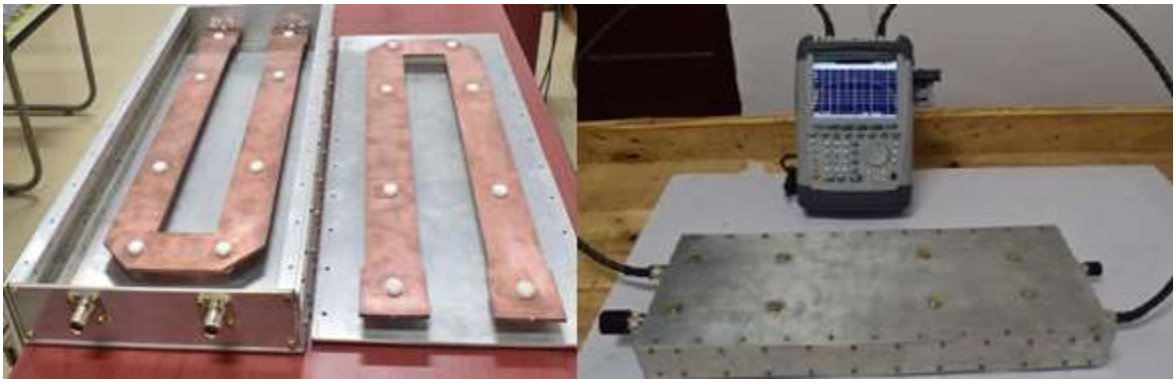

Figure 3.7: Fabricated design of tandem hybrid coupler.

The fabricated hybrid coupler is tested using a two ports Vector Network Analyzer (VNA). The prospective comparison of simulation and experimental results are shown in Figure 3.8, where Figure 3.8(a) shows coupling characteristic, Figure 3.8(b) shows the output, Figure 3.8(c) shows

return loss and Figure 3.8(d) shows isolation characteristics of the hybrid coupler. In simulation results, the coupling and output parameters are found as -3.001dB and -3.031dB respectively at the center frequency, 182.5MHz, whereas the experimental results provide the coupling and output -2.96dB and -3.14dB respectively. The comparison shows that the test results are found in close agreement with the simulation results. In given comparison, the coupling in test result is found slightly greater than simulation outcome. These differences are found -3.001dB and -2.96dB in coupling, whereas -3.031dB and -3.14dB in output, which can be due to the fabrication and material tolerances such as Teflon studs and heavy weight of copper strip-line. The weight of copper strip-lines also result in very small sagging when hanged over metallic enclosure using Teflon studs. The sagging introduces decrease in distance between the strip-line. As the coupling coefficient is inversely proportional to the distance between the strip-line. These constraints result in small differences between simulation and test results which is acceptable. The developed coupler found providing coupling of -3 ± 0.3 dB, return loss better than -25dB and isolation better than -32dB for the full frequency range of 155-225MHz. Also, Figure 3.8(c) and Figure 3.8(d) shows return loss and isolation characteristics respectively. The simulated return loss found better than -30dB i.e. 0.1% loss of total power, whereas the return loss from test results comes out to be better than -25dB i.e. 0.3% loss for the full frequency range of 155-225 MHz, which are in good agreement with the simulated results.

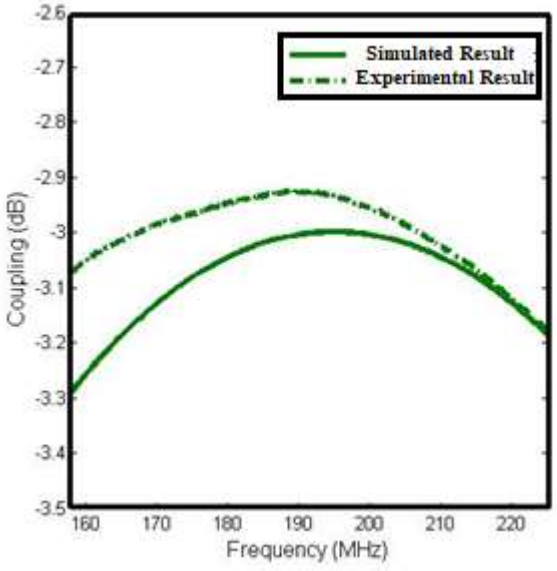

(a) Coupling in dB

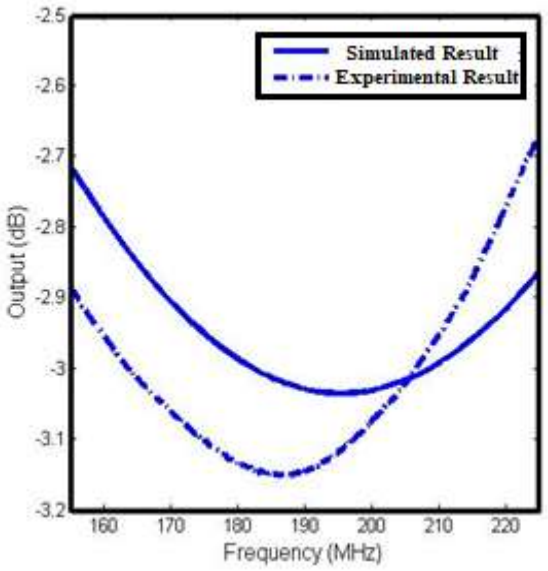

(b) Output in dB

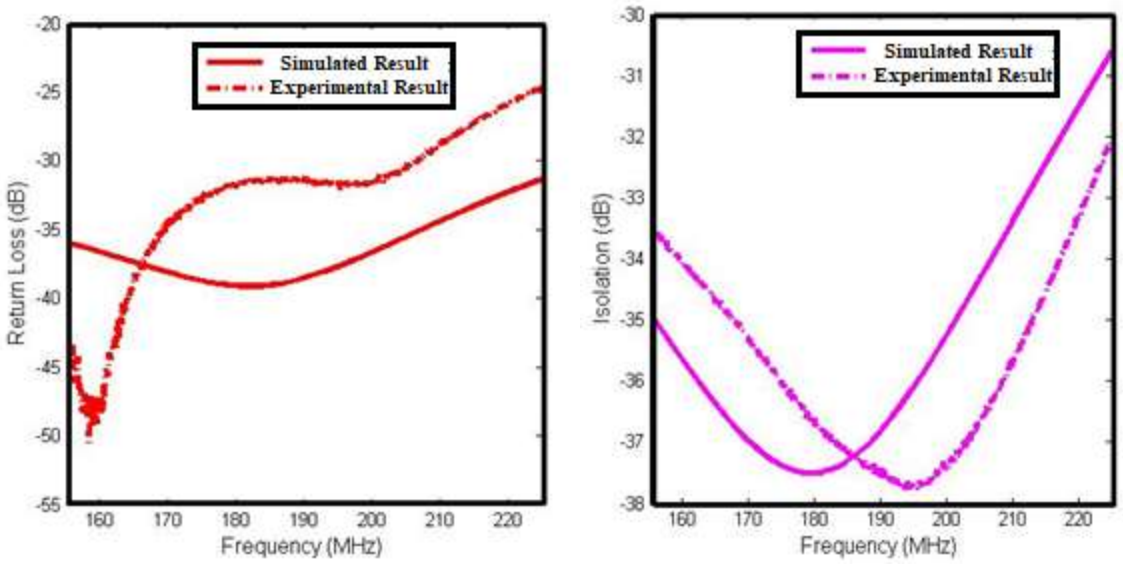

(c) Return Loss in dB **(d) Isolation in dB**

Figure 3.8: Measured S-parameters for fabricated coupler using VNA ((a) coupling, (b) output, (C) return loss and (d) isolation).

3.3.2. VARIABLE DUAL DIRECTIONAL COUPLER

The variable directional coupler [57, 58] is a passive RF component of the RF system. It couples the forward and reflected power in RF system [59-70, 102-107]. In an RF matching network, the magnitude and phase of the forward and reflected power are measured to analyze the standing wave ratio, which has to be ideally in the range of 1-2 for the matched RF system. In high power ICRH system, the forward propagating power is much more prominent as compared to the reflected power. Therefore, power in each direction should be coupled with different coupling magnitude. The development of dual directional coupler is inevitable. An automated RF matching network is proposed under the thesis, where we have to work on the development of computer programs for the matching of variable unknown loads. The initial establishment of the system would be passed through the numerous calibration where the coupling of forward and reflected power with different magnitude is required. A rigid coaxial line based variable loop type dual directional coupler has been developed. The developed coupler is to be utilized for calibration of the proposed system.

3.3.2.1. Theory of dual directional coupler

Schematic of a loop type directional coupler is shown in Figure 3.9, where a U-shaped coupling loop is incorporated inside rigid coaxial line. Coupling loop intercepts over main line with length, *L* and coupling gap *x*, another symbol references are described as follows,

D represents the gap between inner and outer conductor,

W, *L*, and *t* are the width, length, and thickness of the coupled lines respectively,

C_{11}, C_{22} are the self-capacitance between coupled loop element and inner coaxial conductor in ground reference,

C_{12}, C_{21} represent mutual capacitance between the loop element and the inner conductor of a coaxial line, whereas Z_{oe} and $Z_{oo}$are the even and odd mode characteristic impedance.

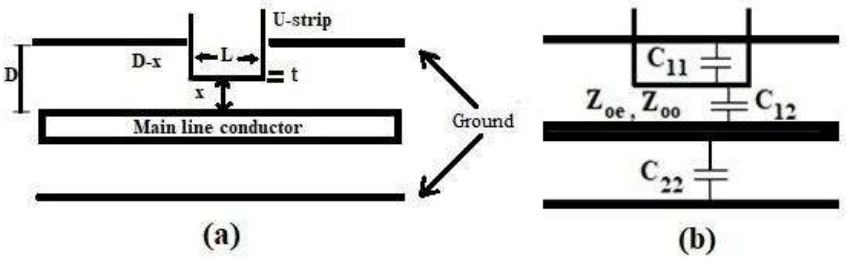

Figure 3.9: Loop type coupler (a) Schematic, (b) Equivalent Circuit

The main coaxial transmission line is designed for 50 Ω characteristic impedance, where inner to outer dimensions are calculated using standard equations [96]

$$Z_o = \frac{60}{\sqrt{\varepsilon_r}} ln\ \frac{b}{a}\ \ , \varepsilon_r = 1 \tag{3.8}$$

Where, a and *b* are the inner and outer radius of the coaxial line.

The coupling between two coupled elements is mainly function parameters, coupling length ($\theta = \beta L$), the separation between two conductors (coupling gap), *x* and even and odd mode impedances Z_{oe} and Z_{oo}. The coupling coefficient of the coupled line, *C* is given by

$$C = \frac{Z_{oe}-Z_{oo}}{Z_{oe}+Z_{oo}}, \tag{3.9}$$

Whereas

$$Z_{oe} = \frac{1}{v_P C_e}; \quad Z_{oo} = \frac{1}{v_P C_o}. \tag{3.10}$$

Here, v_P is phase velocity of wave, ε_r= 1 is the relative permittivity for air dielectric, and C_e and C_o are even and odd mode capacitance which are mentioned as,

$$C_e = C_{11} = \frac{2\varepsilon_r W}{D-x} \tag{3.11}$$

$$C_0 = C_{11} + 2C_{21} = \frac{2\varepsilon_r W}{D-x} + \frac{2W\varepsilon_r}{x} \tag{3.12}$$

From equation (3.10), (3.11), (3.12) and (3.9), Z_{oe} and Z_{oo} are derived as,

$$Z_{oe} = \frac{D-x}{2W\varepsilon_r}\ , Z_{oo} = \frac{(D-x)x}{(2W\varepsilon_r D)} \tag{3.13}$$

Where coupling coefficient,

$$C = \frac{Z_{oe}-Z_{oo}}{Z_{oe}+Z_{oo}} = \frac{D-x}{D+x} \tag{3.14}$$

Here, coupling coefficient is proportional to coupling gap. The derived coupling coefficient is utilized to get voltage coupling, [97]

$$\frac{V_3}{V_1} = jC\ sin\ \theta\ e^{-j\theta} = \frac{D-x}{D+x} sin\left(\frac{2\pi fL}{c}\right) e^{-j\theta}. \tag{3.15}$$

The coupling characteristic of directional coupler is derived as a function of electrical length, (θ), operating frequency, f and physical length, L ($\theta = \beta L$, $\theta = ((2\pi f L)/c)$). This means, the desired coupling response can be obtained by having the desired value of these parameters. The coupling response gets flat, if the physical size of the loop is very small as compared to the wavelength. In particular, physical size of the loop is taken as approximately $\lambda/40$. The coupling performance is being analyzed and shown in Figures 3.10, 3.11 and 3.12. The Figure 3.10 shows coupling response with variable coupling gap, x (3.5 to 11.5) and frequency, f (50 to 500 MHz). Figure 3.11, shows coupling response for variable length, L (26-42mm) with frequency (50 to 500 MHz) with x=3.5, whereas Figure 3.12, shows coupling response for variable length, L (26-42mm) with frequency (50 to 500 MHz) with x=11.5. It can be observed that a variable coupling response, −35 to −10 dB can be obtained by selecting the proper values of, L and x.

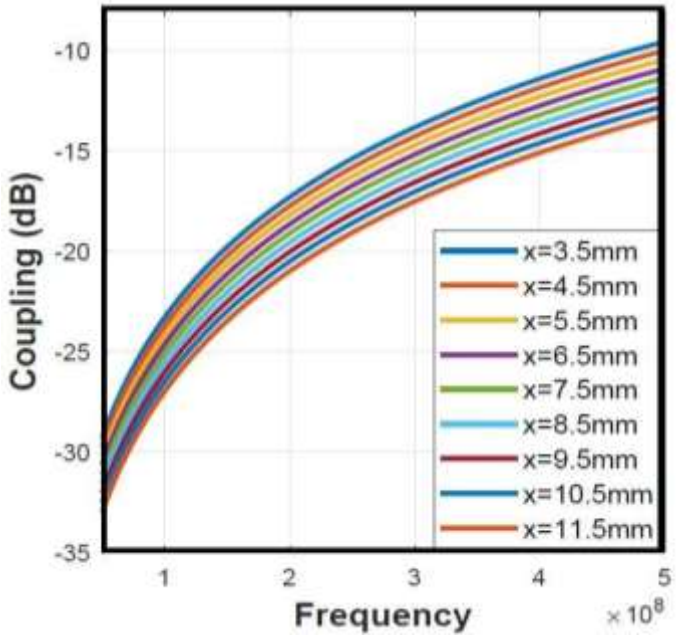

Figure 3.10: Coupling characteristics with variable coupling gap (x) at constant length (L), 40 mm.

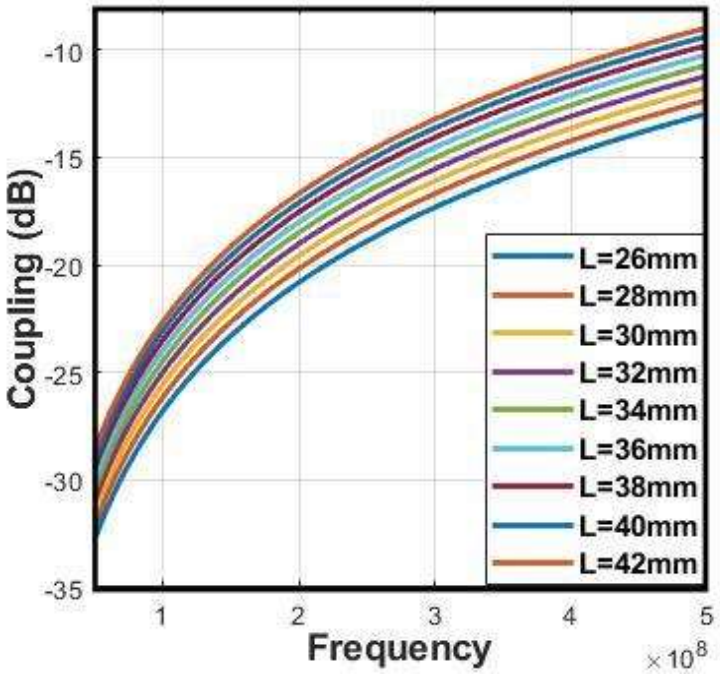

Figure 3.11: Coupling Characteristic with variable length (L) at constant coupling gap (x), 3.5 mm.

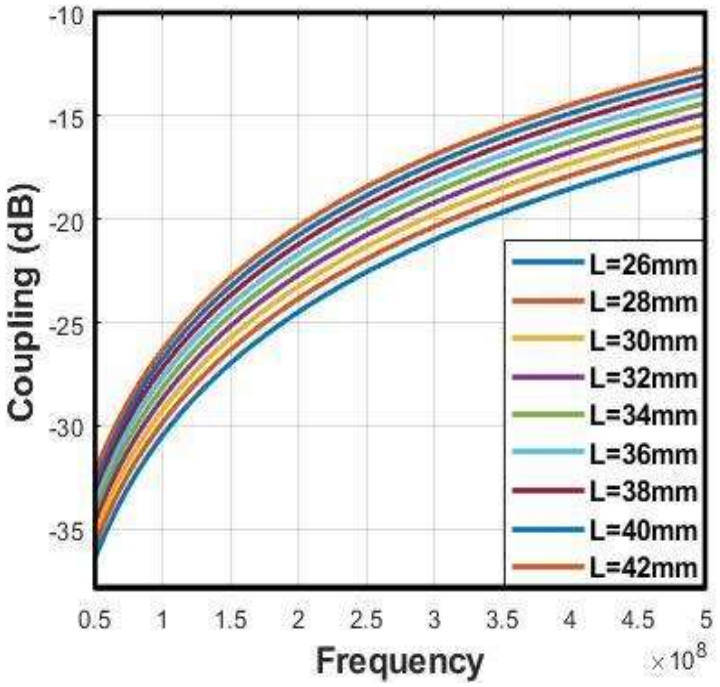

Figure 3.12: Coupling characteristics with variable length (L) at constant coupling gap (x), 11.5 mm.

3.3.2.2. Sensitivity Analysis

The sensitivity of the directional coupler defines as the robustness of design for manufacturing or assembly tolerances. The sensitivity as a function of even and odd mode impedances is written as [101]

$$S_{Z_{oe}}^{C} = -S_{Z_{oo}}^{C} = \frac{1 - C^2}{2C} \tag{3.16}$$

Equation (3.16) is also known as closed form expression, where $S_{Z_{oe}}^{C}$ and $S_{Z_{oo}}^{C}$ represent the coupling sensitivity in even and odd mode, respectively. By substituting the value of *C* in equation (3.16), we get,

$$S_{Z_{oe}}^{C} = -S_{Z_{oo}}^{C} = \frac{2 \times Z_{oe} \times Z_{oo}}{(Z_{oe}^2 - Z_{oo}^2)} \tag{3.17}$$

The overall sensitivity of directional coupler represents the fractional change of coupling coefficient, $\Delta C_{max}/C$. The $\Delta C_{max}/C$ is evaluated from equation (3.17) which is given by

$$\frac{(\Delta C)_{max}}{C} = \left|\frac{\Delta Z_{oe}}{Z_{oe}} S_{Z_{oe}}^{C}\right| + \left|\frac{\Delta Z_{oo}}{Z_{oo}} S_{Z_{oo}}^{C}\right| \tag{3.18}$$

Equation (3.18) defines the overall sensitivity. Figure 3.13 shows the plot of sensitivity with respect to the coupling coefficient. Ideally, coupler should be insensitive to the small changes in the value of coupling coefficient. In particular, a very insignificant variation is observed in sensitivity (0.05–0.095) as coupling coefficient varied (0–1), which is desirable for our design in reference to the robustness.

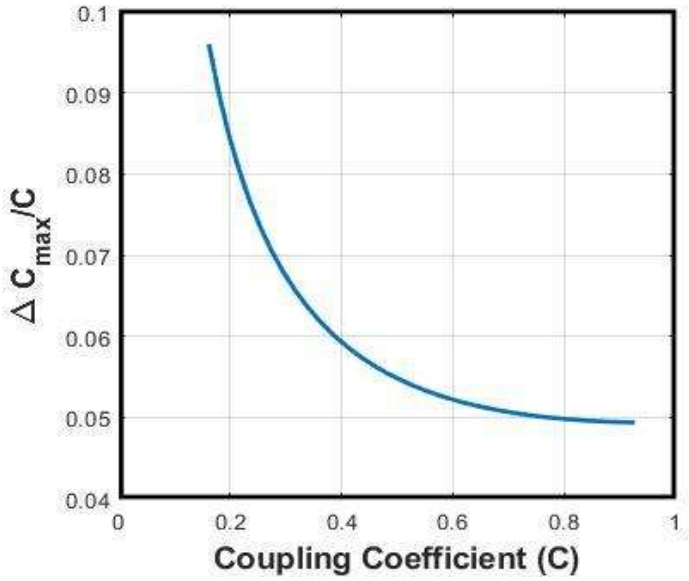

Figure 3.13: Sensitivity plot with respect to coupling coefficient.

3.3.2.3. Design and Simulation

The assembly drawing of the proposed coupler is shown in Figure 3.14. Aluminum is used as a conductive material for the fabrication of inner and outer conductors due to the weight concern. The coaxial N-type connectors are attached for RF input and output. Any one of two N-type connector ports can be used for input/output, whereas other four BNC connectors can be utilized as coupling ports. The two variable rectangular coupling arrangement made up with copper is used for forward and reflected power. The magnitude of the coupling is <−10 dB in throughout the band. Therefore, Bayonet Neill-Concelman (BNC) connectors have been used to conduct this low power. The coupler design is incorporated with four ports for forward and reflected power coupling. Any of two nearby ports of coupling arrangements are needed to be matched terminated for the measurement of forward and reflected power and to avoid multiple reflections. The coupling arrangement is designed with a compact size so that multi-octave bandwidth can be achieved without having any significant deterioration in performance at the higher end of the frequency band.

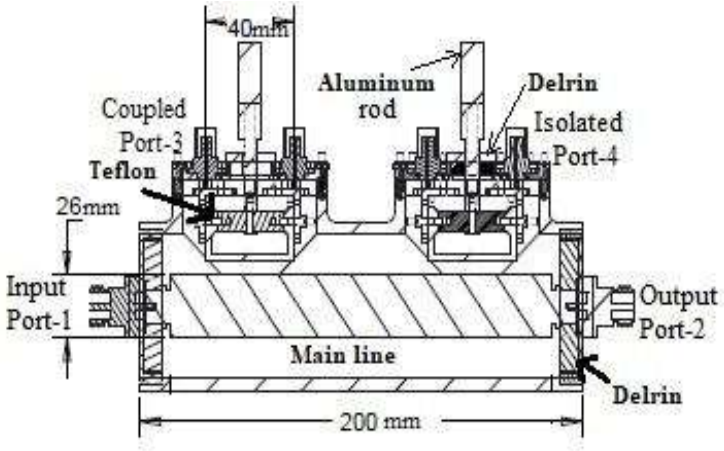

Figure 3.14: Assembly drawing of the directional coupler.

These coupling arrangements are incorporated with the movable tap that moves the inner coupling loops upward and downward direction and provides reasonable variable coupling. The rods consist of eight threads, each of 1 mm which can make eight rotations. Delrin (ε_r = 3.7) is used for support and insulation purpose inside the assembly. The volume of dielectric material has been minimized to avoid the discontinuity and the shape of the transmission structure is modified accordingly to get the proper matching for optimum performance. The dimensions of directional coupler are optimized using 3D EM simulation software, CST and are described as, inner and outer

diameter of the main coaxial line is 26mm and 60mm respectively, the length of the main line is 200mm, $l \times b \times h$ of rectangular strip is $40 \times 8 \times 3$. The designed model of the coupler has been simulated using CST microwave studio software.

Simulation results in terms of S-parameter is shown in Figures 3.15, 3.16 and 3.17. Figure 3.15 shows the coupling response with variable coupling gap, x (3.5 to 11.5), where the coupling varies from -12 to -37 dB in prescribed frequency, f (50 to 500 MHz). Figure 3.16 shows the isolation characteristic for variable, x (3.5 to 11.5). The isolation is found better than -21dB in prescribed frequency, f (50 to 500 MHz). Figure 3.17 presents the output S_{21} and return loss S_{11} parameters, which are found variable, 0.0 to − 0.8 dB and -42dB to -30dB respectively in the prescribed frequency band. The designed coupler is providing desired results in simulation. It can be fixed at any value of coupling within -12 to -37dB in in frequency band 50-500 MHz.

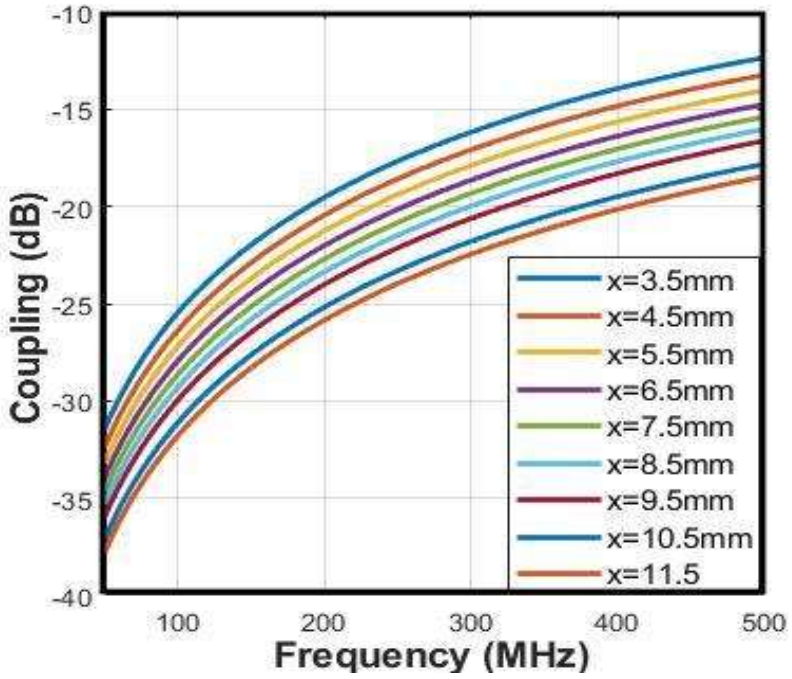

Figure 3.15: Simulation result presents the coupling for different coupling gap (x).

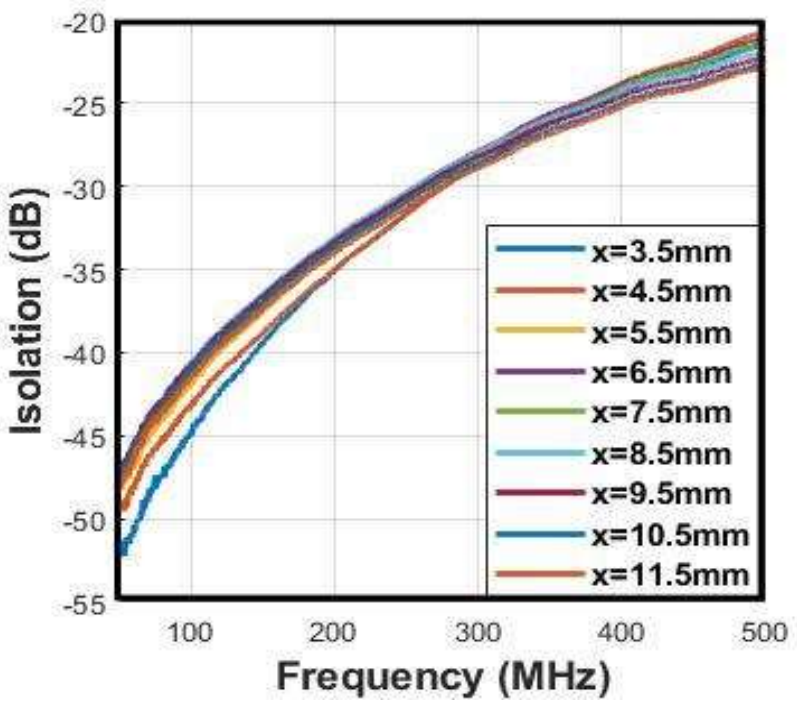

Figure 3.16: Simulation result present the isolation for different coupling gap (x).

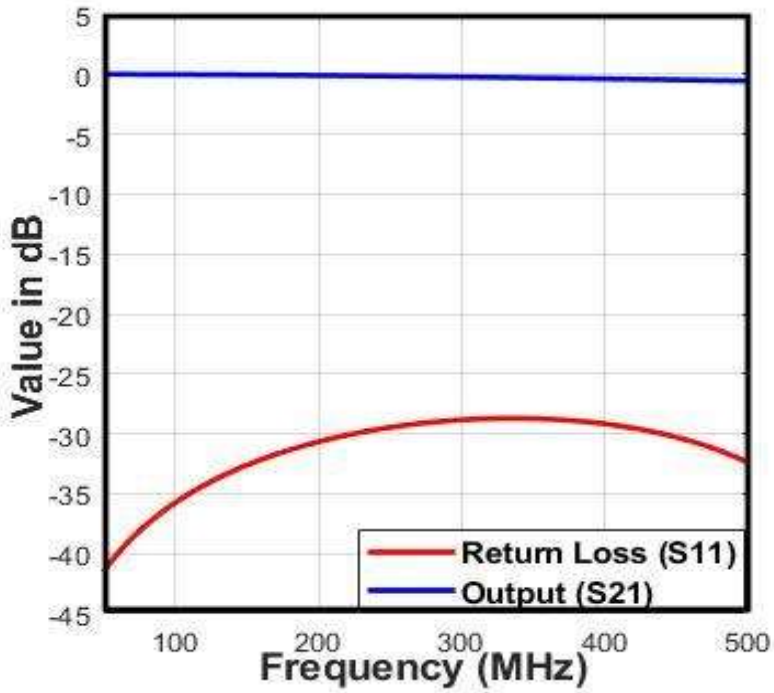

Figure 3.17: Simulation results present return loss and output in dB.

Figure 3.18 shows the electric field mapping inside directional coupler. Its maximum value is found 1.59×10^5 V/m at 2kW input, which is comparatively very less than the rated breakdown

strength of 1.47×10^6 V/m [14, 94] as discussed in section 3.2. As per our analysis at 2kW CW RF input, 8.6°C temperature rise is estimated from ambient (25°C) inside coupler and equilibrium will be attained afterward with natural cooling. Therefore, coupler design is estimated for 2kW power handling capability.

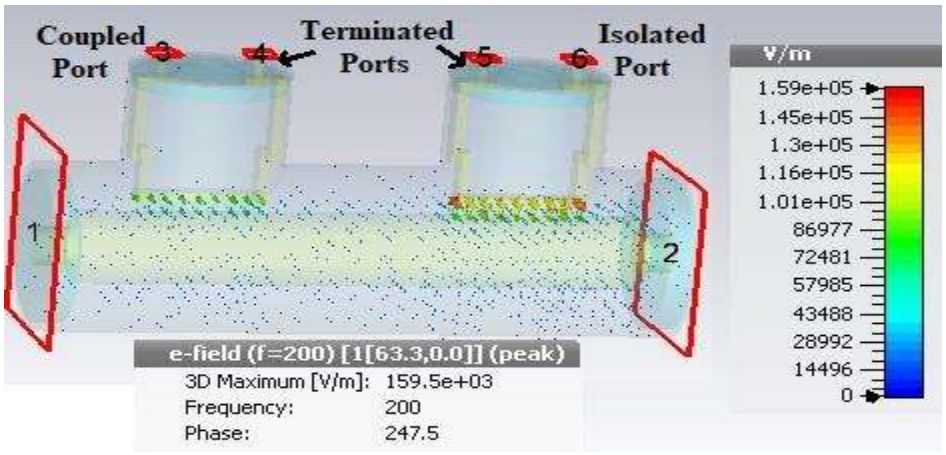

Figure 3.18: Electric field plot of dual-directional coupler.

3.3.2.4. Fabrication and Test results

A photograph of the fabricated dual-directional coupler is shown in Figure 3.19. The inner and outer conductors are separated with the delrin ring that provides needful insulation. The rest of the space between the inner to outer is filled with air. The U-shaped rectangular copper strips are hanged over the inner conductor and supported by the Teflon rod. These strips are connected to a rotating shaft that provides the linear sliding motion to the U-strip. The resulting motion provides the variable coupling gap.

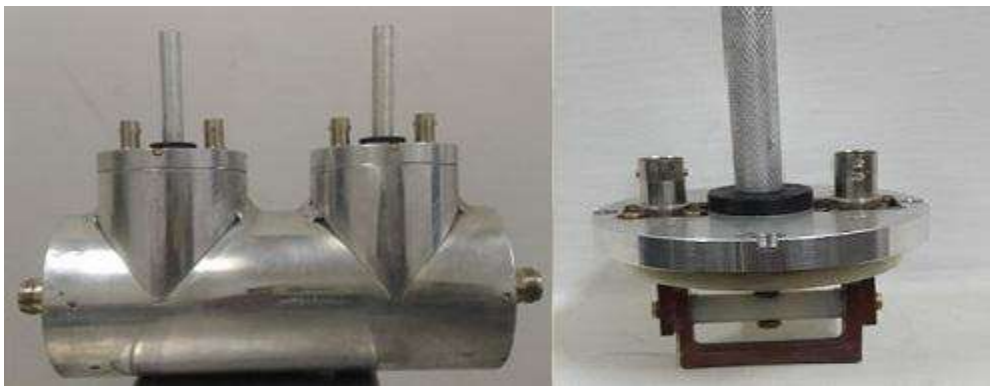

Figure 3.19: Photograph of the fabricated dual-directional coupler.

Coaxial N-type connectors are applied to input and output terminals which can handle the rated power, whereas BNC connectors are applied to the coupling ports. The fabricated hybrid coupler

is tested using two ports of vector network analyzer (VNA). Figure 3.20 shows the coupling response with variable coupling gap, x (3.5 to 11.5), where coupling varies from -10 to -40 dB whereas, Figure 3.21 shows the isolation response with variable coupling gap, x (3.5 to 11.5), where isolation varies from -22 to -55 dB in prescribed frequency, f (50 to 500 MHz).

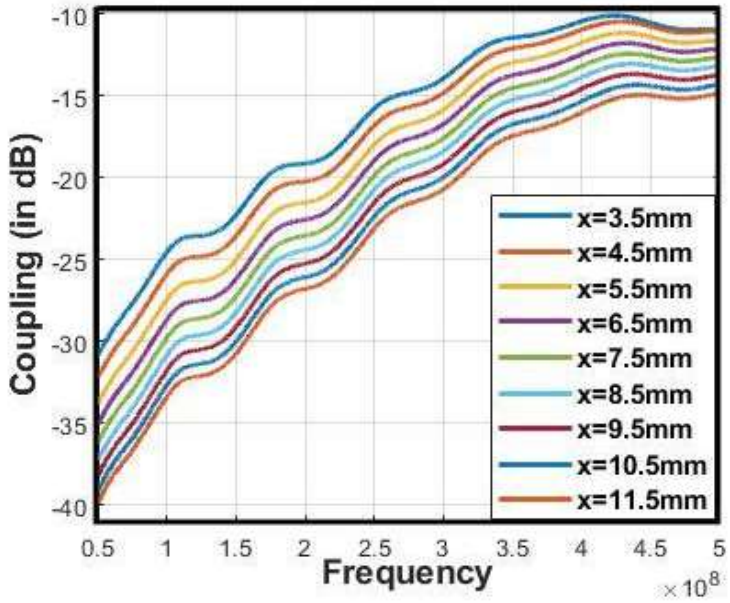

Figure 3.20: Test result presenting coupling characteristics in dB.

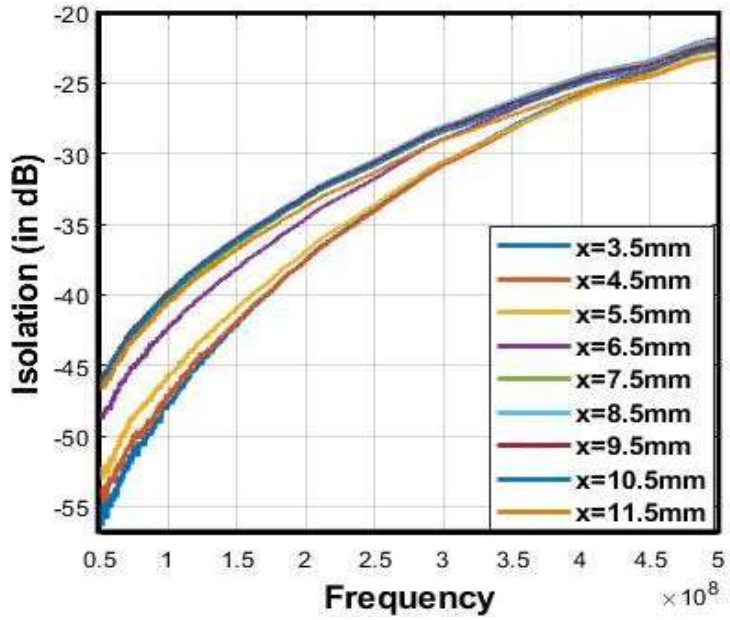

Figure 3.21: Test result presenting isolation characteristics in dB.

The details about the variability in coupling along with isolation performance is shown in Table 1. Prospective comparison of simulation and test results is presented in Figure 3.22, 3.23 and Figure 3.24, respectively, which shows the comparison of coupling, isolation, output and return loss S-parameters. The overall test results are found as per desired where coupling varies from -10 to -40 dB , isolation -21 to -53 dB, output from −0.12 to −1.8 dB, return loss better than −15 dB. The small deviation is observed between the test and simulation results which are found under desired limit. These deviations are found due to the resultant effect of inbuilt transition and sliding contact presents inside the fabricated model.

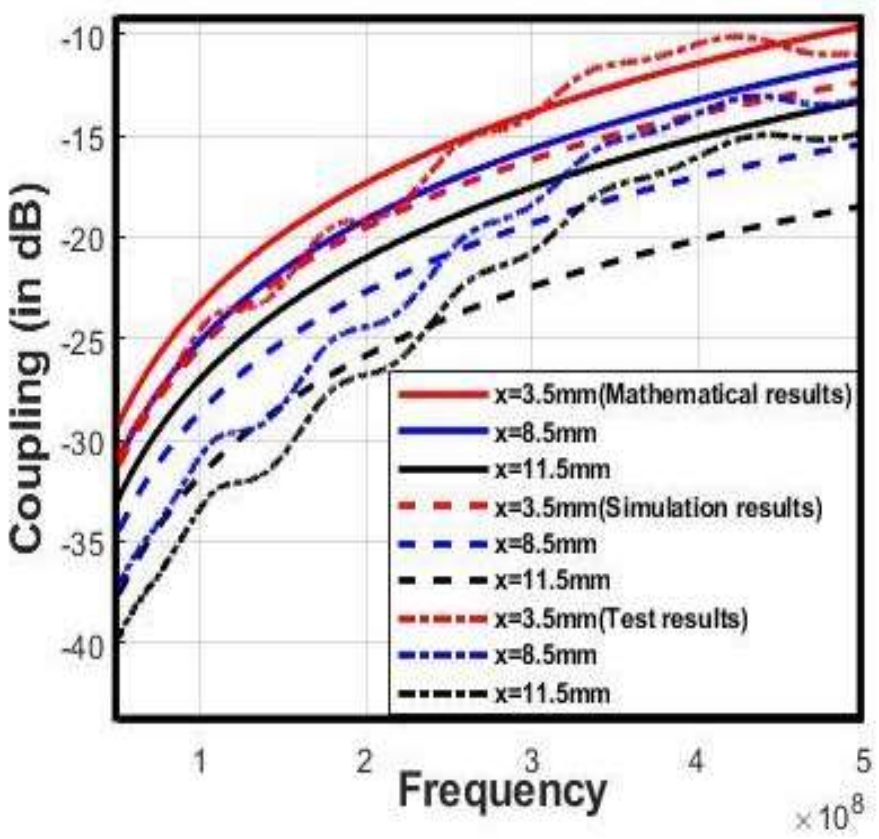

Figure 3.22: Respective comparison between theoretical, simulation and test results of Coupling.

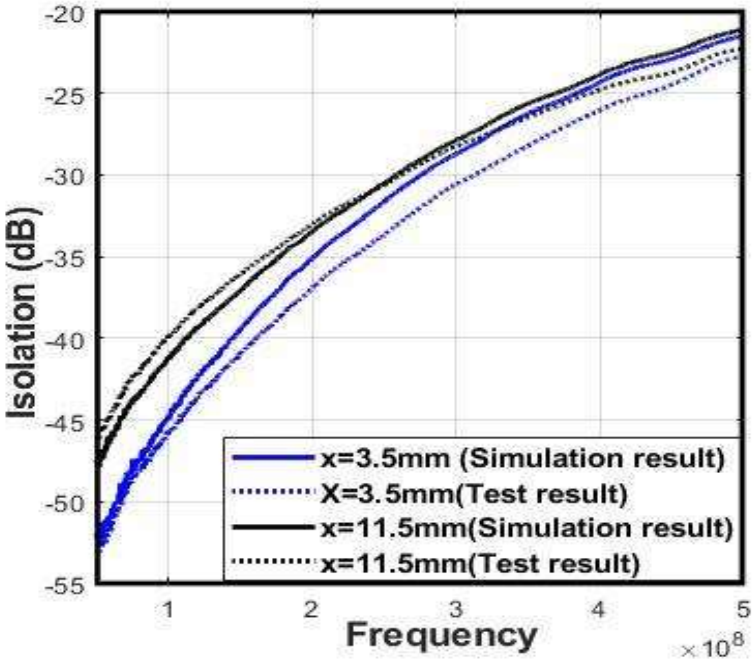

Figure 3.23: Comparison between simulation and test results of isolation.

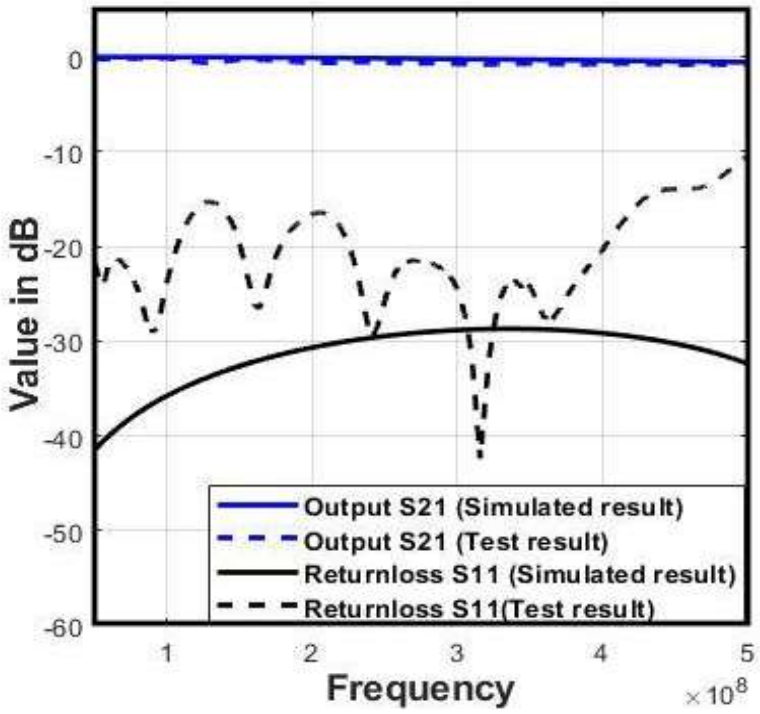

Figure 3.24 Comparison between simulation and test results of output and return loss in dB.

Table 3.1: Value of coupling and isolation for different coupling gap.

Parameter	Variable distance between the two strips, mm	Frequency range, MHz	Typical variation range, dB
Coupling	x=3.5-11.5	50-200	-19 to -39
		200-400	-10 to -26
		400-500	-10 to -16
Isolation	x=3.5-11.5	50-200	-33 to -56
		200-400	-25 to -38
		400-500	-22 to -26

The VSWR measures how effectively RF power is transmitted from input to output port. Directivity and VSWR of directional coupler are correlated parameters which are described as

Directivity (dB) = Isolation (dB) – Coupling (dB).

Based on a given equation, a plot for directivity and VSWR of coupler is shown in figure 3.25. The fabricated variable coupler shows VSWR from 1.15-1.65dB and directivity from −12 to −23 dB in the frequency band 50–500 MHz which are as per desired. Figure 3.26 shows the phase transmission response of the developed coupler. A Table of comparison of coupler characteristics in terms of coupling, power handling capability, directivity, and coupling flatness with earlier works is shown in Table 2. As per the observation, the developed coupler is providing better overall response in comparison to similar work as reported earlier.

The CWRF power test also has been conducted to test the average power handling capability, where 36 W is given as input at 200 MHz. The schematic of high power set-up is shown in Figure 3.27. The resulting peak voltages at the input, output, coupled, and isolated ports captured using oscilloscope are shown in Table 3 which are found in agreement to the VNA outcomes.

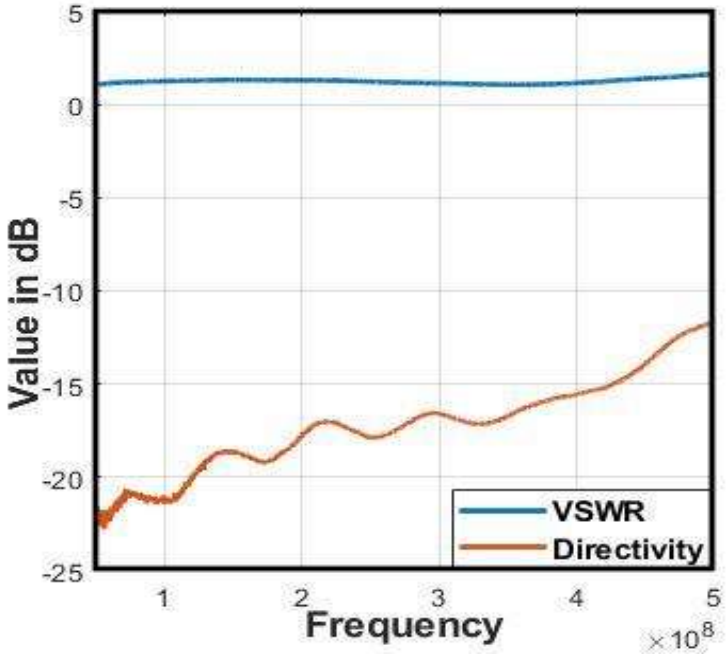

Figure 3.25 Test result present VSWR and directivity in dB.

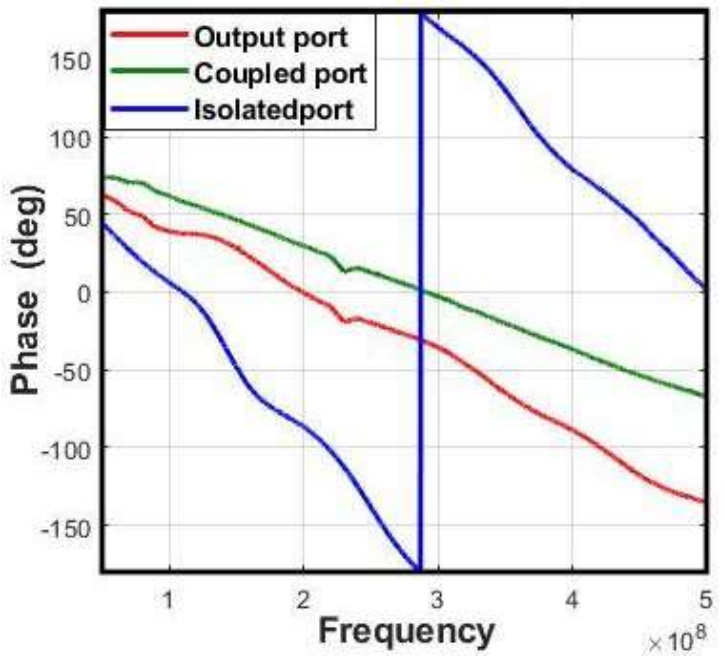

Figure 3.26: Phase response of direction coupler.

Table 3.2: Quantitative comparison between the presented design and other similar designs.

Sr. No.	Reference	Frequency Range	Coupling, dB	Band width	Coupling flatness	Type of Coupling	Rated Power	Directivity
1.	[102]	2.1-3.1Ghz	1.4-7.1	1.476	3.86	Variable	Very low	-
2.	[65]	1.6-2.4GHz	2-20	1.50	12	Variable	Low	-
3.	[103]	2.7-5.3GHz	4-20	1.96	8.16	Variable	Low	16-29dB
4.	[104]	0.1-500MHz	20	-	-	Fixed	200W	20dB
5.	[105]	10-2000MHz	30	-	-	Fixed	75W	18dB
6.	[106]	30-512MHz	10	-	-	Fixed	50W	13dB
7.	[107]	60-345MHz	1-50	5.75	8.52	Variable	1kW	-
8.	Presented design	50-500MHz	10-40	10	3	Variable	2kW	12-23dB

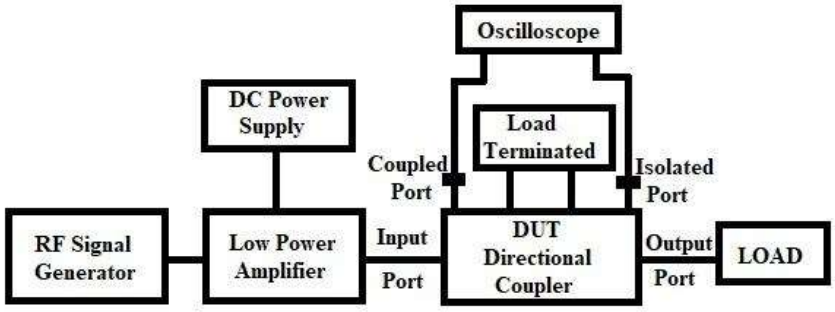

Figure 3.27: Schematic representation of high power test set-up.

Table 3.3: High power measurement

Input, V	Output, V	Coupling, V	Isolation, V
6	5.6	0.61	0.039

3.3.3. 20dB DIRECTIONAL COUPLER

The directional couplers with fix coupling magnitude are proposed to be utilized under a mock-up ICRH system to couple the forward and reflected power [59-70, 108-113]. The couplers are placed at position 3 as mentioned in Figure 3.1. The fixed directional coupler is supposed to couple 1% of total RF input power inside the proposed mock-up ICRH system.

A simple 20dB directional coupler along with miniaturization, easy to manufacture design, has been developed for this purpose. It consists of two symmetrical edge coupled lines having an electrical length of λ⁄4 at 182.5MHz. It is about 41 cm, which is very long and very difficult for practical realization. In order to miniaturize the coupler, the length of the coupler is reduced with 90^0 bends. The 90^0 bend in the strip-line generates extra capacitance due to the accumulation of charges at the corner of the bend, which is compensated by chamfering at the corner.

The even and odd mode impedance of edge coupled strip-line are mentioned as follow,

$$Z_{oe} = \frac{30\pi}{\sqrt{\varepsilon_r}} \frac{K(k_{e'})}{K(k_e)}\ ohms\ ,\ \ Z_{oo} = \frac{30\pi}{\sqrt{\varepsilon_r}} \frac{K(k_{o'})}{K(k_o)}\ ohms \tag{3.19}$$

where, $k_{e'} = \sqrt{1 - {k_e}^2}\ ,\ k_e = tanh\ tanh\left(\frac{\pi}{2}.\frac{w}{b}\right).tanh\left(\frac{\pi}{2}.\frac{w+s}{b}\right)$ and

$$k_{o'} = \sqrt{1 - {k_o}^2}\ , k_o = tanh\ tanh\left(\frac{\pi}{2}.\frac{w}{b}\right).Coth\left(\frac{\pi}{2}.\frac{w+s}{b}\right).$$

Here, K is the complete elliptic integrals of the first kind,

ε_r is the relative dielectric constant of the material.

w, b, and s represents the width of strip, total height of the conductor box and the coupling gap.

For calculating w/b and s/b

$$\frac{w}{b} = \frac{2}{\pi} tanh^{-1}\sqrt{k_e k_o} \ \text{ and } \ \frac{s}{b} = \frac{2}{\pi} tanh^{-1}\left(\frac{1-k_o}{1-k_e}\sqrt{\frac{k_e}{k_o}}\right) \tag{3.20}$$

Equations (3.6, 3.7, 3.19 and 3.20) has been utilized for the calculation of coupled strip-line dimensions which is shown in Figure 3.28. For 20dB coupling, Z_{oe} = 55.277Ω and Z_{oo} = 45.227Ω are calculated.

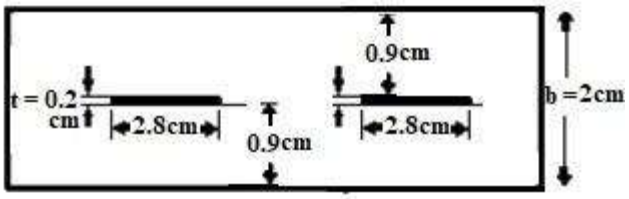

Figure 3.28: Dimension of 20 dB conventional directional coupler.

As per the calculated dimensions, assembly drawing of directional coupler is shown in Figure 3.29, where two similar copper strips are placed in edge coupled configuration and are hanged with Teflon studs through outer ground metallic enclosure. The air act as a dielectric and space between the copper-strips and outer box provides better heat dissipation and average power handling in continuous wave application.

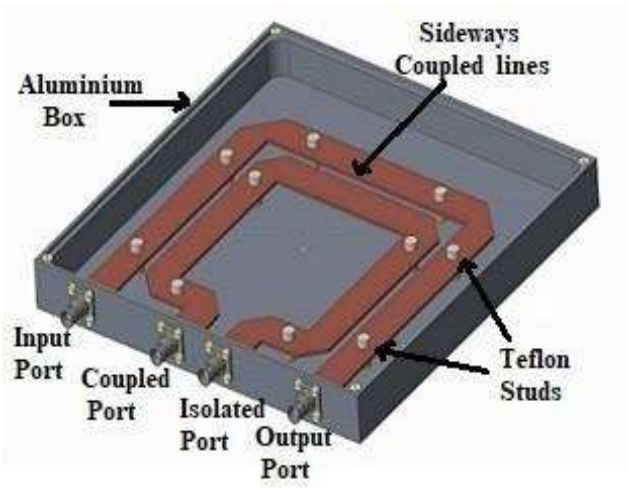

(a) Layout design of prototype 20dB coupler.

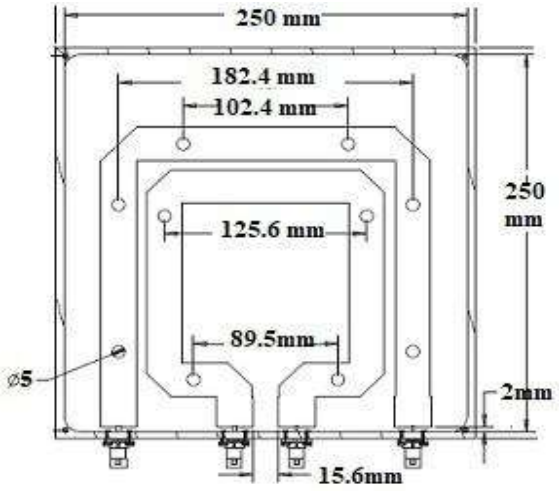

(b) Top view with detailed dimensions.

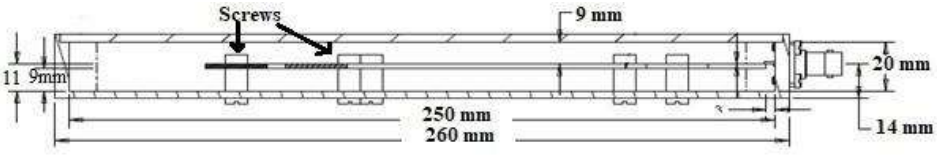

(c) Side view of assembly drawing.

Figure 3.29: Detailed Assembly drawing ((a) Layout design (b) Top view (c) Side view of 20dB coupler)

3.3.3.1. Fabrication and Test results

Photograph of fabricated directional coupler is shown in Figure 3.30. The rectangular box is made of aluminum metal using a die casting process. The thickness of the box is 3mm and having dimensions of 250 × 250 × 20 mm^3. The design consists of two copper strips each of 2 mm thickness arranged in edge coupled configuration to provide the needful coupling. The copper

strips are hanged using Teflon studs inside a rectangular box and the space is filled with air as dielectric. The N-type coaxial connectors are connected at all ports of the device.

Figure 3.30: Photograph of fabricated directional coupler.

Fabricated coupler is tested with two-port handheld Vector Network Analyzer (VNA). The obtained test results are shown in Figure 3.31 in prospective comparison with simulation results. The fabricated coupler provides excellent coupling flatness of -20 ± 0.3dB in full frequency band of 140-200MHz, whereas the obtained return loss and isolation are better than -30dB and -36dB, respectively. The overall directivity found to be more than 16.5 dB in frequency band 140-200MHz. The overall test results are found in close agreement to simulation results. For more comprehensive analysis, a table of comparison is also shown in Table 3.4, which compares the key parameters of the coupler with earlier work.

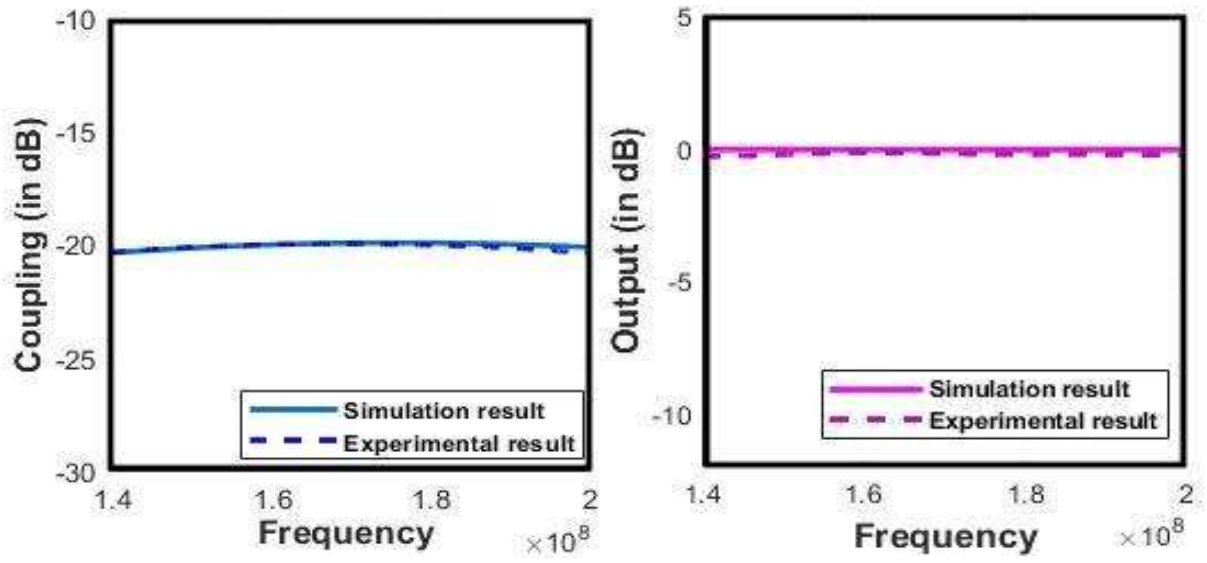

(a) **(b)**

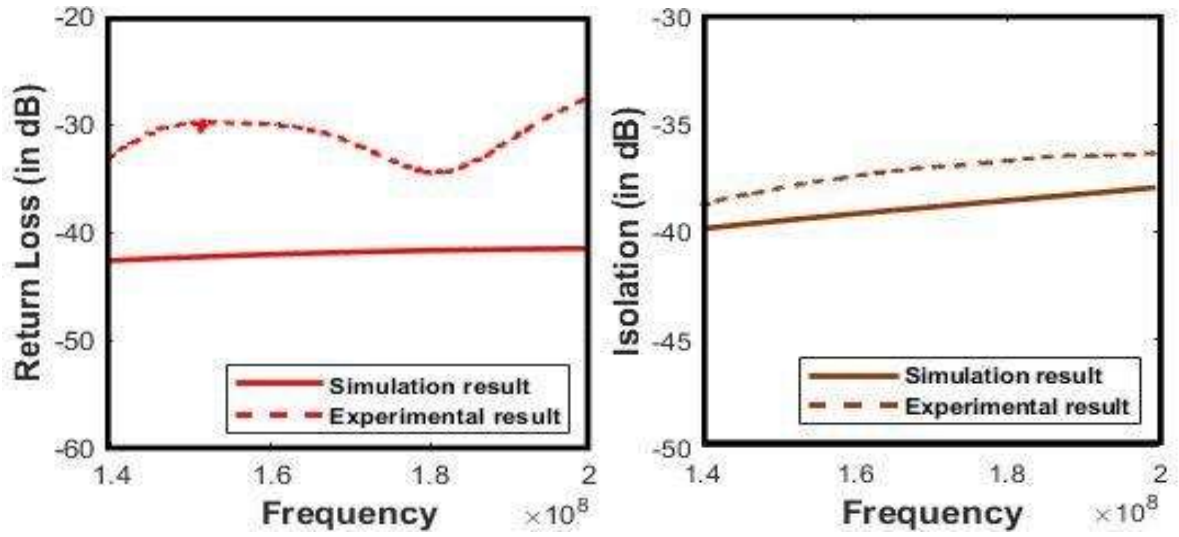

(c) **(d)**

Figure 3.31: Measured S-parameters characteristics comparison of the simulation and experimental result using VNA ((a) coupling, (b) output, (C) return loss and (d) isolation).

Table 3.4: Comparison between the proposed design and other similar work.

Sr. No.	Reference	Frequency Range	Coupling Range	Power Capability (W)	Directivity	Remarks
1.	[108]	20-30 GHz	20.5-22 dB	Low	15 dB	Very low power capability
2.	[109]	0.75-1.25 GHz	3±0.2 dB	Low	20 dB	Increased size of compensating elements
3.	[110]	500-1000 MHz	20 dB	50	20 dB	Very low power capability
4.	[111]	500-1000 MHz	20±1.25 dB	200	20 dB	Very low power capability
5.	[112]	0.1-500 MHz	20 dB	200	20 dB	Moderate power
6.	[113]	30-512 MHz	10dB	50	13 dB	Low directivity and power
7.	Presented design	140-200 MHz	20±0.3 dB	2000	16.5-20 dB	Good coupling flatness and high power capability

Figure 3.32 shows the electric field mapping inside the directional coupler. Its maximum value is found 1.04×10^5 V$/m$ at 2kW input, which is comparatively very less than the rated breakdown strength of 3×10^6 V$/m$ as discussed in section 3.2. We have estimated the power handling capability of directional coupler for 2kW.

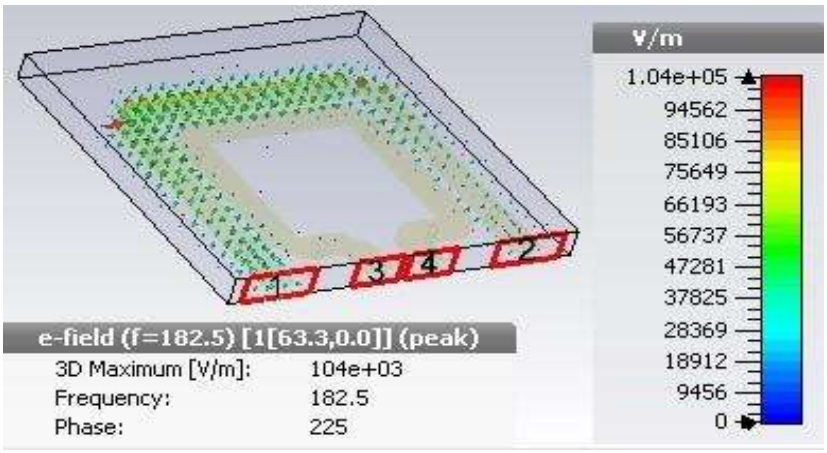

Figure 3.32: Electric field plot of directional coupler.

3.3.4. HIGH POWER RF ANTENNA

The high-power RF antenna [83] has been applied in RF heating of fusion Tokamak [84-93]. The RF power is directed inside Tokamak via various antennae to heat the plasma at ion cyclotron resonance frequency in which RF energy is transferred to the charged particle through resonant interaction. Various designs of high power antenna has been presented earlier by different Tokamak groups. In a very early stage, a double loop antenna is developed by Oak Ridge National Laboratory (ORNL) for TORE SUPRA [17, 36]. A similar antenna design has also been developed for JET [30, 32, 34], TFTR [35], and Alcator C-Mod Tokamak [16–18]. Recently, development of ITER-like antenna is reported by JET, where four resonant double loops (RDLs) are connected to achieve the required power handling capability. The ITER has also proposed the ICRH antenna with 24 radiating shorted straps that have to be feed with 20 MW RF power to the plasma [38-48]. The earlier works were mainly focused on the application of high power antenna in ICRF heating reference. However, the earlier literature is not well explained about high power ICRH antenna design. This thesis hypothesizes the high power antenna design technique for the Tokamak application. A 2kW, 182.5 MHz prototype of the ICRH antenna has been developed and tested for the desired performance. This section mainly focused on the theoretical analysis of the ICRH

antenna design and its optimization for the desired radiation parameters. The RF Antenna is placed at position 6 as shown in Figure 3.1.

3.3.4.1. Design and Simulation

The proposed design of the ICRH antenna is based on the composite right/left-handed transmission line (CRLH-TL) unit cell. The CRLH-TL possesses through the left-handed (LH) and right-handed (RH) combined attribute [114-120]. The distributed series and shunt LC components decide RH and LH nature of the transmission line. An equivalent circuit model of a CRLH TL unit cell is shown in Figure 3.33, where series inductance (L_S) and shunt capacitance (C_P) provide RH attribute and series capacitance (C_S) and shunt inductance (L_P) provide LH attribute to the transmission line.

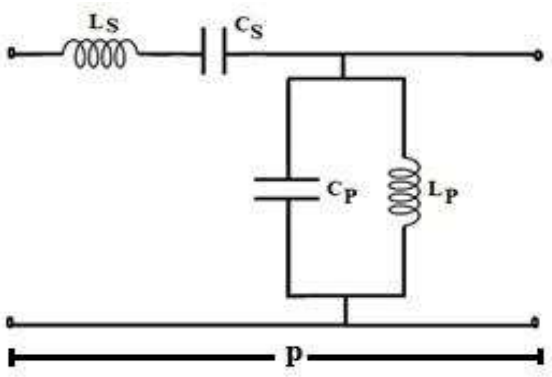

Figure 3.33: Unit cell of CRLH-TL.

The CRLH TL unit-cell's dispersion relation is determined by following [112],

$$\beta(\omega) = \frac{1}{p}\left(1 - \frac{1}{2}\left(\frac{\omega_L^2}{\omega^2} + \frac{\omega^2}{\omega_R^2} - \frac{\omega_L^2}{\omega_{sc}^3} - \frac{\omega_L^2}{\omega_{sh}^2}\right)\right) \tag{3.21a}$$

where,

$$\omega_L = \frac{1}{\sqrt{L_L C_L}}, \qquad \omega_R = \frac{1}{\sqrt{L_R C_R}} \tag{3.21b}$$

$$\omega_{se} = \frac{1}{\sqrt{L_R C_L}}, \qquad \omega_{sh} = \frac{1}{\sqrt{L_L C_R}} \tag{3.21c}$$

In general, series (w_{se}) and the shunt (w_{sh}) resonance are not equal in nature and present two non-zero frequency points. These resonance points are referred to as infinite wavelengths and are determined by the series and shunt LC elements. The series and shunt resonance frequencies can

be calculated using equation (3.21c). To realize a resonant type planar antenna, a CRLH-TL structure that supports an infinite wavelength at its fundamental mode is required.

The schematic of the proposed ICRH antenna design is shown in Figure 3.34a. It presents the asymmetrical TEE of transmission line with left and right shorted end at length L_f and L_b respectively. For $\frac{\lambda}{4} < L_f < \frac{\lambda}{2}$ and $L_b < \frac{\lambda}{4}$, the shorted end provides the parallel LC resonance equivalent. The full arrangement can be realized as an equivalent circuit shown in Figure 3.34b. Here, shunt and series elements of the circuit decide the resonance frequency and characteristic impedance of the antenna, respectively. This arrangement is known as inductor-loaded TL. In the case of an open boundary, the infinite wavelength frequency is determined by the shunt resonance frequency w_{sh}.

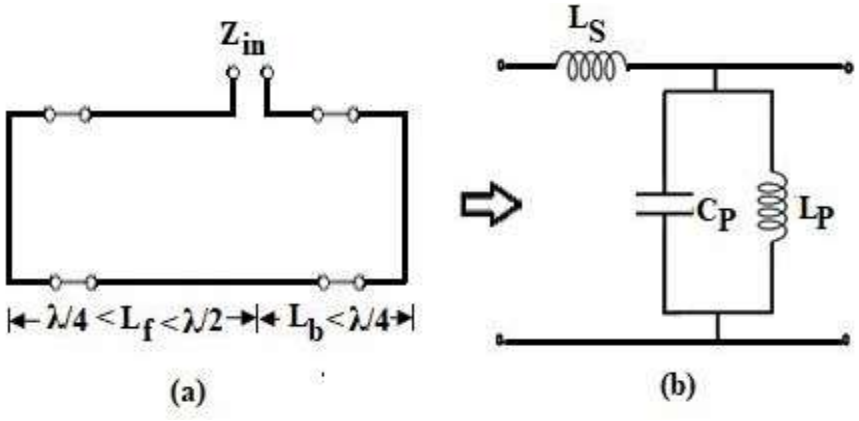

Figure 3.34: Proposed ICRH antenna (a) Schematic (b) Equivalent circuit.

The resonance frequency and propagation constant of the open end, inductor loaded unit cell are given by [119,120],

$$\beta(\omega) = \frac{1}{p}\left(1 + \frac{1}{2}\left(\frac{L_R}{L_L} - \frac{\omega^2}{\omega_R^2}\right)\right) \tag{3.22}$$

Transmission matrix (ABCD) for given equivalent circuit of ICRH antenna as shown in Fig. 2b is written as,

$$\begin{bmatrix} A_o & B_o \\ C_o & D_o \end{bmatrix} = \begin{bmatrix} 1 & j2\pi f L_S \\ 0 & 1 \end{bmatrix} \begin{bmatrix} 1 & 0 \\ j(2\pi f C_P) & 1 \end{bmatrix} \begin{bmatrix} 1 & 0 \\ \frac{1}{j(2\pi f L_P)} & 1 \end{bmatrix}, \tag{3.23a}$$

$$\begin{bmatrix} A_o & B_o \\ C_o & D_o \end{bmatrix} = \begin{bmatrix} 1 & j2\pi f L_S \\ 0 & 1 \end{bmatrix} \begin{bmatrix} 1 & 0 \\ j\left(2\pi f C_P - \frac{1}{2\pi f L_P}\right) & 1 \end{bmatrix}, \tag{3.23b}$$

$$\begin{bmatrix} A_o & B_o \\ C_o & D_o \end{bmatrix} = \begin{bmatrix} 1 - 2\pi L_S(2\pi f C_P - \frac{1}{2\pi f L_P}) & j2\pi f L_S \\ j(2\pi f C_P - \frac{1}{2\pi f L_P}) & 1 \end{bmatrix}. \quad (3.23c)$$

From equation (3.23c), transmission matrix parameter for CRLH inductor loaded TL can be written as,

$$A_o = 1 - 2\pi L_S\left(2\pi f C_P - \frac{1}{2\pi f L_P}\right),$$

$$B_o = j2\pi f L_S,$$

$$C_o = j\left(2\pi f C_P - \frac{1}{2\pi f L_P}\right), D = 1.$$

In resonance condition, substituting $f = f_{sh} = \frac{1}{2\pi\sqrt{L_P C_P}}$ in above gives,

$$A_o = 1, B_o = j\left(\frac{L_S}{\sqrt{L_P C_P}}\right), C_o = 0, D_o = 1.$$

From above, it can be found that C_o = 0 satisfies the resonance criteria. However, the resonance frequency is not affected by the series inductance (L_S) as shown in equation (3.23c).

The ICRH antenna has been realized as a single inductor-loaded TL unit-cell, where resonance frequency depends on the shunt LC elements. It has been designed at 182.5 MHz, which is five times the frequency (36.5 MHz) used in SST-1 for ICRF heating [6]. The assembly drawing of a strip-line based prototype ICRH resonant loop antenna is shown in Figure 3.35, where side and isometric view of the antenna are shown in (a) and (b), respectively. The outer assembly of the antenna is designed with aluminum metal, where the air is used as a dielectric. Teflon studs are utilized for the insulation of inner strips that support the strips in metallic enclosures. The antenna front end is covered with the faraday shield. Faraday shield filters the external electric field parallel to the static magnetic field. The spacing between conductors in the antenna is taken in such a way that it can be capable to withstand maximum 2 kW RF power. Inner strip-line conductors are shorted with the outer box at L_f and L_b in left and right end, respectively. The resultant assembly of the strip-line introduces the parallel LC network element at the feed point. As shown in Figure 3.35*b*, the strip-line is folded back from the front end and formed broadside overlapping with itself. The overlapping of folded strip-line introduces the internal series capacitance (C_{se}) which has been utilized for matching the overall antenna at 50 ohms. The C_{se}

has been incorporated in the equivalent circuit of an antenna as shown in Figure 3.34*b*. Now, the modified equivalent circuit of an antenna is shown in Figure 3.35*c*.

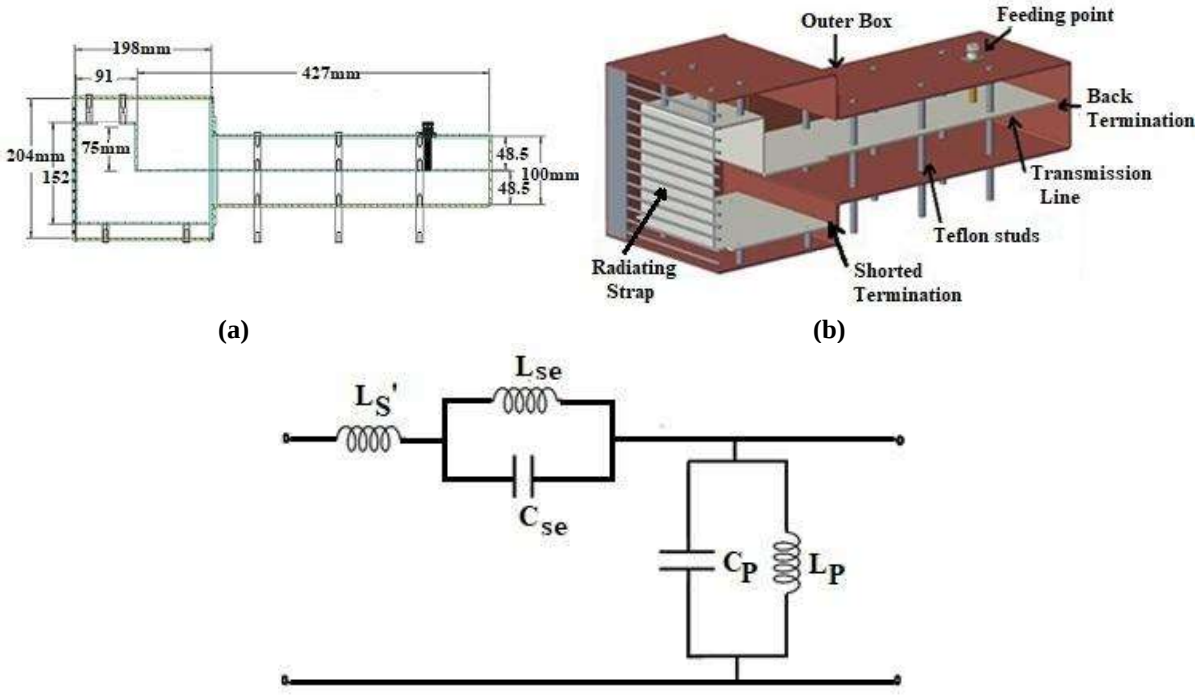

Figure 3.35: Assembly drawing of prototype ICRH resonant loop antenna (a) Side view, (b) Isometric view and, (c) Equivalent circuit with series coupling Capacitance.

Transmission matrix for modified equivalent circuit of ICRH antenna can be is written as,

$$\begin{bmatrix} A_1 & B_1 \\ C_1 & D_1 \end{bmatrix} = \begin{bmatrix} 1 & j2\pi fL_S \\ 0 & 1 \end{bmatrix} \begin{bmatrix} 1 & j\left(2\pi fL_S - 2\pi fL_{se} - \frac{1}{2\pi fC_{se}}\right) \\ 0 & 1 \end{bmatrix} \begin{bmatrix} 1 & 0 \\ j\left(2\pi fC_P - \frac{1}{j(2\pi fL_P)}\right) & 1 \end{bmatrix}$$

$$A_1 = \left(1 - 2\pi fL_S - 2\pi fL_{se} - \frac{1}{2\pi fC_{se}}\right)\left(2\pi fC_P - \frac{1}{j(2\pi fL_P)}\right)$$

$$B_1 = j\left(2\pi fL_S - 2\pi fL_{se} - \frac{1}{2\pi fC_{se}}\right)$$

$$C_1 = j\left(2\pi fC_P - \frac{1}{j(2\pi fL_P)}\right) \qquad (3.24)$$

$$D_1 = 1$$

From equation (3.24), it can be found that the resonance frequency is not affected by the series capacitance (C_{se}).

The input impedance of an antenna is given as

$$Z_{in} = Z_{11} = \frac{Z_{12}Z_{21}}{Z_{22} + Z_L}, \qquad (3.25)$$

where

$$Z_{11} = \frac{A_1}{C_1}, Z_{12} = \frac{A_1 D_1 - B_1 C_1}{C_1}, Z_{21} = \frac{1}{C_1}, Z_{22} = \frac{D_1}{C_1} \tag{3.26}$$

Substituting the values from equation (3.26) in (3.25) gives,

$$Z_{in} = \frac{A_1 Z_L + B_1}{C_1 Z_L + D_1} \tag{3.27}$$

It can be observed that the input impedance *Z*in depends on C_{se} and can be utilized for matching overall antenna impedance.

3.3.4.2. Physical Parameters of Antenna design

The calculation of physical antenna parameters is given in this section. Antenna design passes through various transitions and the strip-line impedance is varying in various places according to the design. The impedance segments are highlighted in Figure 3.36a. The equivalent of antenna design is shown in Figure 3.36b, where Z_1, Z_2, Z_3, Z_4, Z_5 and L_1, L_2, L_3, L_4, L_5 represent the impedances and progressive lengths of respective segments. Here, the left and right end have been shorted at L_f = 745mm and L_b = 198mm, respectively. The shorted line with impedance of Z_1 and Z_5 is replaced with its equivalent reactance $X_f = Z_1 tan(\beta L_1)$ and $X_b = Z_5 tan(\beta L_5)$. The other antenna segments are presented as same with their respective impedance.

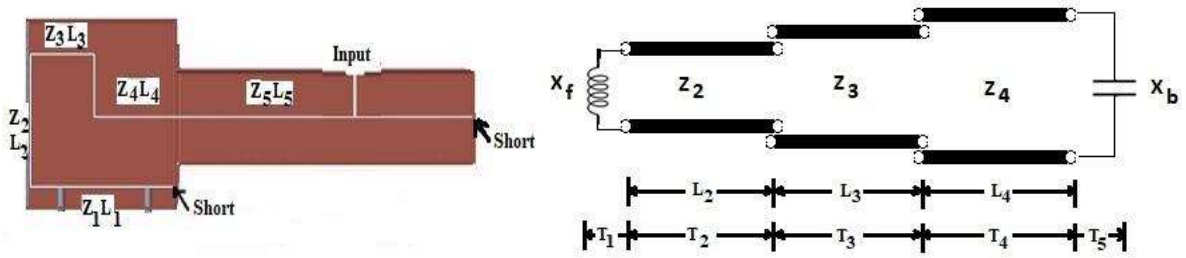

(a) **(b)**

Figure 3.36: Antenna transitions and its equivalent design (a) Proposed antenna structure with various impedance segments and, (b) Equivalent of antenna design.

The overall design is optimized using transmission matrix which is written as,

$$[A_t] = \begin{bmatrix} A & B \\ C & D \end{bmatrix} = T_1 T_2 T_3 T_4 T_5 \tag{3.28}$$

where, $T_1, T_2, T_3, T_4, and\ T_5$ are transmission matrix of each segments which are given as,

$$T_1 = \begin{bmatrix} 1 & 0 \\ Y_1 & 1 \end{bmatrix},\ Y_1 = 1/(jZ_1 tan(\beta L_1)),$$

$$T_2 = \begin{bmatrix} Cos(\beta L_2) & jZ_2\text{Sin}(\beta L_2) \\ jY_2\text{Sin}(\beta L_2) & Cos(\beta L_2) \end{bmatrix}$$

$$T_3 = \begin{bmatrix} Cos(\beta L_3) & jZ_2\text{Sin}(\beta L_3) \\ jY_2\text{Sin}(\beta L_3) & Cos(\beta L_3) \end{bmatrix}$$

$$T_4 = \begin{bmatrix} Cos(\beta L_4) & jZ_2\text{Sin}(\beta L_4) \\ jY_2\text{Sin}(\beta L_4) & Cos(\beta L_4) \end{bmatrix}$$

$$T_5 = \begin{bmatrix} 1 & 0 \\ Y_5 & 1 \end{bmatrix} \ , \ Y_5 = 1/(jZ_5 tan(\beta L_5)).$$

The length and impedance of the each segment has been optimized using transmission matrix A_t. In resonance condition C = 0 at 182.5 MHz is applied in equation (3.28) where values of Z_1, Z_2, Z_3, Z_4, Z_5 and L_1, L_2, L_3, L_4, L_5 are calculated as,

$$Z_1 = 25.98\Omega, Z_2 = 10.85\Omega, Z_3 = 50\Omega, Z_4 = 75.50\Omega, Z_5 = 48.66\Omega$$

$$L_1 = 198mm, L_2 = 152mm, L_3 = 91mm, L_4 = 182mm, L_5 = 320mm.$$

The strip-line parameters of the antenna are calculated by well-known Wadell's formula [121]. These parameters are incorporated in 3D Electromagnetic simulation software, CST Microwave Studio and simulated for the radiation characteristics. The obtained results are shown in Figures 3.37-3.49. The simulation results are found as, reflection coefficient is −32 dB, efficiency is −0.7669 dB, directivity is 3.09 dBi, and gain is 2.63 dB at desired frequency 182.5 MHz. The obtained results are found as per desired. The gain and the reflection coefficient of the antenna is optimized by having the appropriate strip line parameters such as strap width, ground spacing, and feeder point. The gain of an antenna varies with radiating strap width. Figure 3.40*a* shows that the antenna gain improves as strap width increases with a slight shift of frequency. The re-centering of the frequency can be made by shifting the feeder position. Figure 3.40*b* shows the respective shift of the center frequency with the change of the feeder location from the back shorted end.

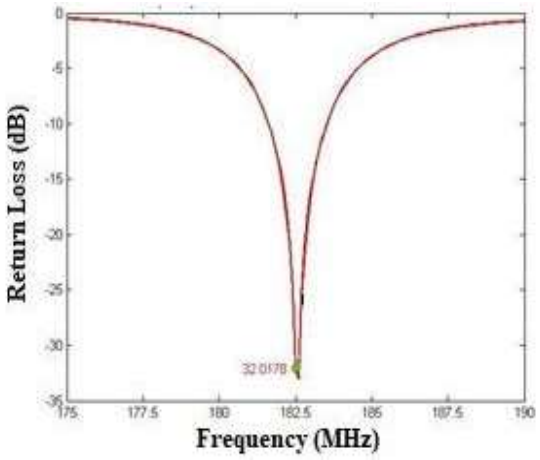

Figure 3.37: Simulation result of Reflection coefficient in dB.

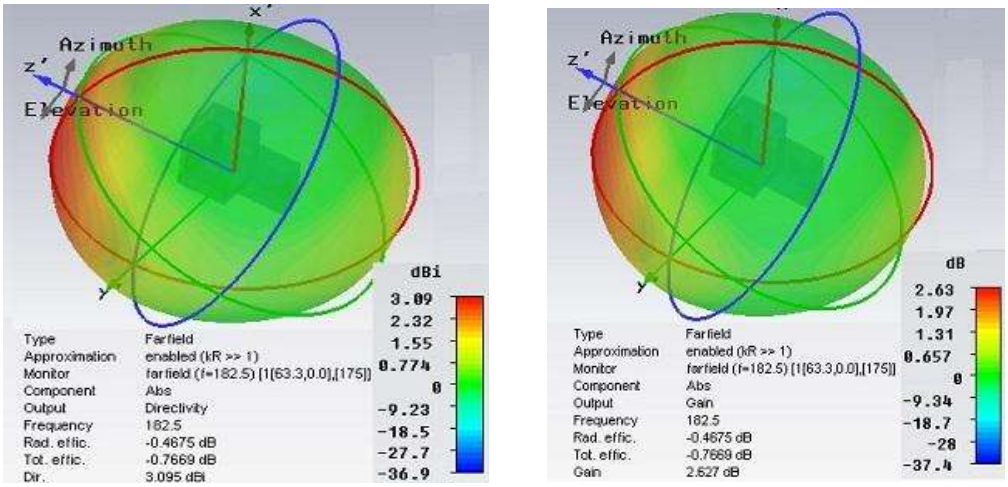

(a) **(b)**

Figure 3.38: Radiation pattern present the (a) Directivity (b) Gain of simulated antenna.

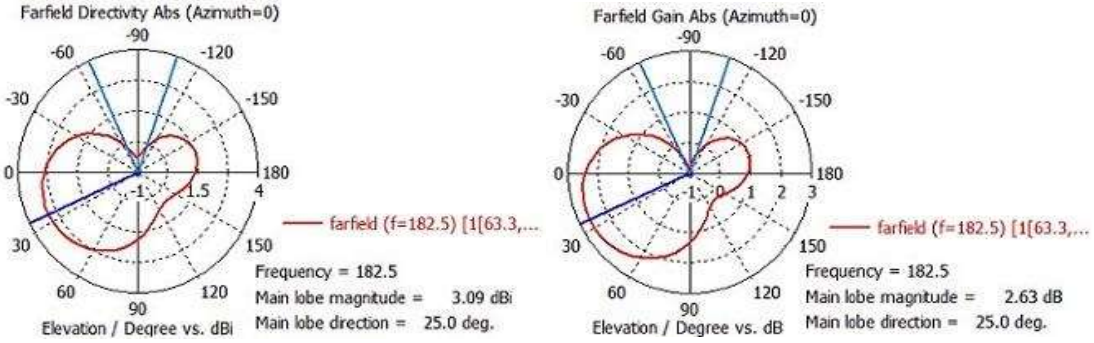

(a) **(b)**

Figure 3.39: Polar plot of (a) Directivity in dBi (b) Gain in dB.

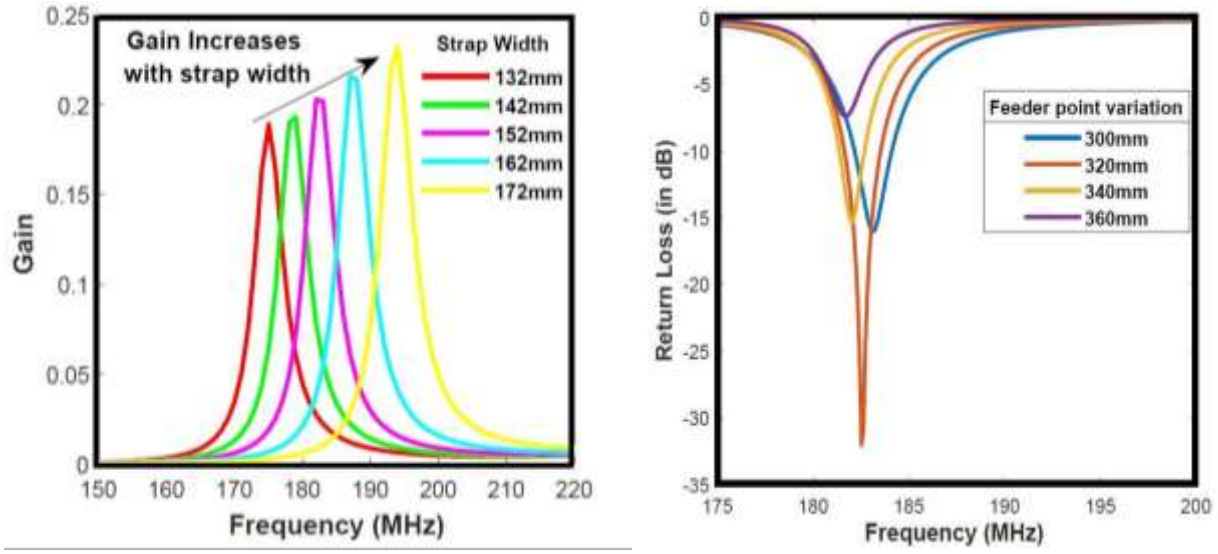

(a) **(b)**

Figure 3.40: Simulation result present (a) Effect of change of strap width, (b) Effect of variation in feeder point.

The electric field distribution inside the designed ICRH antenna is analyzed at 2 kW RF input using CST microwave studio software which is shown in Figure 3.41. Here, the maximum electric field is found to be $1.43 \times 10^5 V/m$ below the breakdown strength. The peak power handling capability depends upon various losses and the maximum value of an applied electric field. The maximum allowable electric field to prevent the breakdown in the air is limited by $1.47 \times 10^6 V/m$ [14, 54-56, 94]. In the simulation result, the maximum electric field is found significantly less than the breakdown limit, which verifies the maximum power rating of the antenna.

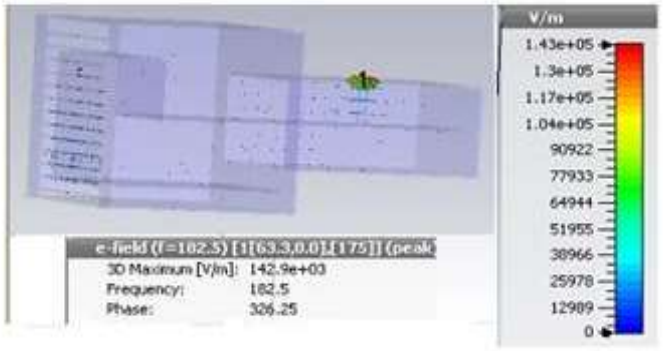

Figure 3.41: Electric field plot of ICRH antenna at 2 kW power.

3.3.4.3. Fabrication and test results

A photograph of the fabricated ICRH antenna is shown in Figure 3.42*a*. The Faraday shield is designed with stainless steel and the other components are made with commercial-grade aluminum. The N-type connector is attached to withstand high power up to 2 kW RF input.

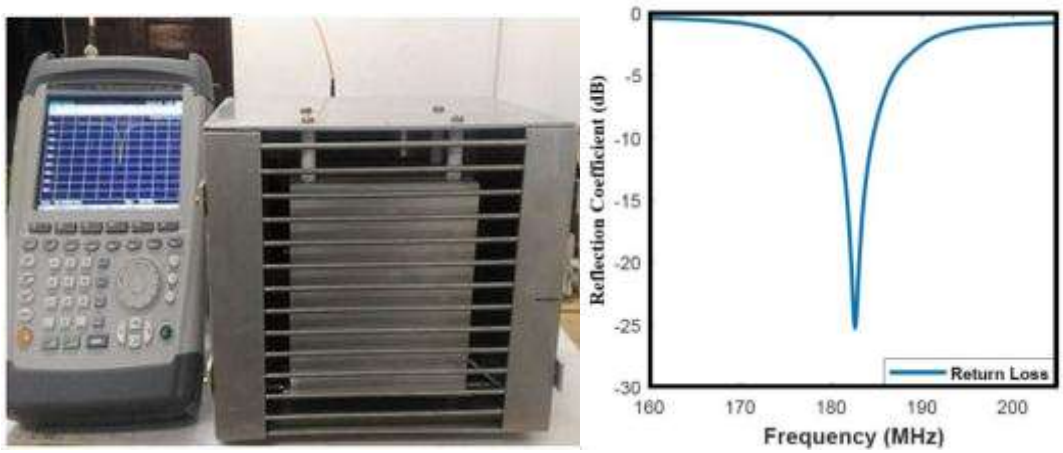

(a) **(b)**

Figure 3.42: Fabricated antenna and its test result (a) Photograph of fabricated ICRH antenna, (b) Test result of reflection coefficient in dB.

The fabricated antenna is tested with the help of a vector network analyzer (VNA). The reflection coefficient obtained is − 24.65 dB, as shown in Figure 3.42b. The result obtained after fabrication is in good agreement with the simulation result. The measurement setup for the polar radiation pattern of an antenna is shown in Figure 3.43, where Figures 3.43*a* and 3.43*b* present the schematic and a photograph of the real system, respectively. The setup consists of multiple AC servo motors and controller, network analyzer, RF signal generator, and a computing device. The RF signal generator Agilent (N9310A) provides 13dBm RF input to the ICRH antenna at 182.5 MHz. The antenna radiates the RF input, where an air-cored helical antenna is used for reception of radiated power. The receiving antenna is on board at moving arm which moves in polar coordinates. Received power at each location is recorded using a spectrum analyzer. The radiation results in terms of polar coordinates are shown in Figure 3.44 in prospective comparison with the simulation results. The test results are found in close agreement with the simulated result.

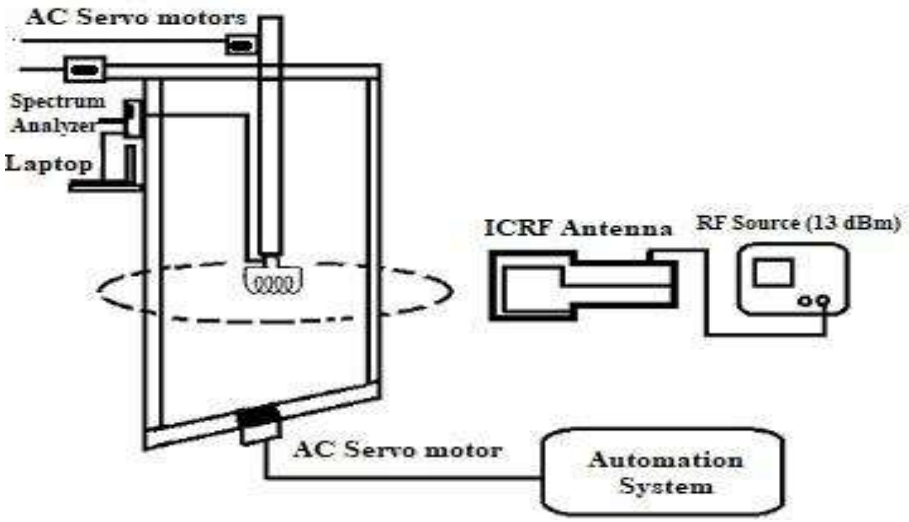

(a)

(b)

Figure 3.43: Radiation measurement set-up (a) Schematic, (b) Photograph of real system.

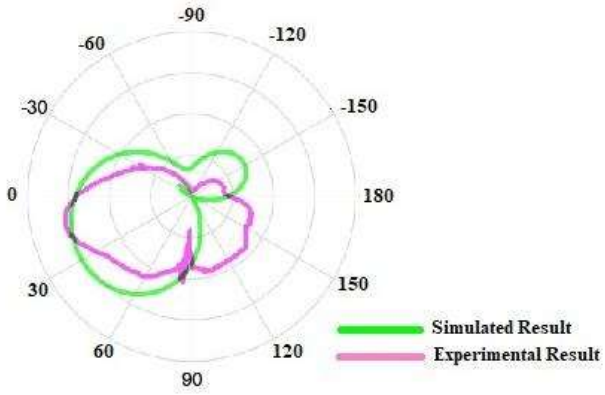

Figure 3.44: Comparison of polar plot for simulated and test result.

The directivity of an ICRH antenna is calculated using the well-known formulas as given in [122] and is found as ~2.95 dBi. The antenna radiation efficiency (e) is defined in terms of reflection efficiency (e_r), conduction efficiency (e_c), and the dielectric efficiency (e_d) which is given by

$$e = e_r e_c e_d \tag{3.29}$$

Here, e_r =$(1 - {S_{11}}^2)$, S_{11} = − 24.65 dB = 0.0034. So, reflection efficiency is calculated as 99% approximately. Here, dielectric loss can be considered as zero for air dielectric. The maximum resistivity of aluminum and steel is given as 2.65 to 2.82 $\times 10^{-8}$ and 6.9 × 10^{-7}Ωm, respectively, and exhibits conduction losses due to which the efficiency is approximately equal to 85%. Also, the gain is related to the directivity with antenna efficiency factor as: $G = kD$ where, k is the antenna efficiency factor and equal to 0.85 and also calculated using known formulas as in [122]. So, gain comes out to be 2.5 dB. The measured parameters are in good agreement with the simulated results.

3.3.5. VARIABLE WATER LOAD

In Tokamak, plasma impedance varies dynamically in front of the RF antennae. To emulate the realistic plasma like conditions for mock-up ICRH system, a variable water load has been developed. The variability of the developed load is found in the range, (35 to 260)Ω, resistive + (-j25 to +j220)Ω, reactive due to the high dielectric constant of water [38, 40, 41]. The photograph of the water load in front of the RF antenna is shown in Figure 3.45. A movable water bucket, connected with the controlled motor drive is placed in front of an RF antenna which moves back and forth to introduce variable load impedance. The length of the sliding bed is approximately 600 mm. The variable water load is placed at position 7 as shown in Figure 3.1.

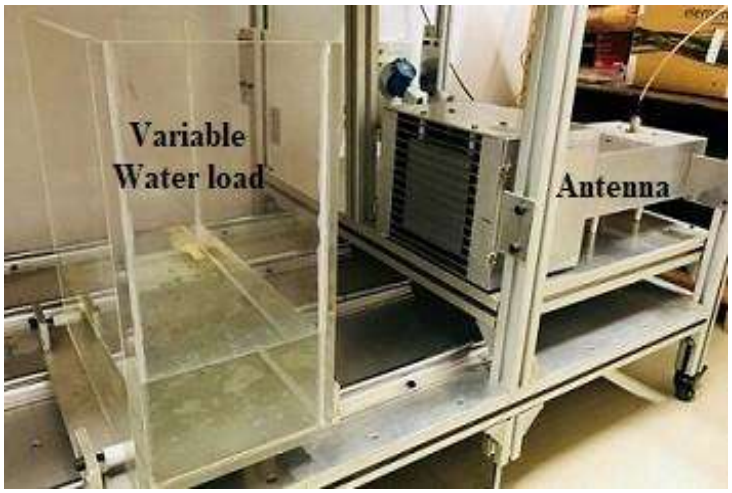

Figure 3.45: Photograph of water load in front of antenna.

3.3.6. TAPPED TRANSMISSION LINE

A rigid coaxial tapped transmission line has been utilized to calculate the phase difference between the forward and reflected wave [6]. The tapped line consists of 15 voltage probes. It is placed between the hybrid coupler and matching unit, which is used to rectify the voltage signals with diode detectors and are sampled to find the VSWR curve at any given instant of time. The VSWR curve is used to find the load impedance, i.e. magnitude and phase. The co-axial transmission line is fabricated from the commercial-grade aluminum. The length of the transmission line is selected approximately one wavelength (1.64m) at the center frequency of 182.5 MHz. For the 50 Ω line, the inner to outer dimensions are selected as standard 1:2.3 [97, 98]. A view of the transmission line and return loss graph is shown in Figure 3.46.

Figure 3.46: Fabricated coaxial transmission line and return loss (dB).

3.3.7. RF SOURCE

The RF source provides input to the proposed mock-up ICRH system for active test and measurement. An RF signal generator, Key sight model no. N9310A, along with LPA, model no. Mini-Circuit ZHL-100W-52-S+ is used as an RF source in the system, which is shown in Figure 3.47. It can produce RF output up to 100 watts in the frequency range 50 to 500MHz. The RF source is placed at position 1 as mentioned in Figure 3.1.

Figure 3.47: Photograph of the source along with LPA.

3.3.8. CONTROLLER UNIT

A controller unit used in the mock-up ICRH system has been designed to control the matching components on the basis of feedback received from detectors, and the controller unit is placed at position 8 as mentioned in Figure 3.1. The schematic of the matching system along with a controller is shown in Figure 3.48. The photograph of the controller unit is shown in Figure 3.49 consists of Motion controller, Human-Machine interface (HMI), Servo drive module, A/D converter and power supply unit. The motion controller is inbuilt with ARM Cortex A9 800 MHz Processor which can control servo motors up to 16 nos. at a time [123]. The forward and reflected magnitude obtained from the power detector is fed to A/D converter for conversion to a digital value. The motion controller processes the digital value using an algorithm at the server end and the controller generates feedback to the AC servo motor connected with encoder. An encoder converts the electrical signals to the mechanical motion and thus moves the stub position. The user can use HMI to change modes like manual and automatic processing of the system.

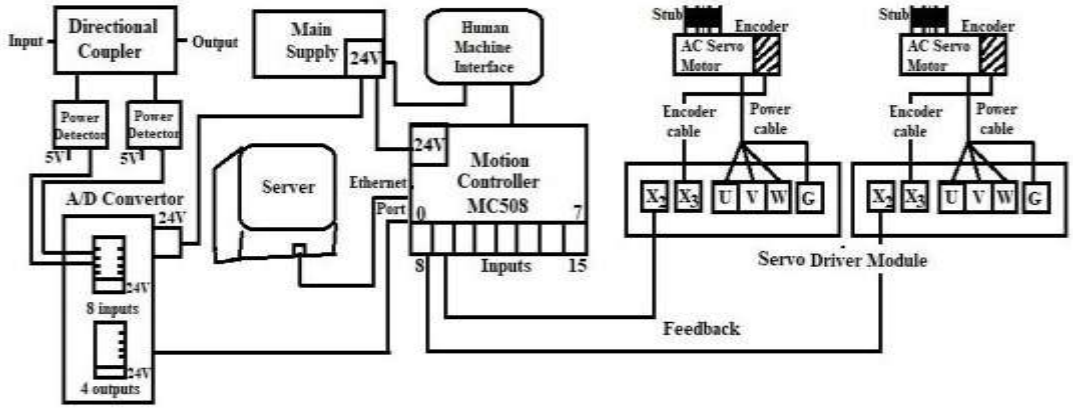

Figure 3.48: Schematic of controller with matching network.

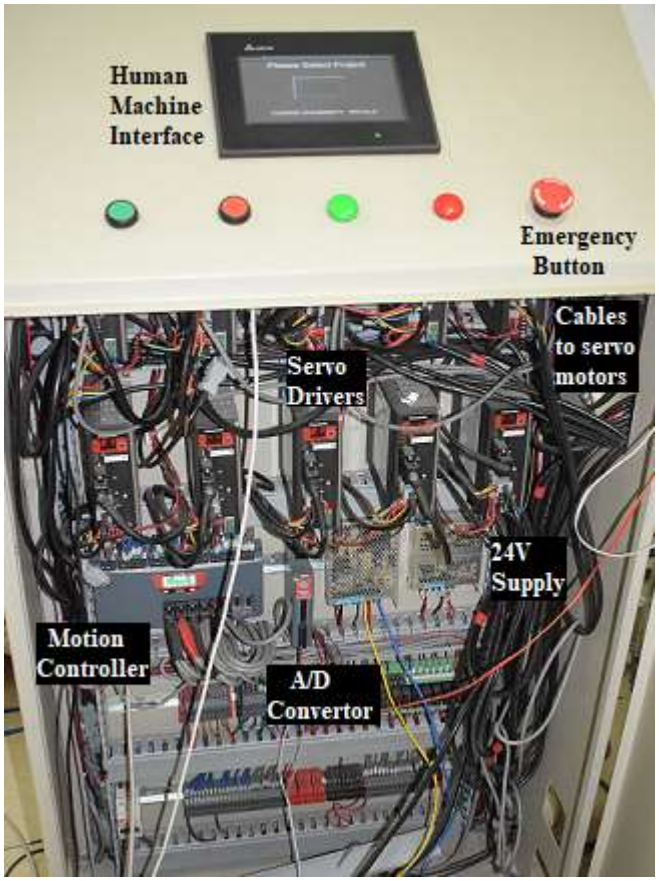

Figure 3.49: Photograph of controller unit.

The controller uses the M/s Trio Motion Technology's software [124], motion perfect v4.1.4 for controlling purposes. It is a Windows-based software for the PC, which has been developed using the latest .NET and WPF technologies. Programming is as simple like C, where standard instruction sets such as variables, loop, input/output, math, conditions, etc. can be executed. It

facilitates the wide variety of motion control facilities, such as single-axis moves, synchronized and unsynchronized multi-axis moves, and control of the digital I/O.

Figure 3.50 shows the program window of the Trio controller for writing the instruction set for communicating the device.

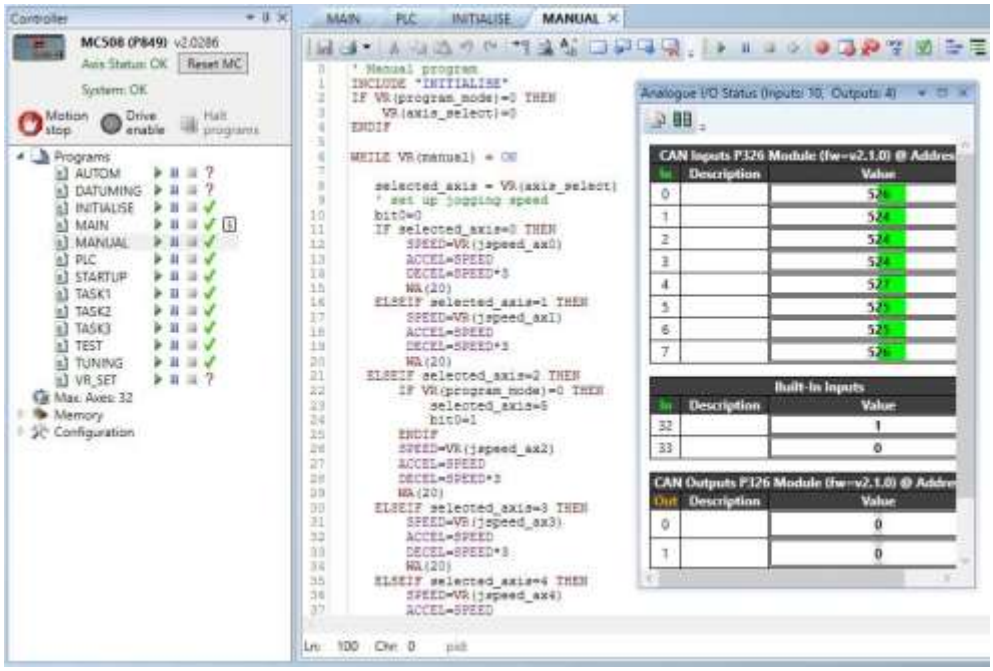

Figure 3.50: Program window of the Trio controller.

3.3.9. STUB TUNER

A high-power stub tuner is used for matching and tuning of the ICRH network at the operating frequency. Various designs of stub tuner have been presented earlier. At present, tuner designs are based on cavity type, micro-strip, coaxial line, dielectric liquid stub tuner, fast ferrite tuner, MEMS designs, etc. as discussed earlier [71-78]. In high power systems, rigid coaxial line based stub tuners are used. Therefore, for the mock-up ICRH system, the rigid coaxial line based variable stub tuner, which is capable to tune at any frequency in the range of 80 to 850 MHz, has been developed. The stub tuner is placed at position 4 as mentioned in Figure 3.1.

3.3.9.1. Design and Analysis

The schematic of high power RF stub is shown in Figure 3.51. Stub design is based on a rigid coaxial line that incorporates a movable shorting ring. It is housed inside the transmission line and moved along the length of the stub. Shorted stub introduces a reactance in microwave or RF circuit, which can be utilized for the matching of RF system. Stub parameter can be analyzed using

distributed lumped equivalent circuit of a transmission line, which is shown in Fig 3.52, where R, L, G, C are resistance, inductance, conductance, capacitance per unit length. Z_{in} is the input impedance of short circuited line and L_g represents the per unit length of transmission line. Here, values of L and C vary with the stub length. A slot on the outer conductor of the coaxial line is assumed as an equivalence of L'in the circuit.

For lossless transmission line, equivalent circuit parameter are given by [97],

$$L = \frac{\mu}{2\pi} ln\, ln\, \frac{b}{a}\ , C = \frac{2\pi\varepsilon'}{ln\frac{b}{a}}\ and\ R = G = 0.$$

Where, a and b are the inner and outer diameter of the conductor respectively.

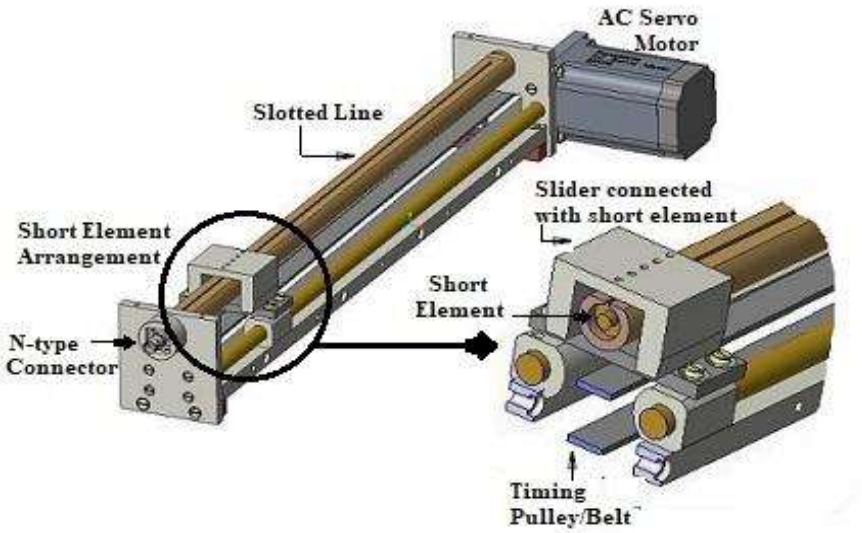

Figure 3.51: Schematic of high power RF stub.

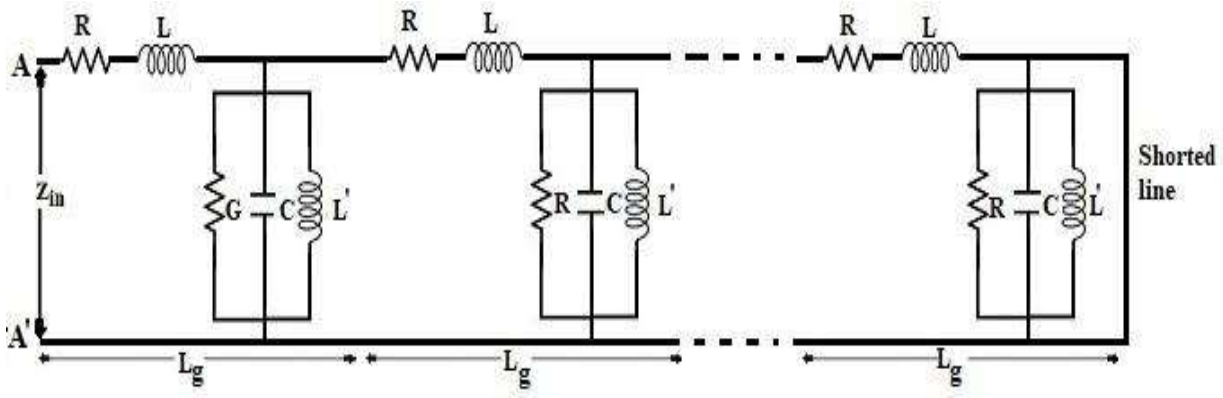

Figure 3.52 Distributed lumped equivalent circuit of slot line transmission line.

The characteristic impedance for the equivalent circuit, shown in Figure 3.52 is calculated using telegrapher's equations [97, 98] and given as below:

$$Z_o = \sqrt{\frac{L}{C - 1/\omega^2 L'}} \tag{3.30}$$

$$Propagation\ constant\ (\gamma)\ = j\beta = j\sqrt{\omega L\left(\omega C - \frac{1}{\omega L'}\right)}$$

Input impedance at AA' is calculated as,

$$Z_{in} = jZ_o\ tan\ tan\left(\beta L_g\right)\ = j\sqrt{\frac{L}{C - 1/\omega^2 L'}}\ tan\ tan\left(\sqrt{L\left(C - \frac{1}{\omega^2 L'}\right)}L_g\right) \tag{3.31}$$

$In\ case\ \frac{1}{\omega^2 L'} \ll C$,

$$Z_{in} = j\sqrt{\frac{L}{C}}\ tan\ tan\left(\sqrt{LC} * L_g\right) \tag{3.32}$$

Equation (3.32) represents the impedance of uniform shorted stub without slot. This thesis hypothesizes the fabrication of shorted stub, which can be upgradable up to MW power handling capability, where the size of the outer conductor goes up to 9" diameter and slot size is also significantly wider. Therefore, the significance of the slot cannot be avoided. Significance of $1/\omega^2 L'$ deteriorates the impedance of stub and it highly dominates when frequency goes high. This deterioration can be compensated by tapering of inner space within the coaxial line.

The assembly drawing of the stub tuner is shown in Figure 3.53. The shorting ring is placed between the inner and outer conductor, and a linear slot is cut through the outer conductor to move the ring along the length using a fast belt pulley arrangement, which is integrated with a controlled drive. Air is used as a dielectric for the high power handling capability, where Teflon supporting studs are used at one end near to connector to provide the insulation between inner and outer conductors.

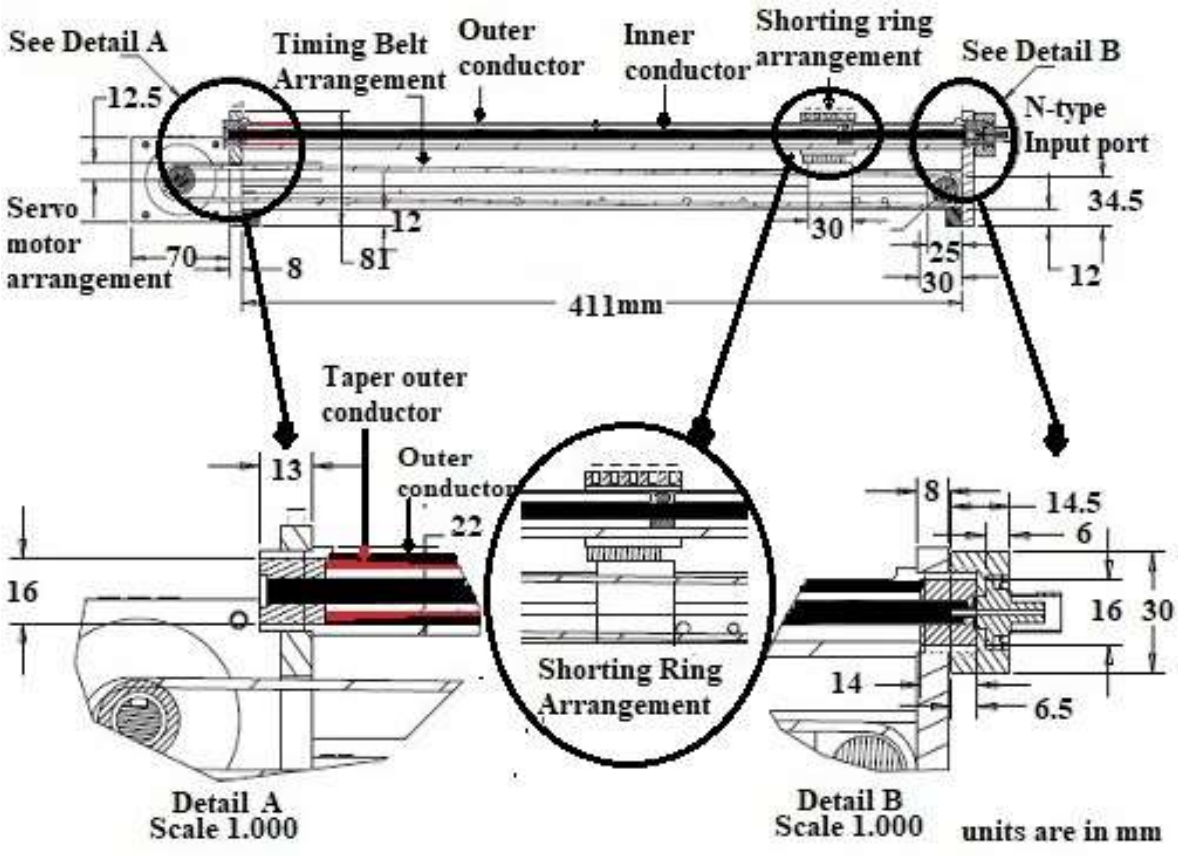

Figure 3.53: Assembly drawing of stub tuner.

The dimensions of the inner and outer conductors have been calculated for 50Ω impedance. To compensate the slot discontinuity, a tapered profile is incorporated at the outer of a coaxial line, which has been optimized using CST software simulation. The final dimensions of the developed model are given in Figure 3.53. The critical dimensions between the inner and outer conductors are selected in such a way that it can support an electric field at 2kW input without any breakdown.

The simulation outcomes are shown in Figure 3.54. The simulation results show that the designed stub is performing excellently in the frequency range of 80 to 850 MHz. It can be tuned at any frequency within the range by changing its length. For example, stub is tuned for frequencies 120, 510, 630 MHz by having the stub length of 410, 300, and 70 mm, respectively, as shown in Figure 3.54. The VSWR, as shown in Figure 3.55 is observed in the range of 1.1 to 1.7 in a prescribed frequency range, which is a desirable parameter. Electric field mapping of inner space of coaxial stub is shown in Figure 3.56 where the maximum electric field at 2kW input is found to be $1.57 \times 10^5\, V/m$ which is much below the breakdown strength of air i.e. $1.47 \times 10^6\, V/m$ as shown in section 3.1 [94].

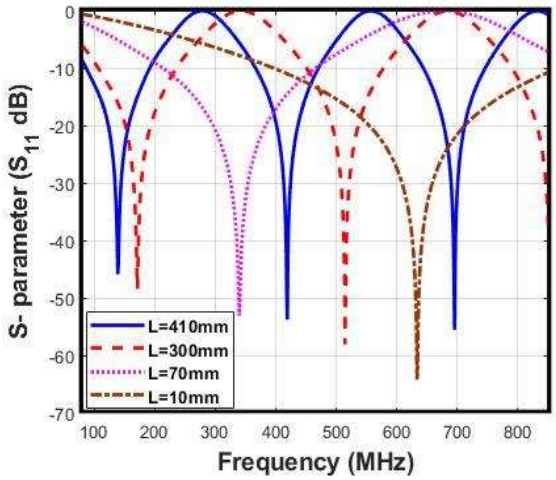

Figure 3.54: Simulation outcome of stub tuner.

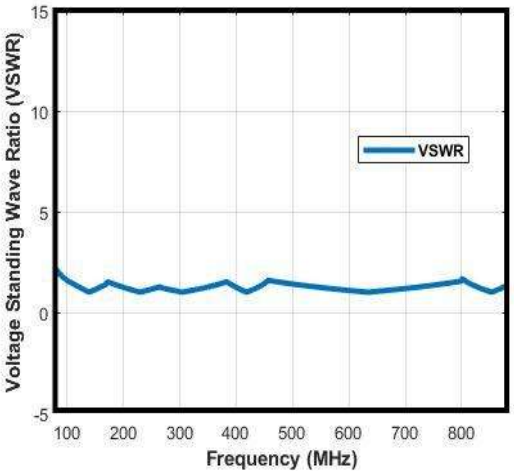

Figure 3.55: VSWR output of stub tuner.

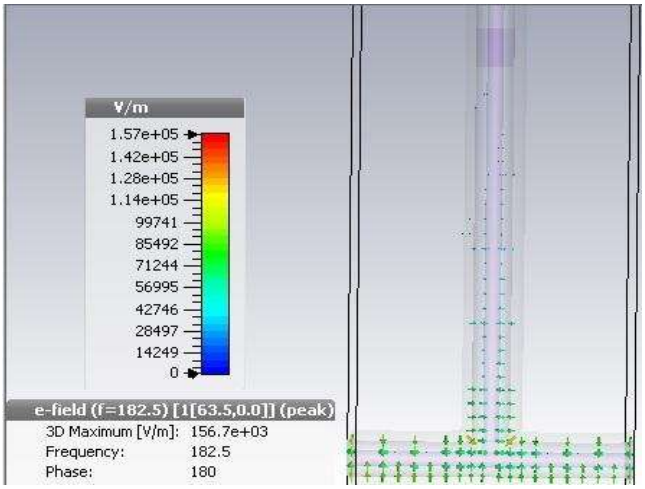

Figure 3.56: Electric field plot of stub tuner.

3.3.9.2. Fabrication and testing

A photograph of the fabricated stub tuner is shown in Figure 3.57. It has been developed as per the assembly drawing shown in Figure 3.53. The Assembly of a stub is connected with a belt pulley arrangement, which moves in linear motion. The maximum speed of the shorted ring is estimated as,

$$S = \frac{Belt\ pitch\ \times Pulley\ teeth \times rpm}{60 \times 1000} = 3.9\frac{mm}{msec}.$$

Where, maximum rpm is 3000, nos. of pulley teeth is 26, and belt pitch is 3.0mm. The full length of stub can be traveled by the shorting ring in 106msec as per the given estimate. This means the stub can be tuned at any frequency in the range of 80 to 850 MHz within 106msec.

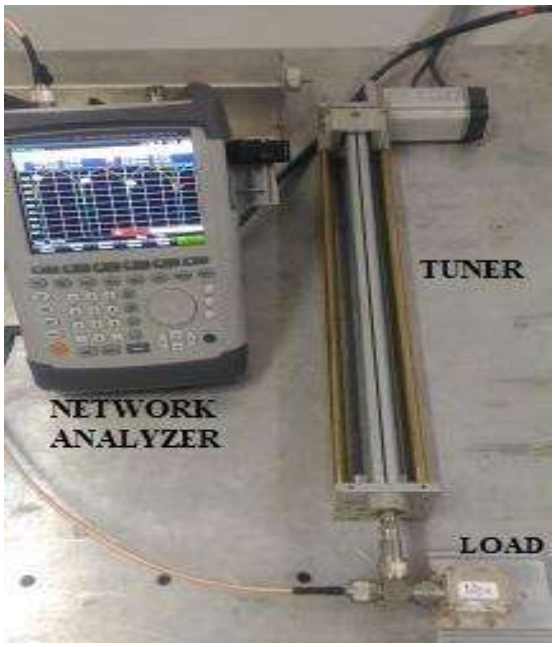

Figure 3.57: Photograph of fabricated stub tuner.

The fabricated tuner is tested using a single port Vector Network Analyzer (VNA). The perspective comparison of simulation and test results for different lengths is shown in Figure 3.58. The test results show that the tuner can operate in the wideband of 80MHz to 850MHz frequency range for matching of unknown impedance and having return loss better than 25dB and VSWR in between 1.1 to 1.9 as shown in Figure 3.59. The test results are in good agreement with the simulation results.

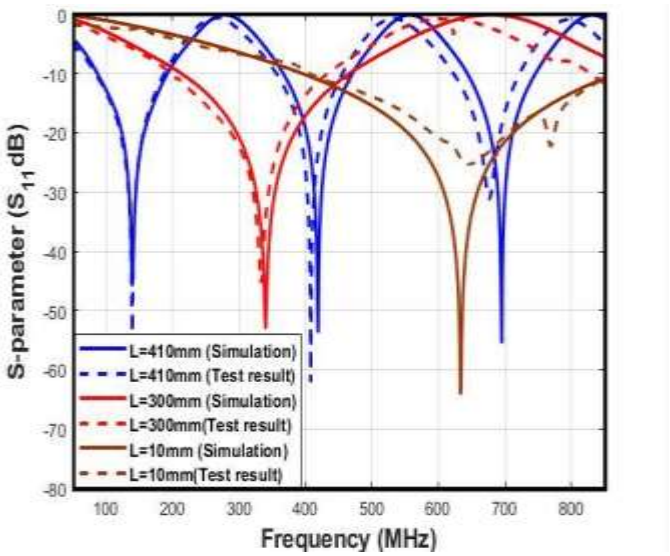

Figure 3.58: Comparison of simulation and test results of stub tuner.

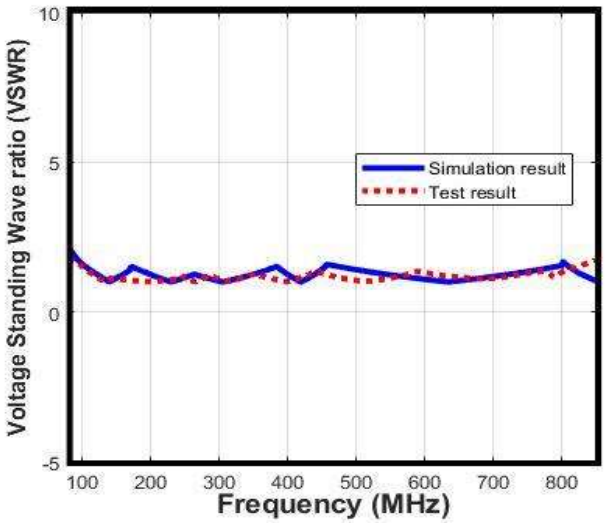

Figure 3.59: VSWR output.

3.3.10. LINE STRETCHER

A high power line stretcher or phase shifter is used to control the phase of RF signal for impedance matching in RF system or testing application. At present, the phase shifter designs are based on electrically controlled co-axial ferrite based, micro-strip based, coaxial transmission line, etc. [79-82]. In high power, a rigid coaxial line based line stretcher is designed that can be moved mechanically using servo motors. A rigid coaxial line based line-stretcher has been developed, which is capable of providing required phase shift for matching in the frequency range of 50-250 MHz, and the line stretcher is placed at position 5 as shown in Figure 3.1. It is designed for 2kW power handling capability and can be upgraded up to MW as per the required applications.

3.3.10.1. Design, fabrication and results

This section presents the design and fabrication of the rigid coaxial line based line stretcher. The assembly drawing of the line stretcher is shown in Figure 3.60. It incorporates two rigid coaxial transmission lines (TL), one is fixed, and the other is movable. The movable TL slides over the fixed one, which changes the overall length of TL. The total length of TL defines the electrical delay and phase of propagation. The sliding assembly introduces the phase shift required for matching in an electrical circuit. The assembly moves to and fro using a fast belt pulley arrangement, which is integrated with a controlled drive. Air is used as a dielectric for high power handling capability, where Teflon supporting studs are used to provide insulation between inner and outer conductors.

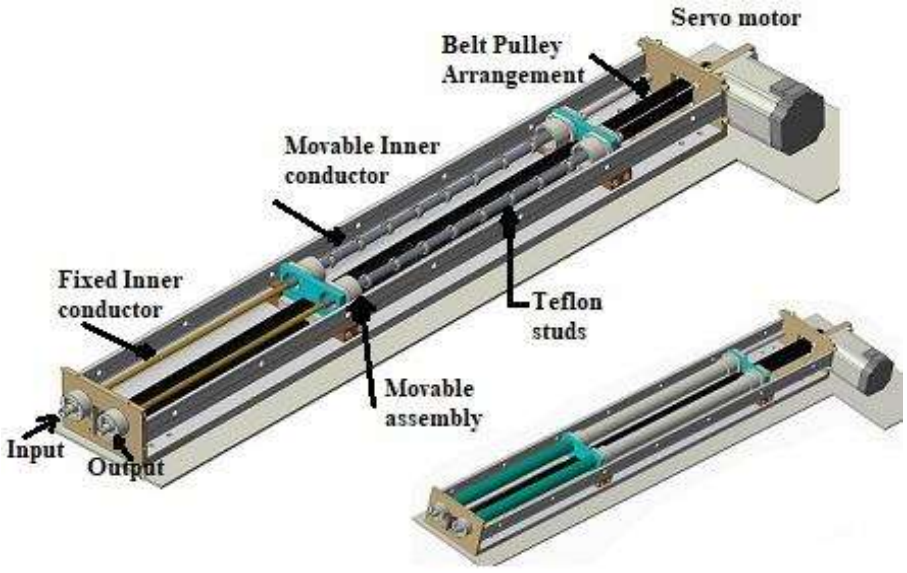

Figure 3.60: Assembly drawing of line stretcher.

The movable TL introduces discontinuity when it slides over the fixed one, which changes the overall impedance of TL due to change in inner and outer radii of TL. To compensate the discontinuity, the Teflon studs are introduced inside the sliding TL at regular intervals, which has been optimized using electromagnetic simulation software, CST. The final dimensions of the developed line stretcher is shown in Figure 3.61.

The rigid coaxial transmission line is designed for 50 Ω characteristic impedance, where inner to outer dimensions are calculated using standard equation [97, 98] as described in equation 3.5.

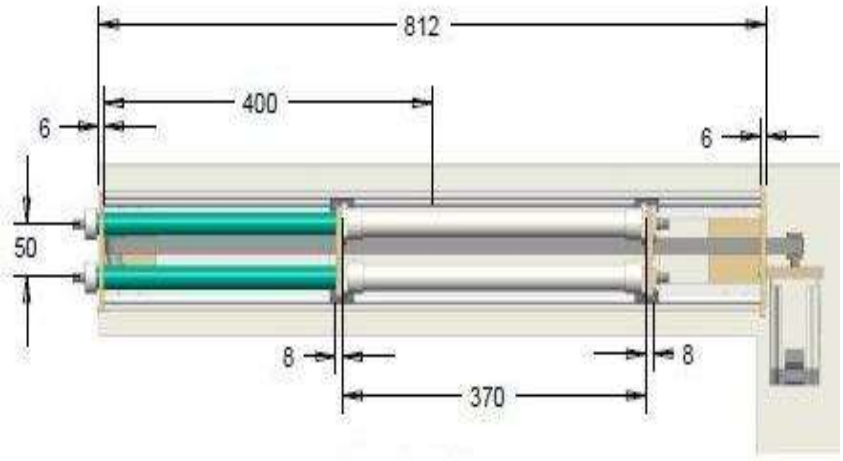

Figure 3.61: Dimensions of line stretcher.

The dimensions of fixed TL, inner conductor, ID=OD=6mm and outer conductor, ID=15.5mm, OD=19mm, whereas the dimensions of moving TL, inner conductor, ID=6mm, OD=9mm and outer conductor, ID=19mm, OD=22mm. The dimensions are selected in such a way that it can support electric field at 2kW input without any breakdown.

A photograph of the fabricated line stretcher is shown in Figure 3.62. It has been designed as per the assembly drawing. The Assembly of the line stretcher is connected with a belt pulley arrangement, which moves in linear motion. The maximum speed of the shorted ring is estimated as,

$$S = \frac{Belt\ pitch\ \times Pulley\ teeth \times rpm}{60 \times 1000} = 3.9\frac{mm}{msec}.$$

Where, maximum rpm is 3000, nos. of pulley teeth is 26, and belt pitch is 3.0mm. The full length of the line stretcher can be travelled in 94.9msec as per the given estimate. This means the line stretcher can provide phase shift at any frequency in the range of 100 to 350 MHz within 94.9msec.

Figure 3.62: Photograph of fabricated line stretcher.

The fabricated line stretcher is tested using a two-port vector network analyzer (VNA). The test results for s-parameter characteristics are shown in Figure 3.63(a) and (b). Figure 3.63(a) shows the reflection coefficient ($|S_{11}|$) and Figure 3.63(b) shows the transmission coefficient ($|S_{21}|$) when the line is elongated from 30mm to 370mm. The phase shift response (angle of S_{21}) has been measured from 50 to 250 MHz. The phase shift measured at 100MHz is around 94.5^o and 150^oat 200MHz, as shown in Figure 3.64.

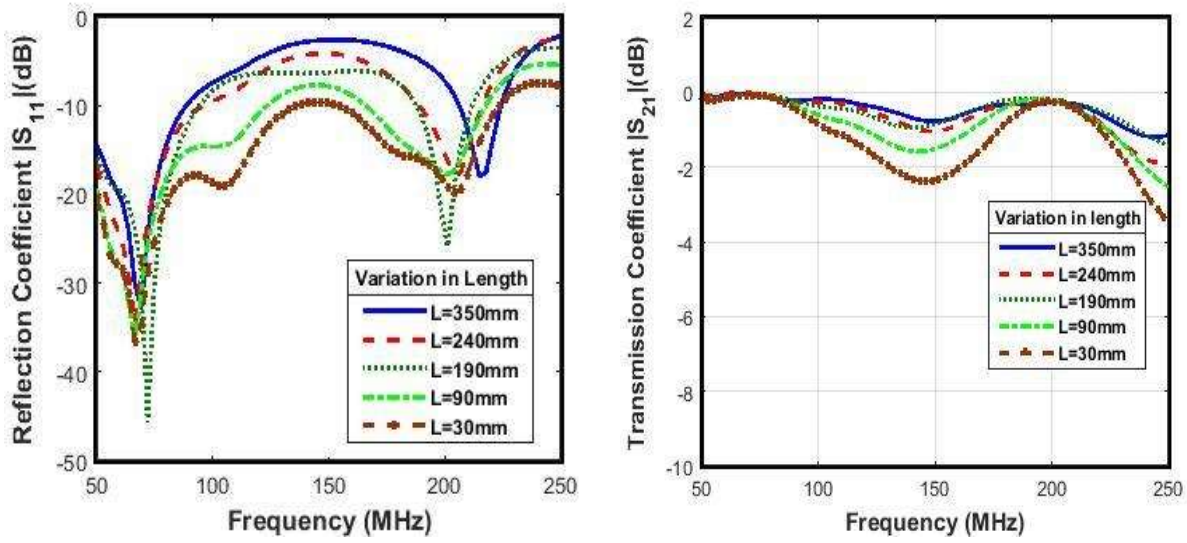

(a) **(b)**

Figure 3.63: S-parameter characteristics of fabricated line stretcher when stretched from 30mm to 350mm (a) Reflection Coefficient, (b) Transmission Coefficient.

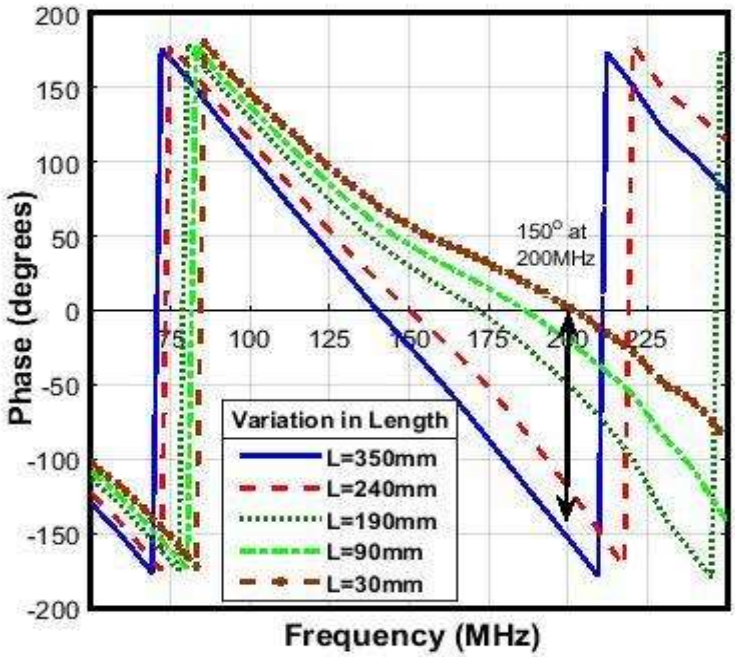

Figure 3.64: Phase shift (angle of the transmission coefficient, S21) of the fabricated line stretcher when stretched from 30 to 350 mm.

3.4. Summary

In this chapter, the components of the mock-up ICRH system have been developed for 170-190 MHz frequency and 2kW power handling capability. These components are designed in such a

way that can be upgradable up to MW power handling capability in any frequency range within HF, VHF, and UHF. Each of the components has been indigenously developed and tested for the desired output. The developed components have wide applications in the field other than the fusion Tokamak, such as telecommunication, defense and electronic warfare, aerospace, satellite, and navigation systems.

CHAPTER 4

HIGH POWER RF MATCHING NETWORK

4.1. Overview

This chapter briefly explains the development of high power double stub automated matching network using developed components, as presented in chapter 3. The ICRH system of Tokamak is mainly based on a double stub matching concept. Therefore, an automated double stub matching network has been developed a stage before the development of full mock-up of ICRH system. Its layout is shown in Figure 4.1 in which a variable double stub tuner along with a line stretcher is used to introduce desirable reactance with appropriate phase change for matching of unknown variable water load. The stub tuners and line stretcher are integrated with AC servo motors, which are controlled and drive using feedback controller in the real-time domain. In this chapter, we have developed a computational program, i.e. based on the double stub RF matching hypothesis. A program algorithm is developed in such a way that the optimum matching speed can be achieved with the matching network.

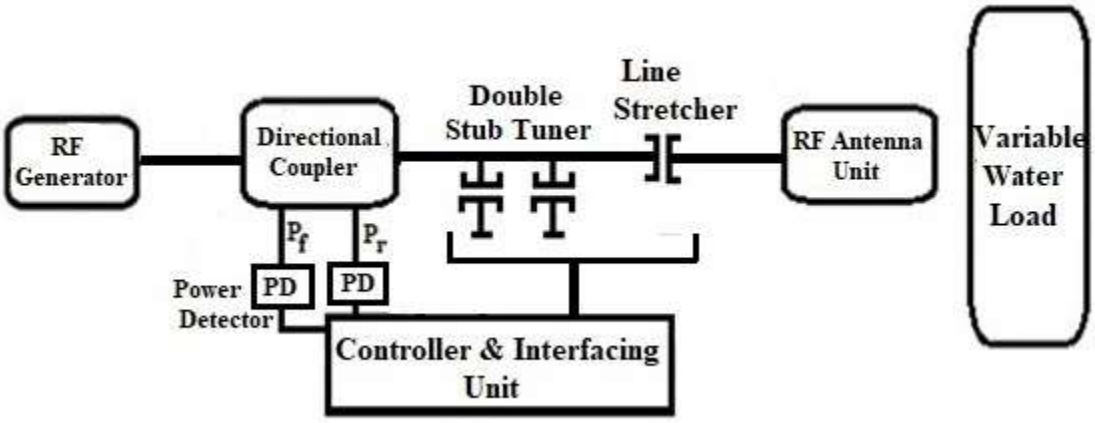

Figure 4.1: Layout of automated matching network.

4.2. Double Stub Tuner based RF matching network

In RF network, stubs are broadly used for the matching of load impedance with impedance of the network. In case of single stub matching, transformed load admittance, $1 + j\beta$ at distance L from the load end is matched by adding the susceptance $-j\beta$ through shorted or open stub. Single stub matching is avoided in case of variable load because the distance L is decided by the load

impedance, and it is very difficult to change the stub position all the time when the load impedance is changed. Therefore, the double stub matching concept has been used. In a double stub matching network, two stubs are placed in parallel at a certain distance l_a (i.e., in general, it is kept $\frac{\lambda}{8} or \frac{3\lambda}{8}$) to match the unknown load. The stub distance from the load is not dependent on the load impedance. Therefore, stubs can be located at a fixed distance in a double stub matching network [97].

Figure 4.2 shows the schematic of a double stub matching network where Stub 1 and Stub 2 are placed L distance apart at node A and node B, respectively. Length L is taken very small as compared to λ, so that transformed impedance will appear the same as found at load point. The length of shorted stubs is decided by shorting ring position inside stubs, which are assumed to l_{sA} and l_{sB} respectively.

Based on stub positions, impedance of the short-circuited stub tuners are given by [97]

$$Z_{sA} = jZ_o \tan(\beta l_{sA}) \ , \ Z_{sB} = jZ_o \tan(\beta l_{sB}). \tag{4.1}$$

where Z_o is the characteristic impedance of the coaxial line used in the stub and β is the phase constant. Corresponding normalized admittance (y_s) for stub1 and stub 2 are given by

$$y_{sA} = jb_{sA} = 1/Z_{sA} \ , \ y_{sB} = jb_{sB} = 1/Z_{sB} \tag{4.2}$$

b_{sA} and b_{sB} represents the susceptance of stub A and stub B respectively.

In particular, a variable load is emulated using a movable water tank in front of an antenna. The antenna admittance (y_{ant}) not only depends upon the structural parameters but also depends on the peripheral medium which is assumed as,

$$y_{ant} = g_{ant} + jb_{ant} \tag{4.3}$$

where g_{ant} and b_{ant} are the conductance and susceptance of antenna load.

By including the stub 1 admittance, transformed admittance at node A is written as

$$y_A = y_{ant} + y_{sA} = (g_{ant}) + j(b_{ant} + b_{sA}) \tag{4.4}$$

Normalized admittance before the stub 2 by transforming through the length (l_a), is given by

$$y_{A'} = \frac{(g_{ant}) + j(b_{ant} + b_{sA} + \tan(\beta l_a))}{1 - (b_{ant} + b_{sA})\tan(\beta l_a) + j(g_{ant})\tan(\beta l_a)} = g_{A'} + jb_{A'} \tag{4.5}$$

So, the real part of $y_{A'}$ must be equal to the 1, whereas it's imaginary part $(jb_{A'})$ is compensated by stub 2. Means admittance at node B,

$$y_B = y_{A'} + y_{sB} = g_{A'} + j(b_{A'} + b_{sB}), \tag{4.6}$$

This represents perfectly matched load admittance. Now the reflection coefficient at node B, $(\Gamma = 0)$ can be taken for perfectly matched condition. So,

$$y_B = g_{A'} = 1, \text{ and} \tag{4.7}$$

$$b_{A'} + b_{sB} = 0 \tag{4.8}$$

Susceptance of stub 1 (b_{sA}) is calculated using eq. (4.7) and eq. (4.5) and given by,

$$b_{sA} = \frac{1}{T_S}((1 - (b_{ant})tan(\beta l_a)) \pm \sqrt{K}) \tag{4.9}$$

Where $K = \frac{(1+tan(\beta l_a)^2)g_{ant}}{\gamma} - g_{ant}^2 tan(\beta l_a)^2$

The susceptance (b_{sB}) of stub 2 is obtained using eq. (4.5) and eq. (4.8),

$$b_{sB} = -b_{A'} \tag{4.10}$$

In matched condition, length of stub 1 and stub 2 are derived as,

$$l_{sA} = -\frac{1}{\beta} tan^{-1}\left(\frac{1}{b_{sA}}\right), \quad l_{sB} = -\frac{1}{\beta} tan^{-1}\left(\frac{1}{b_{sB}}\right), \tag{4.11}$$

which can be achieved by moving the shorting rings at appropriate place inside stubs.

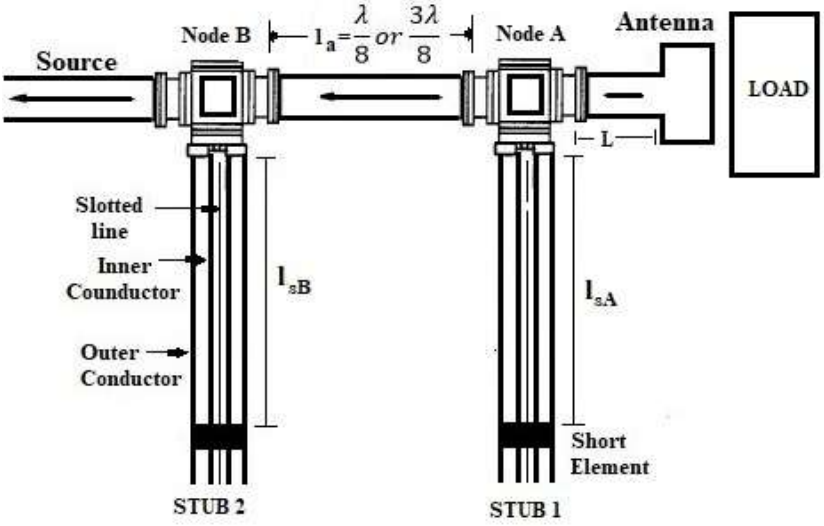

Figure 4.2: Schematic of Double stub matching network.

The double stub matching network is not capable of matching the range of admittance values called as a forbidden gap, which is marked as a forbidden conductance circle in the smith chart [89]. The load admittance under the forbidden gap can be transformed using a line stretcher to get out of the forbidden gap. Therefore, a line stretcher is used along with a double stub tuner to match all the admittances.

4.3. Matching algorithm for high power RF network

The speed of the matching network mainly depends on the inbuilt diagnostics, matching algorithm, and speed of controlled drives. Therefore, an efficient algorithm has been developed for the proposed automated matching network. Its flow chart is shown in Figure 4.3. It includes many steps, and each of the steps is assigned for the specific task, which can be understood using the flow chart.

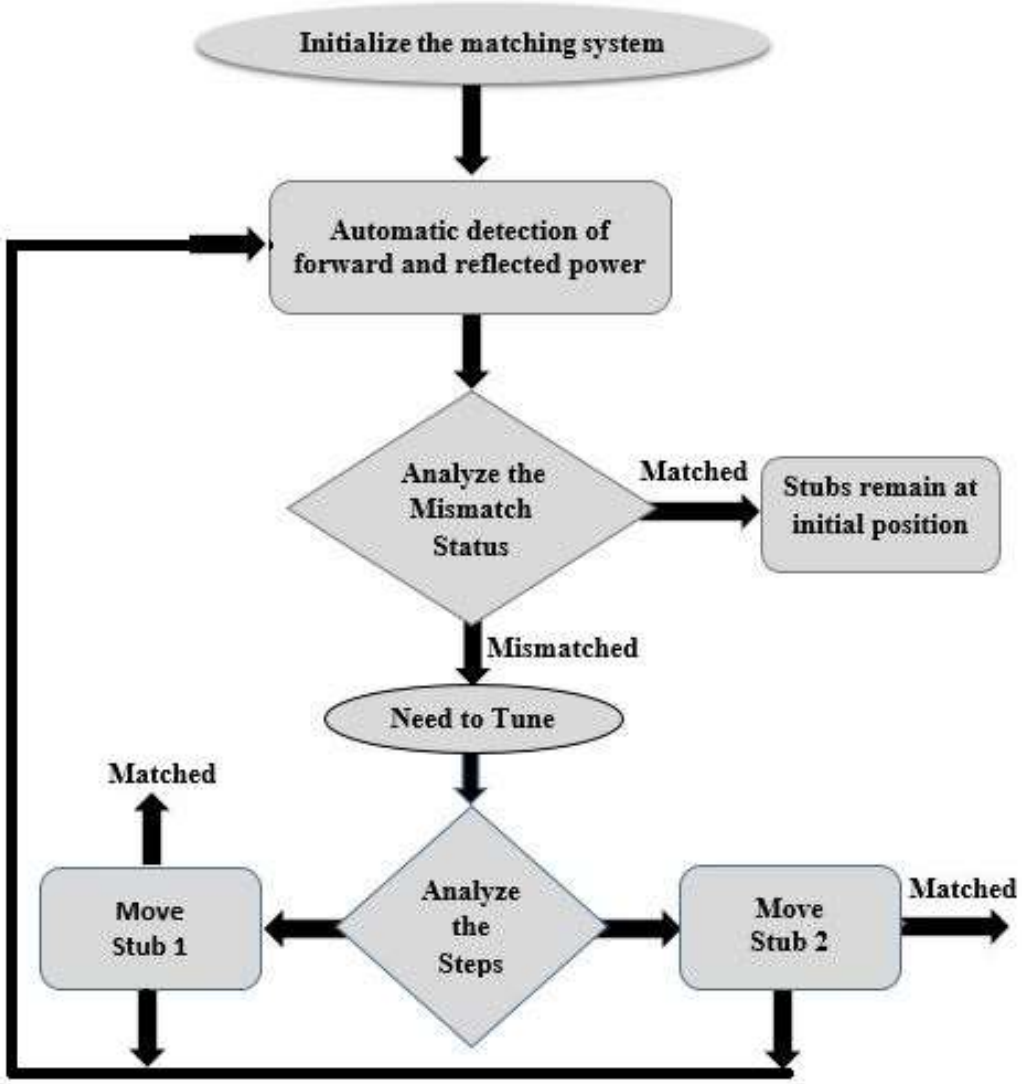

Figure 4.3: Flow chart for proposed matching system.

Steps of the flowchart are defined as follow:

Step 1. This step initializes the system and checks the response from all devices connected to the system. It also ensures that the system is ready for the next step.

Step 2. In this step, the magnitude of forward and reflected power has been measured.

Step 3. On this basis of measured forward and reflected power data, mismatched status has been analyzed. If the system is already matched, stubs remain in the same position; otherwise, the program generates an instruction to start the matching process.

Step 4. The matching process is initiated at this step, where the time taken in matching is minimized by moving both stubs simultaneously towards the match point. Once the system is matched, the controller sends a request to stop the moving stub.

4.4. Signal processing for RF matching network

This section formulates the matched condition on the basis of inbuilt diagnostic response. The system incorporates detectors that continuously measure the forward and reflected power. The power detector, mini-circuit model no. ZX-47-60LN+ outputs are DC voltages, which can be mapped for specific RF power value. It is inbuilt with integrated circuit (IC) AD8318 which has 9-stage demodulating logarithmic amplifier, capable of accurately converting an RF input signal to a corresponding output voltage. The output voltage decreases linearly in the dB scale when RF input power increases. The photograph of the detection unit is shown in Figure 4.4, whose power range is defined as -60dBm to +10dBm for frequency, 10-8000MHz. The output of the detector is specifically plotted for 182.5MHz, which is shown in Figure 4.5. Here, output voltage varies from 0.4 V to 1.2V for -60 to +10dBm input. The detector shows the linear characteristic for -55 to -10dBm input, where the slope is approximately −15.5 mV/dB, which can be utilized for the formulation of the detector output.

Figure 4.4: Photograph of RF power detector.

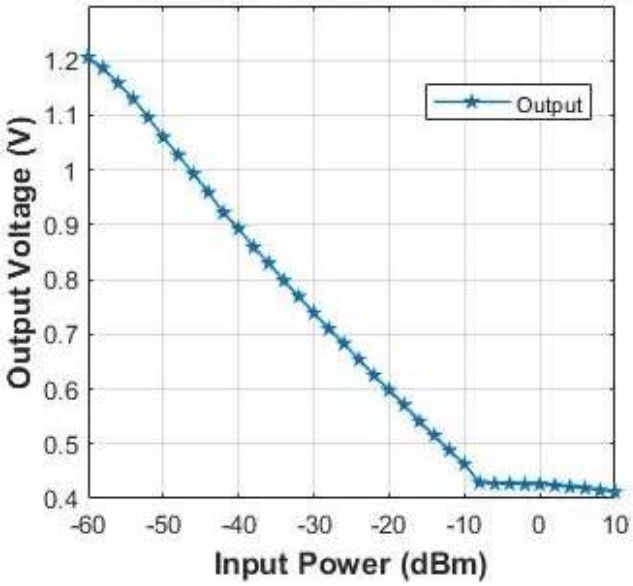

Figure 4.5: Output voltage vs input power at 182.5MHz.

The power output has been formulated in terms of measured voltage which is written as [94, 122],

$$P_d = \frac{-k}{v_d}(dBm) = 10^{\left(\frac{-k}{v_d}\right)}mW \tag{4.12}$$

Where, P_d is detector output power and k is slope of the curve in linear region. Now, Voltage Standing Wave Ratio (VSWR) for RF network is written as [97],

$$VSWR = \frac{1 + \Gamma}{1 - \Gamma}$$

Where Γ is the reflection coefficient.

The matching system utilizes detectors for measuring the forward and reflected power that measures output voltages V_{df} and V_{dr} respectively. Its respective power values can be derived from eq. 4.12, which are supposed to be P_{df} and P_{dr}. Now, VSWR in term of forward and reflected power can be written as,

$$VSWR = \frac{1 + \sqrt{\left(\frac{P_{dr}}{P_{df}}\right)}}{1 - \sqrt{\left(\frac{P_{dr}}{P_{df}}\right)}} \tag{4.13}$$

From Eqn. (4.12), substituting the value of P_{df} and P_{dr} in Eqn. (4.13),

$$VSWR = \frac{1 + 10^{\frac{k}{20}\left(\frac{1}{V_{df}} - \frac{1}{V_{dr}}\right)}}{1 - 10^{\frac{k}{20}\left(\frac{1}{V_{df}} - \frac{1}{V_{dr}}\right)}} \tag{4.14}$$

In matched condition VSWR must be less than 1.5. Therefore,

$$\frac{1 + 10^{\frac{k}{20}\left(\frac{1}{V_{df}} - \frac{1}{V_{dr}}\right)}}{1 - 10^{\frac{k}{20}\left(\frac{1}{V_{df}} - \frac{1}{V_{dr}}\right)}} < 1.5$$

Substituting the value of slope k=15.5mV/dB for 182.5MHz gives,

$$\left(\frac{1}{V_{df}} - \frac{1}{V_{dr}}\right) > 0.901 \tag{4.15}$$

The condition is given in eq. 4.15 represents the matched condition, where reciprocal differences of the voltage output from the detector must be greater than the defined constant (0.901). This has to be satisfied with the matching of unknown load impedance. The condition is used in developed algorithm to analyze the matched condition and interpreted for the controller program.

4.5. An Automated RF Matching Network

The schematic of the proposed RF matching network is shown in Figure 4.6. It comprises of various RF components such as directional coupler, power detectors, coaxial stub tuners, line stretcher, RF antenna, and feedback-controlled drives, etc. To emulate the unknown load conditions, a water bucket is moving back and forth at the antenna front, which introduces time-varying load. Signal generator and low power amplifier (LPA) are used as an RF source to excite the system for testing and measurement. In mismatched conditions, the directional coupler couples the forward and reflected waves at two separate ports that are measured using power detectors. The detector output has been utilized for the analysis to match the unknown load condition. Moving stubs and line stretcher is connected with the feedback controller to match the system in the real-time domain.

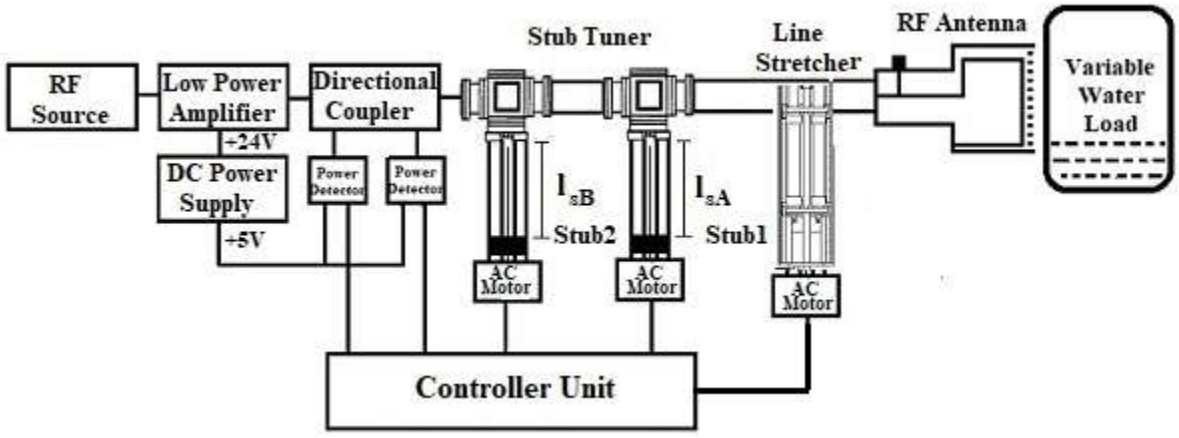

Figure 4.6 Schematic of proposed RF matching network.

The photograph of the developed RF matching network, along with a variable water load is shown in Figure 4.7. System components are connected using coaxial cable (RG142). Initially, it is tested using a Vector network analyzer (VNA). The set-up has been calibrated for the various load positions, where impedance values are measured using VNA and matched as per the computerized program, which has been explained earlier in section 4.3. Figure 4.8 shows the graphical user interface on the Human-machine interface (HMI) screen, which has been specifically designed for matching the system. It continuously reflects the detector voltage and position of stubs and line stretcher.

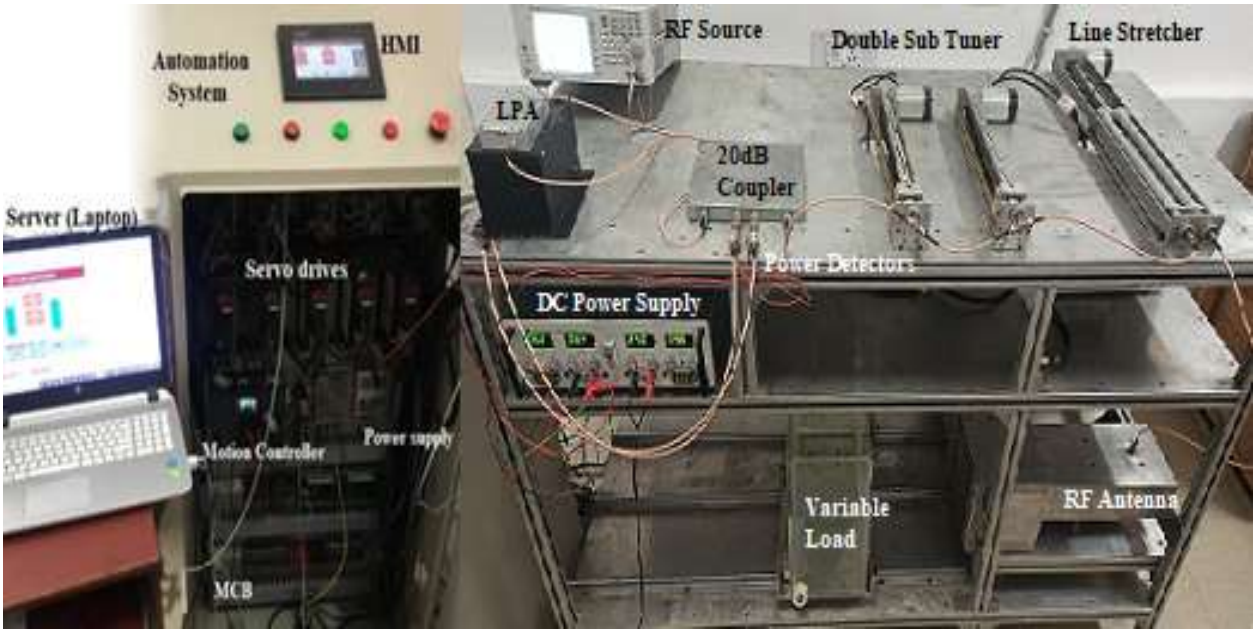

Figure 4.7: Photograph of developed RF matching network.

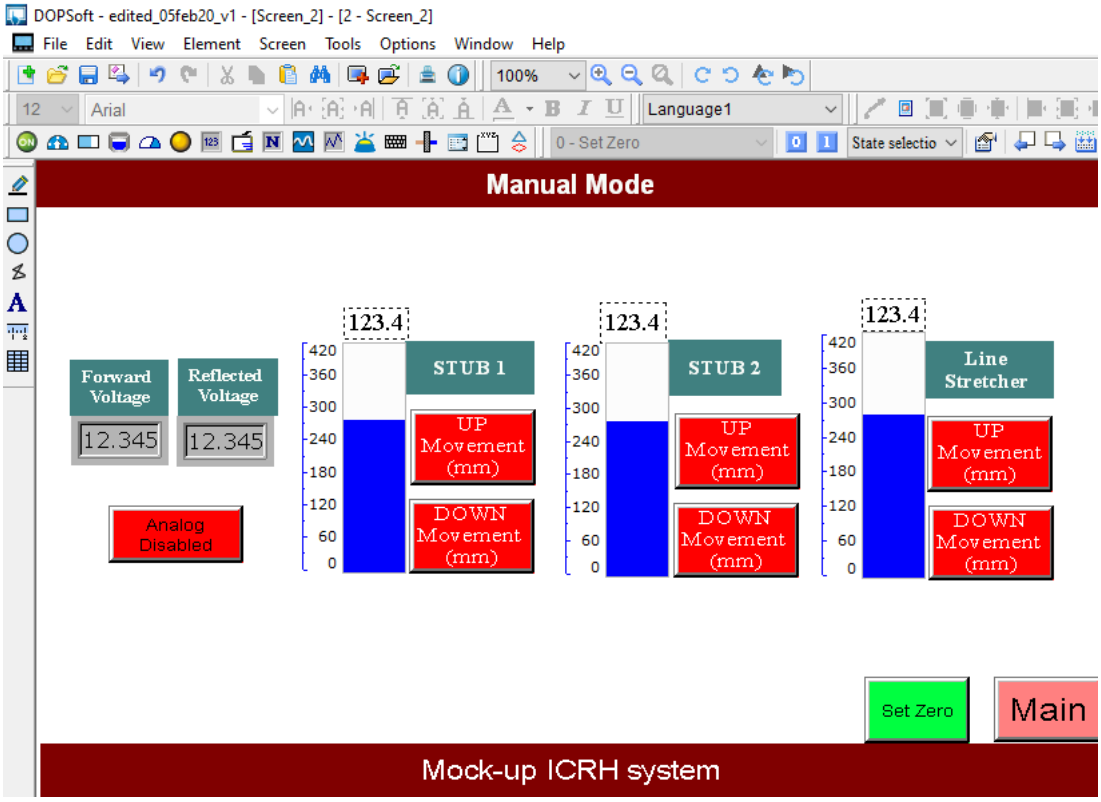

Figure 4.8 Photograph of graphical user Interface for manual matching.

The initial calibration has been tabulated in Table 4.1, which incorporates the measured load impedance before and after matching and the corresponding VSWR, return loss, stub, and line

stretcher positions. The test results are shown in Figure 4.9 (a), Figure 4.9 (b), Figure 4.9 (c) and Figure 4.9 (d), where system response in terms of impedance before and after matching is presented by using the smith chart. The obtained result shows that the developed system is performing as per desired.

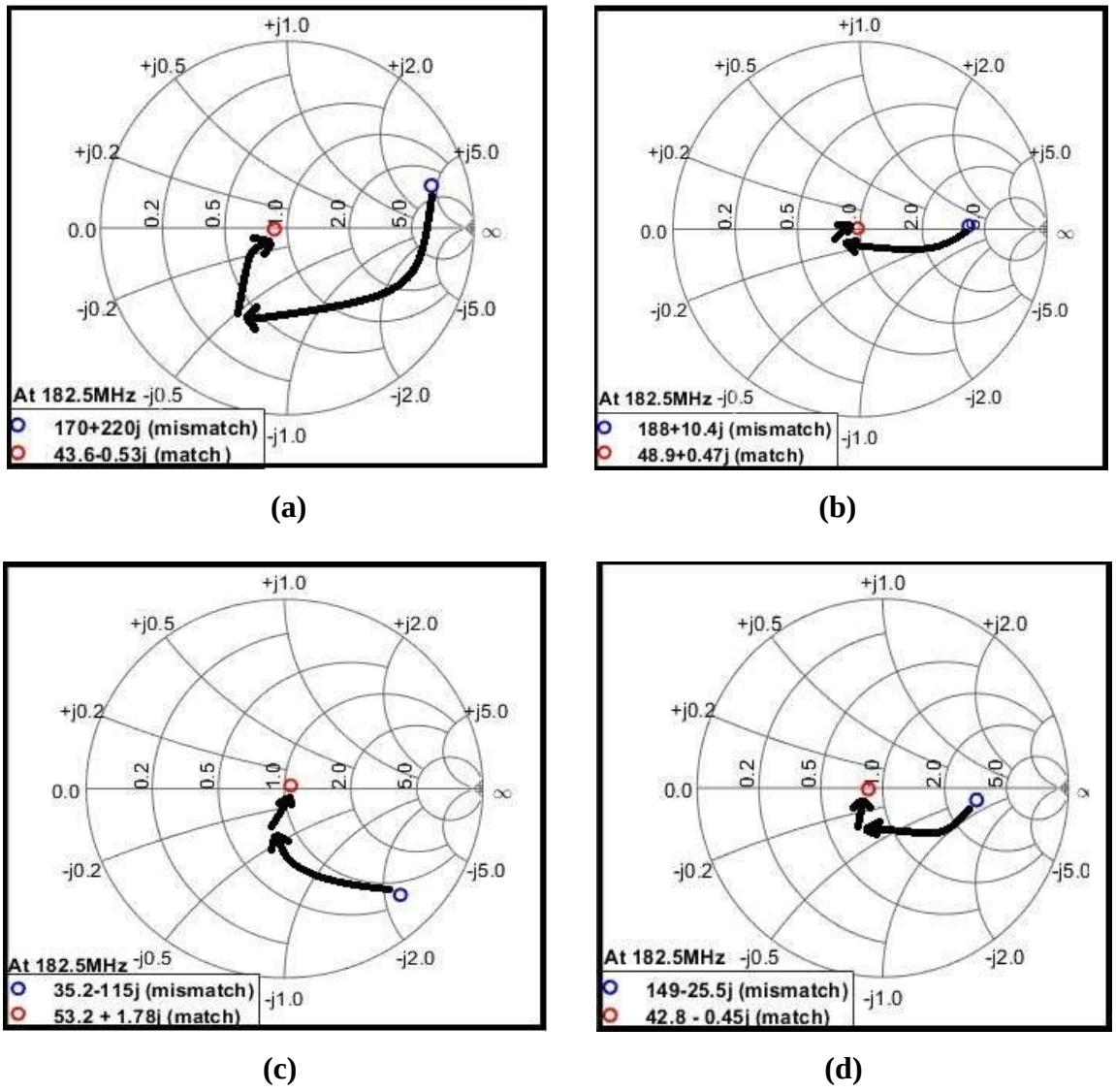

Figure 4.9 (a), (b), (c), (d): Smith chart of system response before and after matching at 182.5 MHz.

Table 4.1: Calibration table.

S. No.	Impedance before matching (Ω)	VSWR	Return Loss (in dB)	Impedance after matching (Ω)	VSWR	Line stretcher (mm)	Double Stub Tuner (mm)	
							Stub 2	Stub 1
1	43.6 - j51.2	2.86	6.30	50.0 - j0.35	1.02	300	240.5	120.5
2	8.91 - j6.27	6.27	2.60	49.2 - j1.34	1.03	150	40	70
3	12.2 - j3.84	4.12	4.30	50.5 - j1.31	1.03	170	50	120
4	8.37 - j8.50	6.22	2.85	49.5 - j0.1	1.01	170	40	150
5	8.39 - j13.6	6.40	2.75	50.8 - j1.03	1.04	140	80	140

In the next step, a signal generator, along with a low power amplifier (LPA) is used as an RF source to excite the system for testing of automatic matching response. The feedback of detectors is used to calculate the mismatch condition and continuously transmits the signal for the movement of line stretcher and stubs until the matched condition is reached out.

Figure 4.10 shows a graphical user interface for an automatic matching network, where a click at the "START" button automatically initiates the matching procedure, and the system automatically stops when the system is matched and displays the mismatch status to "MATCHED".

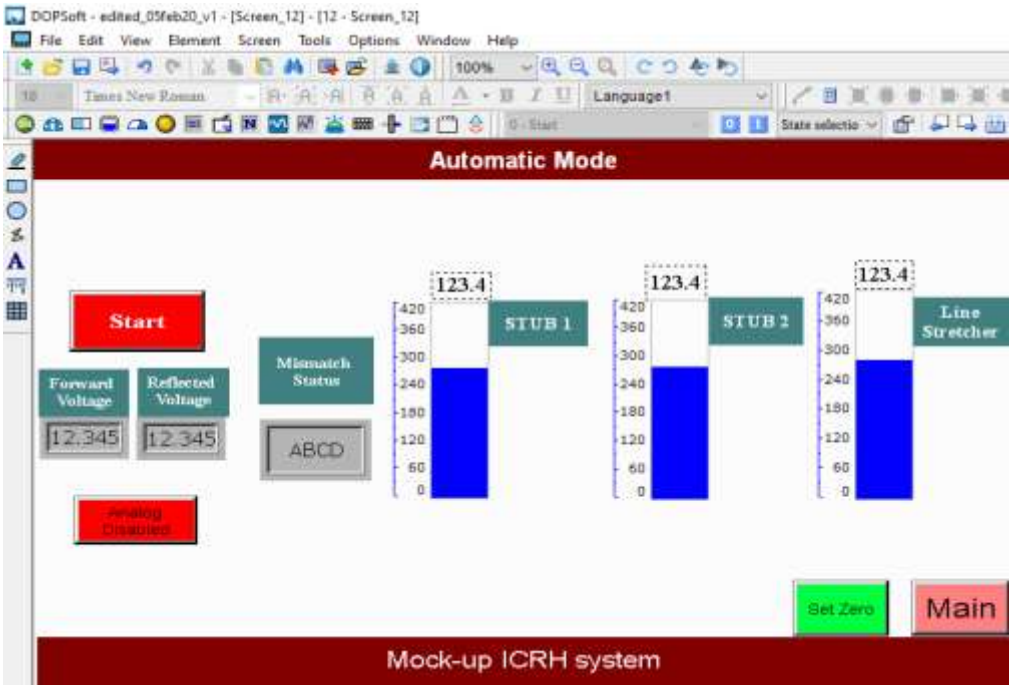

Figure 4.10 Photograph of graphical interface for automatic mode.

The developed system is capable of automatically match any arbitrary load corresponding to VSWR in the range (3.0 to 8.0) within a few 10ms. Test data also have been tabulated in Table 4.2, which shows the VSWR before and after matching, and corresponding stubs and line stretcher positions after matching. The obtained result shows that the system is successfully matched, where VSWR is less than 1.5 after matching.

Table 4.2: Test data before and after matching for automated RF matching network.

Sr. No.	VSWR before matching	Movement of Stub1 length (mm)	Movement of Stub2 length (mm)	Movement of line stretcher length (mm)	VSWR after matching
1	6.21	62.1	142.8	138.4	1.46
2	4.59	38.7	218.4	120.1	1.42
3	6.24	157.4	279.0	94.6	1.48
4	7.24	128.4	145.9	220.4	1.50
5	3.16	55.8	112.1	82.3	1.35
6	5.87	244.2	325.8	175.4	1.46
7	6.52	157.3	314.4	204.6	1.49
8	5.12	98.4	175.2	200.8	1.39
9	3.43	68.9	103.8	88.2	1.41
10	5.21	214.4	282.5	178.6	1.46

4.6. Summary

In this chapter, an automated high power RF matching system has been developed. The automation of a developed matching network is based on the forward and reflected power, which has been detected using power detectors. The detector outputs are utilized to formulate the matched condition, which has been converted into a computer program. The developed matching system is capable of matching any arbitrary load corresponding to VSWR in the range (3.0 to 8.0) within a few 10ms. The developed concept is to be utilized in the development of a mock-up ICRH system of Tokamak. The developed matching system is very robust and simple, which can be used for various applications like RF heating, current drives, sputtering, plasma generation, RADAR, etc. in the RF frequency range.

CHAPTER 5

MOCK-UP OF ICRH SYSTEM

5.1. Overview

This chapter briefly explains the development of a mock-up ICRH system for matching of continuously variable load as in a real system of Tokamak. The mock-up is a prototype of the ICRH system used in SST-1 Tokamak, India, where the components are designed for lower power and five times the scaled frequency ($5 \times 36.5 = 182.5MHz$). The main objective of this chapter is to present the developed mock-up in relation to a real ICRH system of tokamak. The detailed description of the mock-up ICRH system has been given below.

5.2. Layout of mock-up ICRH system

The layout of the proposed mock-up ICRH system is shown in Figure 5.1. The RF source can produce 100 Watt RF power by using a signal generator with LPA. In the ICRH system of Tokamak, RF power from the source is divided into two equal parts using 3dB hybrid coupler and is feed to antennae via matching network. The 3dB coupler also provides essential protection to the RF generator by coupling the reflected power at matched terminated isolated port. The other components of mock-up like a tapped transmission line, directional coupler, power detectors, double stub tuner, line stretcher, service stub, de-coupler, etc. are used for detection and matching. The layout of the mock-up is arranged in a similar way to that of SST-1. A basic matching network has been discussed in earlier chapter-4, which can be appeared like an integrated part of the overall mock-up, as shown in Figure 5.1, where branches of mock-up consist of a double stub tuner arrangement. The water loads are independently placed in front of the antennae to emulate the plasma-like conditions of Tokamak.

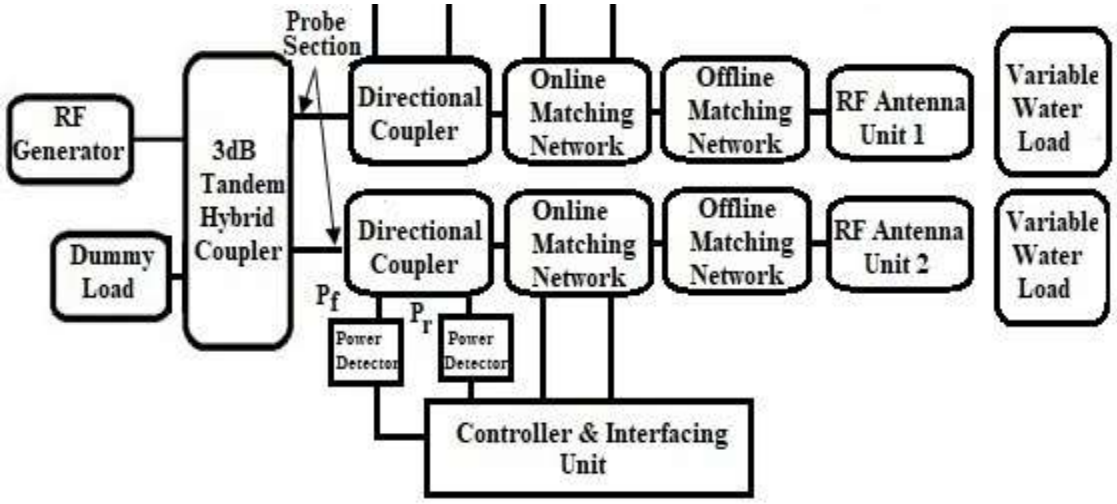

Figure 5.1: Layout of the mock-up ICRH system.

5.3. Real Time Control sequence

The components of mock-up are designed to control in a sequence as per the requirements. The working of each of the components, along with its sequential importance, are discussed herewith in detail.

5.3.1. The 3dB hybrid coupler

In mock-up ICRH system, 3dB hybrid coupler is used as a power divider to feed both RF antennae. It also protects the RF source by coupling of reflected power to isolated port, i.e. terminated with a dummy load. The isolation of reflected power depends on the load impedance, and it is conditional. Therefore, it can also be used as secondary protection other than the applied matching unit which, includes tuners, line stretchers, service stubs, and de-couplers, as shown in Figure 5.2. Working of 3dB hybrid coupler in different loading circumstances is explained as follow:

- In case both the antennae interface passes through a similar mismatched condition, a hybrid coupler completely isolates the generator from reflected power. The similar mismatched means, magnitude, and phase of load impedances are the same, and it is mismatched from the source impedance.
- If both the antenna interface passes through different mismatched load impedances, which are not the same, in this case, reflected power is partially coupled at the isolated port, where the degree of coupling mainly depends on the load values.

- In a particular condition, if both the antenna loads are terminated with the same load magnitude and the reflection phase angle is 90^o out of phase then, the total power is reflected back to the source, which is a major disadvantage of 3dB hybrid coupler. To avoid this condition, a de-coupler arrangement has been utilized to produce a similar phase difference between the antennae, as shown in Figure 5.2. It also reduces the possibility of mutual coupling between the antennae.

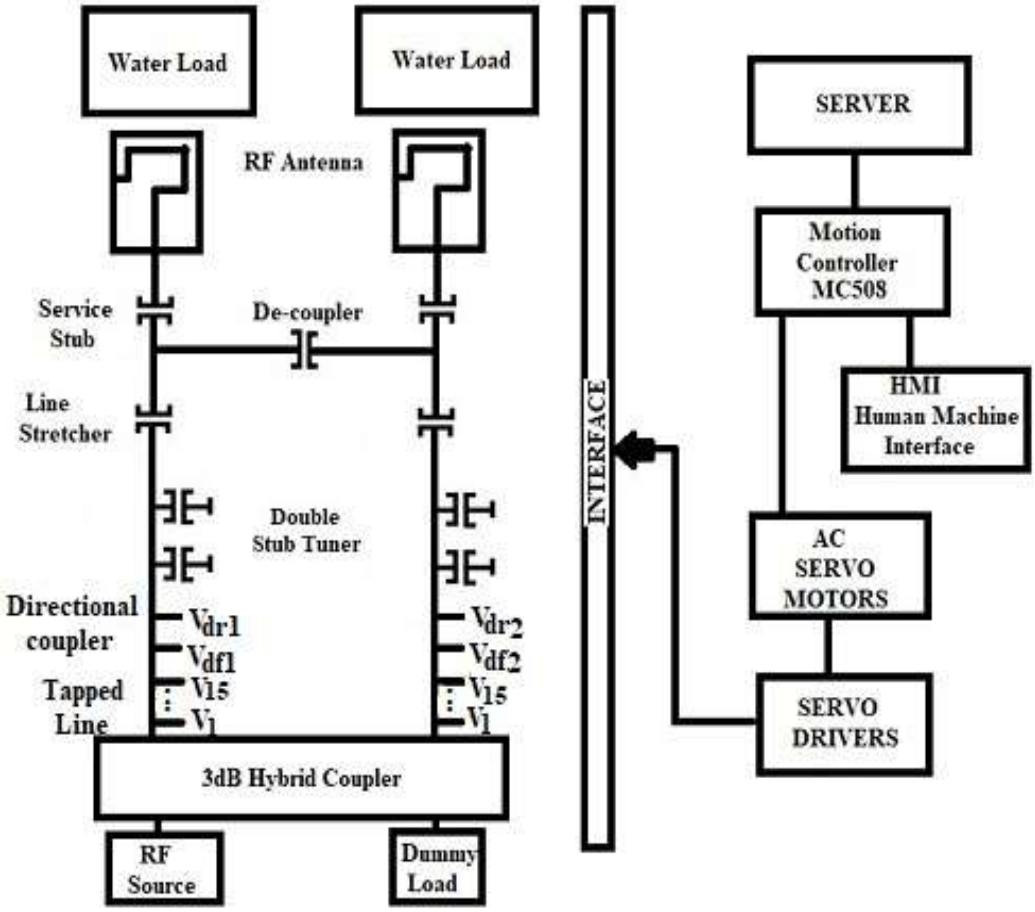

Figure 5.2: Schematic representation of mock-up ICRH system of tokamak.

5.3.2. Detection Control

The mismatching at the antenna load increases the Voltage Standing Wave Ratio (VSWR) in the transmission line, which is detected using the detection unit for analyzing the mismatched condition. The detection unit consists of a tapped transmission line, a directional coupler, and power detectors. The tapped transmission line utilizes 15 probes, which are used to calculate the phase difference between the transmitted and reflected signal. The directional coupler couples the forward and reflected power at two separate ports that are connected to power detectors. The power

detectors sense the magnitude of forward and reflected power in the transmission lines. The detector output has been utilized for the analysis of the VSWR or reflection coefficient (Γ) to match the unknown load condition. VSWR is controlled or lowered in a step by step matching algorithm sequence. Stubs, line stretchers, de-coupler, and service stubs have been utilized with the feedback controller to match the system in the real-time domain. The controller refreshes the detected values after every 2ms time period.

VSWR and reflection coefficient (Γ) is given by

$$VSWR = \frac{1+\sqrt{\left(\frac{P_{dr}}{P_{df}}\right)}}{1-\sqrt{\left(\frac{P_{dr}}{P_{df}}\right)}}, \quad \Gamma = \frac{VSWR-1}{VSWR+1}$$

On the basis of measured Voltage Standing Wave Ratio (VSWR), the matching algorithms take the decision through feedback controller.

- First, a very simple turn by turn approach has been followed for impedance matching where the matching components are adjusted to control the VSWR. In this approach, the stubs and line stretcher either move upward or downward in one by one fixed fashion depending on the VSWR with the motive to decrease the VSWR. The feedback loop works on the principle of generating two outputs, whether to increase or decrease the length of shorted stub till the VSWR approaches 1. This algorithm is very robust for matching.
- Due to long matching time taken by the turn by turn approach for the matching of mock-up ICRH system, an algorithmic approach based on the measured VSWR through both branches has been followed, as discussed in the next section. In this approach, the matching components of both branches are adjusted simultaneously in real-time, depending on the received forward and reflected power.

5.4. Matching algorithm for mock-up ICRH system of Tokamak

An efficient algorithm has been developed for the automated matching network for the mock-up ICRH system of Tokamak. Its flow chart is shown in Figure 5.3. It includes many steps, and each step is assigned for the specific task, which can be understood using the flow chart.

Steps of the flowchart are defined as follows:

Step 1. This step initializes the system and checks the response from all devices connected to the system. It also ensures that the system is ready for the next step.

Step 2. In this step, the magnitude of forward and reflected power has been measured.

Step 3. On this basis of measured forward and reflected power data, VSWR or reflection coefficient has been analyzed for three conditions for both the branches which are described as given:

Condition 1: If $VSWR \leq 1.5$ or $\Gamma \sim 0$, this means the system is matched, and the matching components remain at the same position.as

Condition 2: If $1.5 < VSWR \leq 2$ or $\Gamma < 0.33$, this means the system is mismatched, where the reflected power is less than 12%. For this condition, the program generates an instruction to start the matching process. Here, the double stub and line stretcher initiate the matching process as per the developed hypothesis explained in chapter 4 and are moved simultaneously towards the matching point. Once the system is matched, the controller sends a request to stop the matching process. The controller refreshes the detected values after every 2ms time period.

Condition 3: If $VSWR > 2$ or $\Gamma > 0.33$, this means the reflected power greater than 12%. In this case, the system is mismatched, and at first, the system will check the reflection phase angle of two branches using tapped transmission line. If the antenna loads at both branches are out of phase, then a de-coupler arrangement has been utilized to match the phase between both the branches along with double stub, line stretcher hypothesis to achieve the matching point. If the antenna loads are in phase to each other than the condition 2 hypothesis has been utilized to achieve matching.

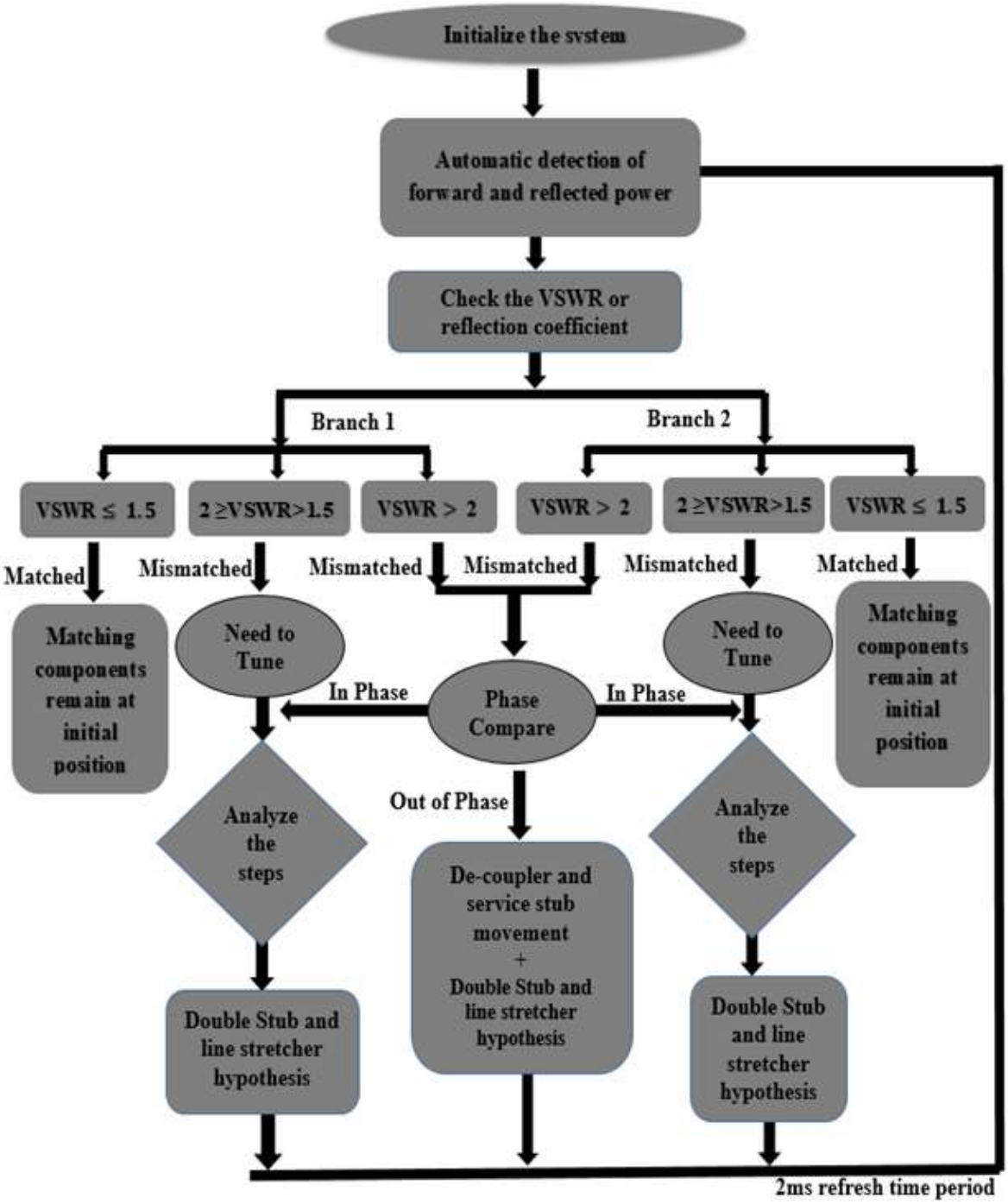

Figure 5.3: Flowchart for mock-up ICRH system of tokamak.

5.5. Automated mock-up ICRH system

The photograph of the fully developed mock-up ICRH system of the Tokamak is shown in Figure 5.4. Here, the mock-up system supplies RF power using a combination of signal generator with LPA. The 3dB coupler is used to divide equal RF power in both the branches. Each branch consists of the directional coupler, power detectors, tapped transmission line, double stub tuner, line stretcher, de-coupler between the branches, service stub, RF antenna, and variable water load. The developed components are integrated using coaxial cable (RG142). Input/ output connectors for each component are designed in such a way that it can be easily changed from BNC to N-type and vice-versa as per the power requirements. Initially, the system is tested using a Vector network analyzer (VNA) and matched as per the developed algorithm. The set-up has been calibrated for the various load positions where the sliding water bucket load is moved in 100mm steps, and the impedance values are measured using VNA.

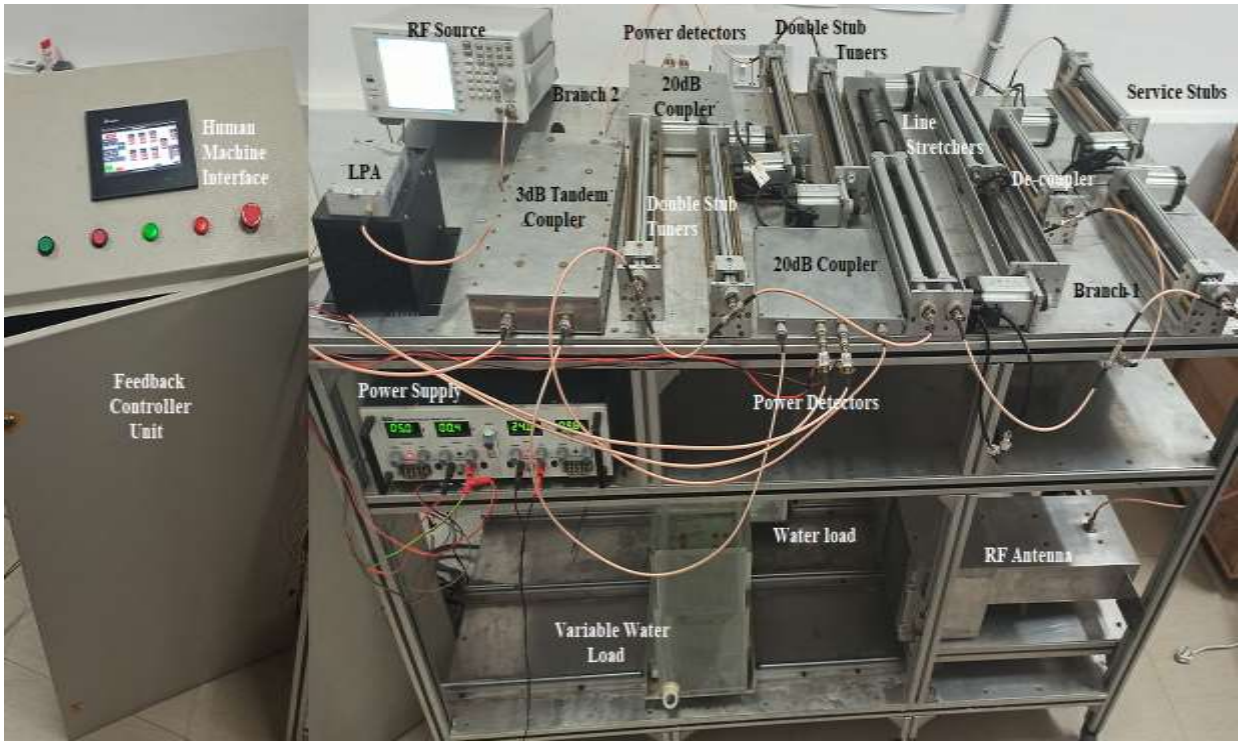

Figure 5.4: Photograph of mock-up ICRF matching network on test bench.

Figure 5.5 shows the graphical user interface on the HMI screen, which has been specifically designed for matching the mock-up ICRH system. The "START" button automatically initializes the mock-up ICRH system. The position of stub tuners, line stretchers, and the detector voltages are continuously reflected on the graphical user interface. The controller refreshes the display

output after every 2ms time period and shows the mismatch status every time, whether the system is matched or mismatched. If the system gets matched, the controller automatically sends a request to stop the movement of motorized stubs and line stretchers.

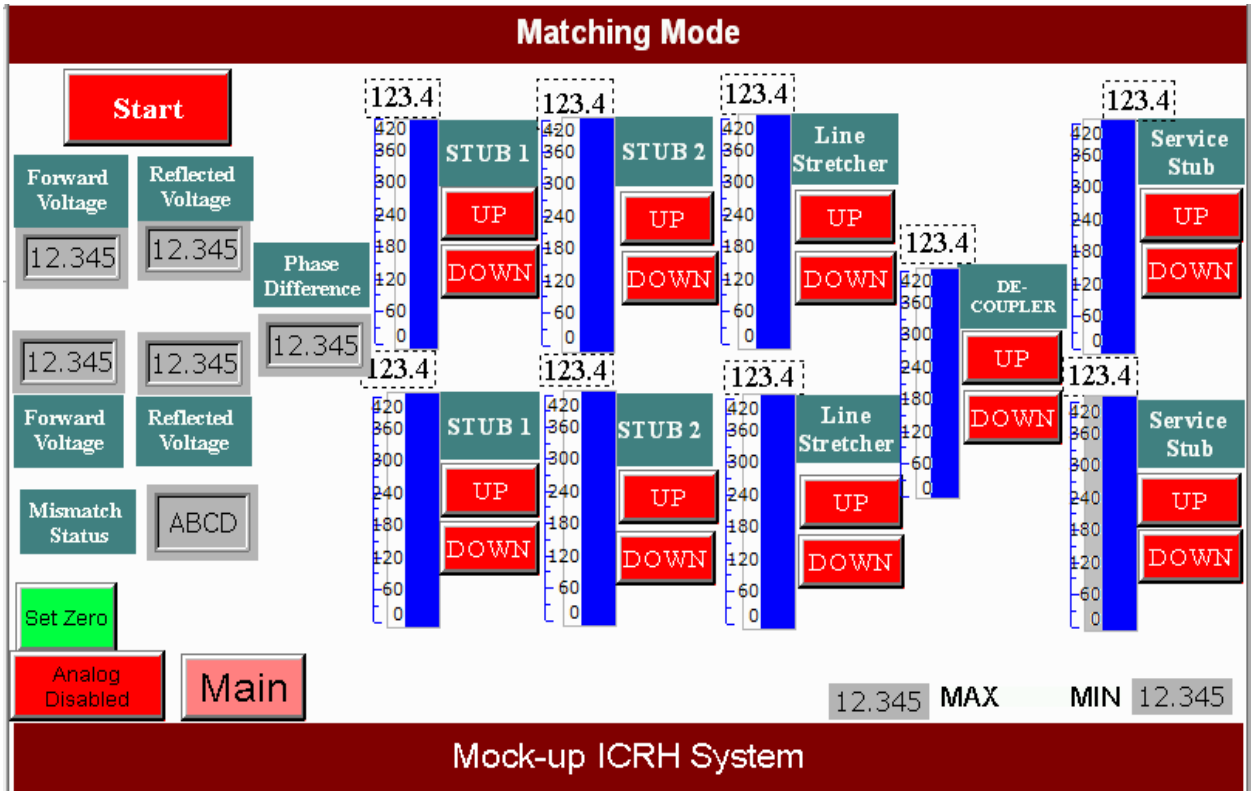

Figure 5.5: Graphical user interface for mock-up ICRH system.

The initial calibration has been tabulated in Table 5.1, which incorporates the measured load impedance before, and after matching and the corresponding VSWR, return loss, stubs, line stretchers, and service stubs positions. The obtained result shows that the developed mock-up system is performing as per desired.

Table 5.1: Calibration table for mock-up system.

							BRNACH 1				BRANCH 2			
S. No.	**Impedance before matching (Ω)**	**VSWR**	**Return Loss (in dB)**	**Impedance after matching (Ω)**	**VSWR**	**De-coupler position**	**Line stretcher (mm)**	**Double Stub Tuner (mm) Stub 1**	**Stub 2**	**Service Stub (mm)**	**Line Stretcher (mm)**	**Double Stub Tuner (mm) Stub 1**	**Stub 2**	**Service Stub (mm)**
1	49.2+j39.8	2.20	8.58	50.2-j2.08	1.04	49.6	240.4	210.1	150.8	52.6	210.1	320.2	90.5	110.8
2	17.6-j9.85	2.96	6.10	48.8-j0.19	1.02	104.2	270	150.2	245.5	90.1	110.5	80.4	320.6	42.3
3	21.2-j14.4	2.63	6.99	51-j2.91	1.07	90.4	290.3	190.6	198.4	41.6	171.9	263.6	272.9	80.5
4	88.1+j5.87	1.77	11.30	48.9+j0.44	1.02	--	224.4	147.9	85.9	--	173.8	162.0	256.1	--
5	83.4-j57.8	2.70	6.78	45.7+j0.12	1.09	40.3	284.7	257.2	179.2	247.3	120.5	110.3	160.9	256.4
6	85.2-j19.7	1.84	10.6	47.0+j1.05	1.07	--	242.5	90.2	63.5	--	80.4	240.6	108.1	--
7	17.0-j25.9	3.81	4.68	45.8-j0.46	1.09	82.2	82.4	113.4	190.1	30.2	251.9	155.1	203.2	45.2

In the next step, a signal generator and low power amplifier (LPA) are used as an RF source to excite the system for testing automatic matching response. The developed system is tested at 182.5MHz. The feedback of detectors are used to calculate the mismatch condition and continuously transmits the signal for the movement of matching components until the matched condition is reached out. The developed system is capable of automatically match any arbitrary load corresponding to VSWR in the range 1.5 to 5.0 within a few 10ms. Test data also have been tabulated in Table 5.2, which shows the VSWR before and after matching and the position of stubs, line stretcher, service stubs, and de-coupler position for both branches after matching. The obtained result shows that the system is successfully matched.

Table 5.2: Test data before and after matching.

		BRANCH 1						BRANCH 2				
Sr. No.	**VSWR before matching**	**Position of Stub1 (mm)**	**Position of Stub2 (mm)**	**Line stretcher (mm)**	**Position of Service Stub (mm)**	**Position of de-coupler**	**VSWR after matching**	**Position of Stub1 (mm)**	**Position of Stub2 length (mm)**	**Line Stretcher (mm)**	**Service Stub (mm)**	**Total Time taken (msec)**
1	2.34	200.5	150.6	114.2	66.8	46.2	1.48	215.6	124.6	148.2	92.3	118
2	3.12	144.6	128.5	120.6	42.6	85.6	1.42	145.6	203.5	204.6	118.5	136
3	2.74	130.5	65.5	178.5	40.3	115.2	1.35	195.0	148.9	102.9	85.4	89
4	4.62	215.9	147.5	247.2	74.2	145.7	1.49	178.2	258.1	285.6	106.4	169
5	1.96	98.2	72..3	112.8	--	--	1.39	103.5	85.4	155.6	--	69
6	3.56	178.6	254.2	198.6	96.2	200.5	1.43	165..4	241.1	214.9	69.3	135
7	1.85	121.3	149.8	95.1	--	--	1.35	147.5	114.6	145.2	--	76

5.6. Summary

In this chapter, a mock-up ICRH system for matching of the continuously variable load has been developed as in a real system of tokamak like SST-1. A computational program has been developed with a defined control sequence to control detectors and matching components used in mock-up as per desired. The developed program has been tested for optimum speed. The developed matching system is capable of matching any arbitrary load within a few 10ms. The developed matching system is very robust and simple, which can be used for various applications in the field of satellite communication, radar technology, RF heating, current drives, sputtering, plasma generation, fusion engineering, navigation, etc.

CHAPTER 6

CONCLUSION AND FUTURE SCOPE

6.1. Conclusion

This thesis presents the development of load resilient mock-up ICRH system of Tokamak. The ICRH system is used in Tokamak for heating of plasma in order to get the fusion reaction. Since plasma offers the variable load impedance, the ICRH system requires a real-time RF matching network to match the load variation with source impedance. Although load variations are very fast that may be in the order of few milliseconds. So, the required matching network need to be very fast. The work presented in the thesis is mainly based on the development of RF equipment that can be easily upgradable to MW power handling capability and also integrate these into a prototype to test the matching techniques to achieve the optimum matching speed. The prototype is rated for low power handling capability (100 W) and scaled up to five times of ICRH frequencies, i.e. ranging from 22-91 MHz. Mock-up of RF matching network consists of various RF components, such as 3dB coupler, directional couplers (dual directional coupler, 20dB coupler), stub tuners, line stretchers, service stubs, RF antennae, and variable water load. Work in the initial stage mainly focused on the theoretical analysis and exploration of new ideas in the development of RF components and matching techniques. The design, fabrication, and testing of each component of mock-up in the frequency range of 170-190 MHz have been carried out at an intermediate stage. The developed components have been integrated on a test bench finally and tested by implementing matching concepts developed to achieve the load resilient behavior of mock-up. The developed components have wide applications other than the fusion tokamak such as telecommunication, defense, and electronic warfare, aerospace, satellite, and navigation systems.

Summary

The major achievements of the thesis can be summarized as follows,

1. The components of the mock-up ICRH system have been developed for 170-190 MHz frequency and 2kW power handling capability, which has broad application scope ranging from communication to defense. These components are designed in such a way that they can be upgradable up to MW power handling capability in any frequency range within HF, VHF, and UHF. Each of the components has been indigenously developed and tested for the desired

output. Brief description of the components has been developed under the thesis is given as follow:

- ***Hybrid coupler*:** 3dB hybrid coupler is a device that is broadly used as a combiner or divider in an RF/microwave network. The developed coupler is developed for 155-225 MHz and 2kW power handling capability. The developed coupler is very robust, easier in fabrication, and can be utilized in many plasma related experiments, radar, and satellite applications in HF, VHF, and UHF range.
- ***RF Antenna:*** The developed RF antenna for the mock-up ICRH system is designed at 182.5MHz for 2kW power handling capability. Its design is based on the CRLH-TL unit cell, where the parameters of the unit cell are decided by the dimension of the shorted loop. The development process of antenna involves a theoretical analysis which can be applied for the development of high power RF antenna for the heating purposes in Tokamak.
- ***Directional couplers:*** In the presented work, the development of variable and fix type directional coupler has been presented, which are applicable in the frequency range of HF, VHF, and UHF. The directional coupler is broadly used in the RF network to couple the forward and reflected power to analyze the system response. The developed couplers are in simple design and construction.
- ***Stub Tuner:*** Tuners are broadly used in the RF network to match the RF system. The work presented in the thesis imparts the indigenous development of feedback-controlled coaxial line based high-speed tuner. It has the capability to move its entire quarter wavelength within 100msec.
- **Line stretcher:** Line stretchers are used for phase matching in the RF circuit. It introduces the required phase shift by changing the length of the transmission line. The rigid coaxial line based line-stretcher has been developed in the frequency range of 50-250 MHz and has 2kW power handling capability and can be upgradable up to MW power handling capability in any frequency range within HF, VHF, and UHF.

2. The development of a load resilient matching network for 100 W power handling capability and upgradeable up to MW is presented. The developed matching network is capable of matching any load variation corresponding to VSWR in the range 1.5 to 8.0 in a few milliseconds. The system is directly applicable for RF matching in the area of telecommunications, broadcasting, small plasma related experiment, etc.

3. A computational program has been developed with a defined control sequence to control detectors and matching components used in mock-up as desired. The developed program has been tested for optimum speed. The detailed analysis about the control and matching sequence has been presented in the thesis, which is useful for similar work.

6.2. Future Scope

- The work presented in the thesis is directly associated with RF heating in Tokamak, which is a controlled reactor for future energy generation. It is a cutting edge of research with wide research scope. The developed mock-up has been tested for matching unknown load in a few milliseconds, which is desired in the real ICRH system of Tokamak. In advance stage, the developed matching technique can be applied directly in the real ICRH system of the Tokamak.
- The matching speed of the drive-based stub tuner is limited up to a certain extent, and the speed of the overall matching network cannot be achieved faster than a few milliseconds. Therefore, for better speed, the ferrite based stub tuner can be used.
- The developed RF antenna is rated for 2kW power handling capability that can be upgraded up to the MW level by using multiple radiating straps, which can be applied in the real ICRH system of Tokamak.
- The components of mock-up can be directly used in small plasma related experiments and can be tested for its matching speed.
- The developed components can also be used in High power RF networks in the field of satellite communication, radar technology, fusion engineering, navigation, etc.

REFERENCES

[1] "Energy policy of India", *En.wikipedia.org.* [online] Available at: https://en.wikipedia.org/wiki/Energy_policy_of_India [Accessed 11th March 2017].

[2] "Nuclear Fusion Basics", *Iaea.org.* [online] Available at: https://www.iaea.org/newscenter/news/nuclear-fusion-basics [Accessed 12 Sep. 2016].

[3] N. Valerie Jamieson, "ITER: A brief history of fusion", *New Scientist.* [online] New Scientist. Available at: https://www.newscientist.com/article/dn17952-iter-a-brief-history-of-fusion/ [Accessed 12 Sep. 2016].

[4] "Tokamak", *En.wikipedia.org.* [online] Available at: https://en.wikipedia.org/wiki/Tokamak [Accessed 2 Oct. 2016].

[5] D. Bora *et al*., "Ion cyclotron resonance heating system on Aditya," *Sadhana*, vol. 30, no. 1, pp. 21-46, Feb. 2005.

[6] D. Bora *et al.,* "Cyclotron resonance heating systems for SST-1," *Nuclear fusion*, vol. 46, no. 3, pp. S72-S84, Feb. 2006.

[7] D. Rathi, R. Singh and S. V. Kulkarni, "Design, fabrication and testing of pressurized co-axial directional coupler for high RF power measurements for SST-1 ICRH system," *International Conference on Recent Advances in Microwave Theory and Applications*, Jaipur, India, 2008, pp. 590-592.

[8] M. S. Parihar, *et al.* "Testing and Optimization of Matching Response Time for the Real Time Feedback Controlled ICRH-Automatic Matching Network (AMN) System for SST-1," IPR Technical Report, Nov. 2007.

[9] R. Joshi, ICRH-RF Group *et al.*, "Automatic impedance matching network for ICRH-RF experiments on SST-1," in *23rd National symposium on Plasma Science and Technology, Journal of Physics: Conference Series* 208 (2010) 012015.

[10] S. Pradhan et al., "The first experiments in SST-1," *Nuclear Fusion*, vol. 55, no. 10, p. 104009, June. 2015.

[11] S. K. Mishra, S. Misra and M. Sodha, "Charging and de-charging of dust particles in bulk region of a radio frequency discharge plasma", *Physics of Plasmas*, vol. 20, no. 3, p. 033705, 2013.

[12] R. Joshi, ICRH-RF Group *et al.*, "Online impedance matching system for ICRH-RF experiments on SST-1 tokamak," *Fusion Engineering and Design*, vol. 100, pp. 293-300, Nov. 2015.

[13] R. Joshi *et al*., "Integration of PLC based offline impedance matching system for ICRH experiments," in *International Conference on Contemporary Computing and Informatics (IC3I),* Noida, India, 2016, pp. 564-567.

[14] R. P. Yadav, Ph.D. thesis, Institute for Plasma Research (IPR), 2014.

[15] A. C. England, "Electron cyclotron heating experiments in tokamaks and stellarators," *IEEE transactions on plasma science*, vol.12, no. 2, pp. 124-133, Jun. 1984

[16] R. H. Goulding *et al.*, "The ORNL fast-wave ICRF antenna for Alcator C-MOD," *IEEE Thirteenth Symposium on Fusion Engineering*, Konxville, TN, USA, 1989, pp. 215-220.

[17] Y. Takase *et al.*, "Engineering design and analysis of the Alcator C-MOD two-strap ICRF antenna," in *IEEE/NPSS Symposium Fusion Engineering*, San Diego, CA, USA: 1991, pp. 118-121.

[18] A. Parisot, M.Sc. thesis, Massachusetts Institute of Technology (MIT), 2004.

[19] Y. Lin, A. Binus and S. J. Wukitch, "Real-time fast ferrite ICRF tuning system on the Alcator C-Mod tokamak," *Fusion Engineering and Design*, vol. 84, no. 1, pp. 33-37, Jan. 2009.

[20] Y. Lin *et al*., "ICRF antenna matching system with ferrite tuners for the Alcator C-Mod tokamak," in *AIP Conference Proceedings*, California, USA, 2015, pp. 0700091-0700094.

[21] S. N. Golovato *et al.*, "Antennas for ICRF heating in the Alcator C-Mod tokamak," *IEEE/NPSS Symposium on Fusion Engineering*, Hyannis, MA, USA, 1993, pp. 1069-1072.

[22] Y. Takase *et al.*, "Alcator C-Mod ICRF antenna design and analysis," *IEEE Symposium on Fusion Engineering*, Knoxville, TN, USA, 1989, pp. 211-214.

[23] F. Hofmeister, F. Braun and F. Wesner, "The RF system and matching procedure for ASDEX and ASDEX Upgrade," *Fusion engineering and design*, vol. 24, no. 1-2, pp. 83-89, Feb. 1994.

[24] M. Prechtl *et al.,* "Theory of dynamic matching with adjustable capacitors for the ICRF system of ASDEX upgrade," *Fusion engineering and design,* vol. 84, no. 7-11, pp. 1539-1543, June 2009.

[25] J. M. Noterdaeme *et al.*, "Matching to ELMy plasmas in the ICRF domain," *Fusion Engineering and Design*, vol. 74, no. 1-4, pp. 191-198, Nov. 2005.

[26] Křivská A. Antenna modelling for ion cyclotron resonant heating of tokamak plasmas. Ph.D. Thesis, Czech technical University, Prague, 2013.

[27] W. M. Manheimer, “Electron cyclotron heating of tokamaks”, in *Infrared and Millimeter Waves: Instrumentation,* K. Button, Ed. New York: Academic Press, New York: Academic Press, 2014, p. 299.

[28] J. Jacquinot *et al.,* “ICRF studies on JET,” *Plasma Physics and Controlled Fusion,* vol. 28, no. 1A, pp. 1-15, Jan. 1986.

[29] D. J. Campbell *et al*., “Stabilization of sawteeth with additional heating in the JET tokamak,” *Physical review letters,* vol. 60, no. 21, p. 2148, May 1988.

[30] R. C. Walton *et al*., “Mechanical design of the ICRH antenna for JET-EP,” in *Symposium on Fusion Engineering*,” Atlantic City, NJ, USA: 2002, pp. 103-106.

[31] ML Mayoral JET-EFDA contributors et al., “Hybrid couplers on the JET ICRF system commissioning and first results on ELMs,” *AIP Conference Proceedings,* 2007, pp. 143-146.

[32] F. Durodié *et al.*, “Commissioning of the ITER-like ICRF antenna for JET,” *Fusion Engineering and Design,* vol. 84, no. 2-6, pp. 279-283, Jun. 2009.

[33] M. Graham *et al*., “Implementation of load resilient ion cyclotron resonant frequency (ICRF) systems to couple high levels of ICRF power to ELMy H-mode plasmas in JET,” *Plasma Physics and Controlled Fusion,* vol. 54, no. 7, p. 074011, Jun. 2012.

[34] I. Monakhov *et al*., “Design and operations of a load-tolerant external conjugate-T matching system for the A2 ICRH antennas at JET,” *Nuclear Fusion,* vol. 53, no. 8, p. 083013, Jul. 2013.

[35] D. J. Hoffman**, “**The design of high-power ICRF antennas for TFTR and Tore Supra,” *AIP Conference Proceeding,* Kissimmee, USA, 1987, pp. 302-305.

[36] K. Vulliez, and A. Argouarch *et al.,* “Validation of the load-resilient ion cyclotron resonance frequency antenna concept on Tore Supra plasmas”, *Nuclear fusion* vol. 48, no. 2008, p. 065007, Apr. 2008.

[37] M. Vervier *et al.*, “Tests and matching analysis of a load resilient ICRH antenna on TEXTOR,” *Fusion engineering and design,* vol. 74, no. 1-4, pp. 377-383, Nov. 2005.

[38] A. Messiaen *et al*., “Realisation of a test facility for the ITER ICRH antenna plug-in by means of a mock-up with salted water load,” *Fusion engineering and design,* vol. 74, no. 1-4, pp. 367-375, Nov. 2005.

[39] P. U. Lamalle *et al*., “Recent developments in ICRF antenna modelling,” *Nuclear fusion,* vol. 46, no. 4, pp. 432-443, Feb. 2006.

[40] A. Messiaen *et al.*, "Study of the ITER ICRH system with external matching by means of a mock-up loaded by a variable water load," *Nuclear fusion*, vol. 46, no. 7, pp. S514-S539, Jun. 2006.

[41] P. Dumortier *et al.*, "Tests of load resilient matching procedure for the ITER ICRH system on a mock-up and layout proposal," *Fusion Engineering and Design*, vol. 82, no. 5-14, pp. 758-764, Oct. 2007.

[42] A. Messiaen *et al*., "Preparing ITER ICRF: development and analysis of the load resilient matching systems based on antenna mock-up measurements," *Nuclear Fusion*, vol. 49, no. 5, p. 055004, Apr. 2009.

[43] P. Dumortier *et al*., "RF optimization of the ITER ICRF antenna plug including its broad banding by a service stub," *Fusion Engineering and Design*, vol. 84, no. 2-6, pp. 707-711, Jun. 2009.

[44] B. Beaumont *et al.*, "ITER ICRF system: R&D progress and technical choices," in *IEEE/NPSS Symposium on Fusion Engineering*, San Diego, USA, 2009, pp. 1-4.

[45] P. Dumortier and A. M. Messiaen, "ICRH Antenna Design and Matching," *Fusion Science and Technology*, vol. 57, no. 2010, pp. 230-238, Feb. 2010.

[46] A. Messiaen and R. Weynants, "ICRH antenna coupling physics and optimum plasma edge density profile. Application to ITER," *Plasma Phys. Control. Fusion*, vol. 53, no. 2011, p. 085020, Jun. 2011.

[47] D. Grine *et al.*, "Summary and results of the study of the hybrid matching option implementation of the ITER ICRH system," *Fusion Engineering and Design*, vol. 87, no. 2, pp. 167-178, Feb. 2012.

[48] M. Vervier *et al.*, "Technical optimization of the ITER ICRH decoupling and matching system," *Fusion engineering and design*, vol. 88, no. 6-8, pp. 1030-1033, Oct. 2013.

[49] H. J. Kim *et al.*, "RF design and tests on a broadband, high-power coaxial quadrature hybrid applicable to ITER ICRF transmission line system for load-resilient operations," *Fusion Engineering and Design*, vol. 96, pp. 498-502, Oct. 2015.

[50] A. Jain A, R. P. Yadav, and S. V. Kulkarni, "Design and development of 2 kW, 3 dB hybrid coupler for the prototype Ion Cyclotron Resonance Frequency (ICRF) system," *International Journal of Microwave and Wireless Technologies*, vol. 11, no. 1, pp. 1-6, Feb. 2019.

[51] H. J. Kim *et al*., "Ultra-wideband coaxial hybrid coupler for load resilient ion cyclotron range of frequency heating at fusion plasmas," *Applied Physics Letters*, vol. 100, no. 26, p. 263506, Jun. 2012.

[52] K. Song *et al*., "Ultra-wideband (UWB) power divider with filtering response using shorted-end coupled lines and open/short-circuit slotlines," *AEU-International Journal of Electronics and Communications*, vol. 67, no. 6, pp. 536-539, 2013.

[53] H. J. Kim *et al.*, "RF design and tests on a broadband, high-power coaxial quadrature hybrid applicable to ITER ICRF transmission line system for load-resilient operations," *Fusion Engineering and Design*, vol. 96, pp. 498-502, Oct. 2015.

[54] R. P. Yadav, S. Kumar and S.V. Kulkarni, "Design and development of 3 dB patch compensated tandem hybrid coupler", *Review of Scientific Instruments*, vol. 84, no. 1, p. 014702, 2013.

[55] R. P. Yadav, S. Kumar and S.V. Kulkarni, "Design and development of ultra-wideband 3 dB hybrid coupler for Ion cyclotron resonance frequency heating in tokamak", *Review of Scientific Instruments*, vol. 85, no. 4, p. 044706, 2014

[56] R. P. Yadav, S. Kumar, and S.V. Kulkarni, "Design of the 1.5 MW, 30-96 MHz ultra-wideband 3 dB high power hybrid coupler for Ion Cyclotron Resonance Frequency (ICRF) heating in fusion grade reactor," *Review of Scientific Instruments*, vol. 87, no. 1, p. 014703, Jan. 2016.

[57] A. Jain, Anurag and R. P. Yadav, "Design and Development of Coaxial Line Based 2kW, 10-30dB Variable Dual Directional Coupler," *2017 IEEE MTT-S International Microwave and RF Conference (IMaRC)*, Ahmedabad, 2017, pp. 1-5.

[58] A. Jain, R. P. Yadav and S. Kumar, "Design and development of high power variable dual-directional radio frequency coupler," in *IET Microwaves, Antennas & Propagation*, vol. 13, no. 14, pp. 2544-2550, 2019.

[59] W. L. Firestone, "Analysis of transmission line directional couplers," *Proceedings of the IRE*, vol. 42, no. 10, pp. 1529-1538, Oct. 1954.

[60] B. M. Oliver, "Directional electromagnetic couplers," *Proceedings of the IRE*, vol. 42, no. 11, pp. 686-92, Nov. 1954.

[61] R. F. Schwartz, P. J. Kelly and P. P. Lombardini, "Criteria for the design of loop-type directional couplers for the L band," *IRE Transactions on microwave theory and techniques*, vol. 4, no. 4, pp. 234-239, Oct. 1956.

[62] S. B. Cohn and R. Levy, "History of microwave passive components with particular attention to directional couplers," *IEEE Transactions on Microwave Theory and Techniques*, vol. 32, no. 9, pp. 1046-1054, Sep. 1984.

[63] C. S. Kim *et al*., "A design of the novel varactor tuned directional coupler," in *IEEE MTT-S International Microwave Symposium Digest,* Anaheim, CA, USA, 1999, pp. 1725-1728.

[64] L. Marcaccioli *et al*., "Design of a broadband MEMS-based reconfigurable coupler in Ku-band," in *European Microwave Conference,* Amsterdam, The Netherlands, 2008, pp. 595-598.

[65] T. Lehmann, H. Mextorf and R. Knoechel, "Design of quadrature directional couplers with continuously variable coupling ratios," in *European Microwave Conference,* Amsterdam, Netherland, 2008, pp. 199-202.

[66] G. Singh, R. P. Yadav, V. Janyani,"Multimode Interference (MMI) coupler based all optical switch: Design, applications & performance analysis", *Int. Journal on Communication* Vol. 1, pp. 9-13, 2010.

[67] L. K. Yeung, "A compact directional coupler with tunable coupling ratio using coupled-line sections," in *Asia-Pacific Microwave Conference,* Melbourne, VIC, USA, 2011, p. 1730-1733.

[68] B. Hur, and W. R. Eisenstadt, "Tunable broadband MMIC active directional coupler," *IEEE Transactions on Microwave Theory and Techniques,* vol. 61, no.1, pp. 168-176, Dec. 2012.

[69] R. Keshavarz, M. Movahhedi, and A. Abdipour, "A broadband and compact asymmetrical backward coupled-line coupler with high coupling level," *AEU-International Journal of Electronics and Communications*, vol. 66, no. 7, pp. 569-574, Jul. 2012.

[70] V. Sarode, K. P. Ray and S. Krishnan, "Parametric study of microwave high power waveguide dual directional coupler," *International Journal of Industrial Electronics and Electrical Engineering,* vol. 4, pp. 38-41, 2016.

[71] R. A. Soares, D. Los Reyes, and J. Guena, "Design of K-band slug tuners," *IEE Proceedings H-Microwaves, Optics and Antennas*, vol. 128, no. 3, pp. 146-150, Jun. 1981.

[72] H. D. Schwarz HD, "Development of a movable plunger tuner for the high-power RF Cavity for the PEP-II B Factory," *In Proceedings of Particle Accelerator Conference*, Vancouver, USA, 1997, pp. 3039-3041.

[73] R. Kumazawa *et al.*, "Liquid stub tuner for ion cyclotron heating," *Review of scientific instruments*, vol. 70, no. 6, pp. 2665-2673, Jun. 1999.

[74] J. Papapolymerou *et al*., "Reconfigurable double-stub tuners using MEMS switches for intelligent RF front-ends," *IEEE transactions on microwave theory and techniques*, vol. 51, no. 1, pp. 271-278, Jan. 2003.

[75] Q. Chengming *et al.*, "Design of a new type of stub tuner in ICRF experiment," *Plasma Science and Technology*, vol. 5, no. 3, pp. 1779-1784, Jun. 2003.

[76] A. Varia, R. Singh, and S. V. Kulkarni, "Design of telescopic stub tuner of 1 5/8″ transmission line," *In Journal of Physics: Conference Series*, Mumbai, India, 2010, p. 012023.

[77] G. Chen *et al*., "High-Power Fast-Response Ferrite Tuner for ICRF Impedance Matching in EAST," *Fusion Science and Technology*, vol. 71, no. 2, pp. 144-149, Feb. 2017.

[78] G. H. Huff and S. Goldberger, "A Coaxial Stub Microfluidic Impedance Transformer (COSMIX)," in *IEEE Microwave and Wireless Components Letters*, vol. 20, no. 3, pp. 154-156, March 2010.

[79] S. Y. Zheng, W. S. Chan and M. F. Man K, "Broadband phase shifter using loaded transmission line," *IEEE Microwave and Wireless Components Letters*, vol. 20, no. 9, pp. 498-500, Jun. 2010.

[80] G. J. Hayes *et al.*, "Microfluidic coaxial transmission line and phase shifter," *Microwave and Optical Technology Letters*, vol. 56, no. 6, pp. 1459-1462, March 2014.

[81] S. Dani *et al.*, "Design of multi limb phase shifter," in *Journal of Physics: Conference Series*, 2010, p. 012032.

[82] R. Mirzavand, B. Honarbakhsh, A. Abdipour and A. Tavakoli, "Metamaterial-Based Phase Shifters for Ultra Wide-Band Applications", *Journal of Electromagnetic Waves and Applications*, vol. 23, no. 11-12, pp. 1489-1496, 2009.

[83] A. Jain, R. P. Yadav, and S. Kumar, "Design and development of resonant loop antenna for mock-up ion cyclotron resonance frequency system of tokamak," *IET Microwaves, Antennas & Propagation*, vol. 13, no. 7, pp. 976-981, Feb. 2019.

[84] T. L. Owens, F. W. Baity, and D. J. Hoffman, "ICRF antenna and feedthrough development at the Oak Ridge National Laboratory," *In AIP Conference Proceedings*, Austin, USA, 1985, pp. 95-98.

[85] S. Raftopoulos *et al.*, "Design of ICRF antennas for TFTR," in *IEEE/NPSS Symposium Fusion Engineering*, San Diego, USA: 1991, pp. 111-114.

[86] P. Dumortier and A. M. Messiaen, "ICRH Antenna Design and Matching," *Fusion Science and Technology*, vol. 57, no. 2T, pp. 230-238, Feb. 2010.

[87] Y. T. Song *et al*., “Design and modification of EAST new-type ICRF antenna,” in *IEEE/NPSS Symposium on Fusion Engineering,* Chicago, IL, USA, 2011, pp. 1-5.

[88] D. Kim, R. Pierce, R. Henderson, S. Doo, K. Yoo and J. Lee, "Liquid metal actuation-based reversible frequency tunable monopole antenna", *Applied Physics Letters*, vol. 105, no. 23, p. 234104, 2014.

[89] S. Dwivedi, A. Rawat and R. N. Yadav, "Design of U-shape microstrip patch antenna for WiMAX applications at 2.5 GHz," *2013 Tenth International Conference on Wireless and Optical Communications Networks (WOCN)*, Bhopal, 2013, pp. 1-5.

[90] S. Sukhija and R. Sarin, "A U-shaped meandered slot antenna for biomedical applications", *Progress In Electromagnetics Research M*, vol. 62, pp. 65-77, 2017.

[91] P. Sharma, K. Vyas and R. P. Yadav, "Design and analysis of miniaturized UWB antenna with tunable notched band", *International Journal of Microwave and Wireless Technologies* Vol. 3, pp. 691-696, 2016.

[92] B. P. Mishra, *et al*., “A Low Loss Broadband Metamaterial Based High Gain W-band Flat Lens Antenna for Radar Application”, *in IEEE India Council International Conference (INDICON)*, Roorkee, India, 2017, pp. 1-4.

[93] R. Pierce, A. Blanchard and R. Henderson, "Broadband Planar Modified Aperture Bowtie Antenna", *IEEE Antennas and Wireless Propagation Letters*, vol. 12, pp. 1432-1435, 2013.

[94] P. A. Rizzi, *Microwave Engineering*, USA: Prentice Hall Publisher, 2006.

[95] I. J. Bahl, and R. Garg, “A Designer’s Guide to stripline circuits,” *Microwave*, vol. 17, pp. 90-96, 1978.

[96] I. J. Bahl, and K. C. Gupta, “Average power-handling capability of microstrip lines,” *IEE Journal on Microwaves, Optics and Acoustics*, vol. 3, no. 1, pp. 1-4, Jan. 1979.

[97] D. M. Pozar, *Microwave engineering*. USA: John Wiley & Sons, 2005.

[98] R. E. Collin, “Foundations of Microwave Engineering,” USA, McGraw Hill, 1992.

[99] S. B. Cohn, “Characteristic impedances of broadside-coupled strip transmission lines,” *IRE Transactions on Microwave Theory and Techniques*, vol. 8, no. 6, pp. 633-637, Nov 1960.

[100] B. Bhat and S. K. Koul. *Stripline-like transmission lines for microwave integrated circuits*, New Age International, 1989.

[101] S. D. Shamasundara, and K. C. Gupta, “Sensitivity analysis of coupled microstrip directional couplers,” *IEEE Transactions on Microwave Theory and Techniques*, vol. 26, no. 10, pp. 788-794, 1978.

[102] M. A. Abdalla, K. Phang and G. V. Eleftheriades, “A compact highly reconfigurable CMOS MMIC directional coupler,” *IEEE Transactions on Microwave Theory and Techniques*, vol. 56, no. 2, pp. 305-319, Feb. 2008.

[103] S. Toyoda, “Variable coupling directional couplers using varactor diodes,” in *MTT-S International Microwave Symposium Digest*, Dallas ,TX, USA, 1982, pp. 419-421.

[104] “Dual directional Coupler”, *Pulsar Microwave Corporation*. [online] Available at: https://www.pulsarmicrowave.com/product/directional_coupler/C40-112-481-5N [Accessed 10th Jan. 2018].

[105] “High power dual directional coupler (HDL series)”, *Microwave communications laboratories, Inc.* [online] Available at: https://mcli.com/documents/HDL-45-30.pdf [Accessed on 10th Jan 2018].

[106] “High power dual directional coupler (HDL series)”, *Microwave communications laboratories, Inc.* [online] Available at https://mcli.com/documents/%20HDL-26-10.pdf [Accessed on 10th Jan 2018]

[107] K. W. Shepard *et al*., “Variable CW RF power coupler for 345 MHz superconducting cavities,” in *IEEE Particle Accelerator Conference (PAC),* Albuquerque, NM, USA, 2007, pp. 2230-2232.

[108] S. Lin, M. Eron, S. Turner and J. Sepúlveda, "Development of wideband low-loss directional coupler with suspended stripline and microstrip line," in *Electronics Letters*, vol. 47, no. 25, pp. 1377-1379, 8 December 2011.

[109] R. Smolarz, K. Wincza and S. Gruszczynski, "Design of low-loss directional couplers with compensated coupled-line sections in suspended microstrip technique", *International Journal of RF and Microwave Computer-Aided Engineering*, vol. 27, no. 8, p. e21125, 2017.

[110] “Dual Directional Coupler”, *Pasternack* [online] Available at: https://www.pasternack.com/images/ProductPDF/PE2CP003-20.pdf [Accessed 05th Feb. 2018]

[111] “Directional Coupler”, *SigaTek.* [online] Available at: https://www.sigatek.com/rf-directional-couplers-N-connectors/SC2010100N.pdf. [Accessed 05th Feb. 2018]

[112] “Directional Coupler”, *Pulsar Microwave Corporation*. [online] Available at: https://www.pulsarmicrowave.com/product/directional$/_$coupler/C40-112-481-5N. [Accessed 05th Feb. 2018]

[113] “Directional Coupler”, *Microwave Communication laboratories.* [online] Available at: https://mcli.com/documents/HDL-26-10.pdf. [Accessed 05th Feb. 2018]

[114] C. J. Lee, K. M. Leong and T. Itoh, "Design of resonant small antenna using composite right/left-handed transmission line," in *IEEE Antennas and Propagation Society International Symposium*, Washington, DC, USA, 2005, pp. 218-221.

[115] A. Lai, T. Itoh, and C. Caloz, "Composite right/left-handed transmission line metamaterials," *IEEE microwave magazine*, vol. 5, no. 3, pp. 34-50, Oct. 2004.

[116] C. Caloz, "Dual composite right/left-handed (D-CRLH) transmission line metamaterial," *IEEE microwave and wireless components letters*, vol. 16, no. 11, pp. 585-587, Oct. 2006.

[117] A. Sanada, C. Caloz, and T. Itoh, "Characteristics of the composite right/left-handed transmission lines," *IEEE Microwave and wireless components letters*, vol. 14, no. 2, pp. 68-70, Feb. 2004.

[118] X. Chen, C. Yin, and C. Guan, "Design and optimization of CPW-based composite right/left-handed transmission line," *International Journal of RF and Microwave Computer-Aided Engineering,* vol. 21, no. 4, pp. 421-31, Jul. 2011.

[119] S. Kochuthundil Lalitha, S. K. Behera, and P. K. Sahu, "Bandwidth improvement of a zeroth-order resonant antenna for WiMax applications," *International Journal of RF and Microwave Computer-Aided Engineering*, vol. 22, no. 4, pp. 569-574, Jul. 2012.

[120] A. Lai, K. M. Leong, and T. Itoh, "Infinite wavelength resonant antennas with monopolar radiation pattern based on periodic structures", *IEEE transactions on antennas and propagation*, vol. 55, no. 3, pp. 868-876, Mar. 2007.

[121] B. C. Wadell, *Transmission line design handbook*. Norwood, NA: Artech House,1991.

[122] C. A. Balanis, *Antenna theory: analysis and design*. Hoboken, New Jersey: John Wiley & Sons Inc, 2015.

[123] Trio motion technologies [online] Available at: http://www.triomotion.uk/ public/ products /p849.php [Accessed 05th Feb. 2018]

[124] Trio motion technologies [online] Available at: http://www.triomotion.uk/public/software/ motionPerfectv4.php [Accessed 05th Feb. 2018].